Efficient Visibility Restoration Method Using a Single Foggy Image in Vehicular Applications

by

Samaneh Ahmadvand

Thesis submitted to the
Faculty of Graduate and Postdoctoral Studies
In partial fulfillment of the requirements
For the M.Sc. degree in
Electrical and Computer Engineering

School of Electrical Engineering and Computer Science
Faculty of Engineering
University of Ottawa

Abstract

Foggy and hazy weather conditions considerably effect visibility distance which impacts speed, flow of traffic, travel time delay and increases the risk accidents. Bad weather condition is considered a cause of road accidents, since it the poor conditions can effect drivers field of vision. In addition, fog, haze and mist can have negative influences on visual applications in the open air since they decrease visibility by lowering the contrast and whitening the visible color palette. The poor visibility in these images leads to some failures in recognition and detection of the outdoor object systems and also in Intelligent Transportation Systems (ITS). In this thesis, we propose an image visibility restoration algorithm under foggy weather in intelligent transportation systems. Various camera based Advanced Driver Assistant Systems (ADAS), which can be improved by applying the visibility restoration algorithm, have been applied in this field of study to enhance vehicle safety by displaying the image from a frontal camera to driver after visibility enhancement.

To remove fog, automatic methods have been proposed which are categorized into two approaches based on the number of input images: 1) methods which are using polarizing filters, 2) methods which are using captured images from different fog densities. In both of these approaches multiple images are required which have to be taken from exactly the same point of view. While these applications can generate good results, their requirements make them impractical, particularly in real time applications, such as intelligent transportation systems. Therefore, in this thesis we introduce a high-performance visibility restoration algorithm only using a single foggy image which applies a recursive filtering to preserve the edge of images and videos in real time and also compute depth map of the scene to restore image. The applied edge preserving filtering is based on a domain transform in which 1-Dimensional edge-preserving filtering is performed by preserving the geodesic distance between points on the curves that is adaptable with wrapping the input signal. The proposed algorithm can be applied in intelligent transportation system applications, such as Advanced Driver Assistance Systems (ADAS).

The main features of the proposed algorithm are its speed, which plays a main role in real time applications, since 1-Dimensional operations are used in the applied filtering leads to remarkable speedups in comparison with classical median filters and robust bilateral filters. Potential of memory saving is considered as another one advantage of the proposed model and also the parameters of applied edge-preserving filtering do not effect on its computational cost. It is the first edge-preserving filter for color images with arbitrary scales in real time. The proposed algorithm is also able to handle both color and gray-level images and achieves the restored image without the presence of artifacts in comparison with other state-of-the-art algorithms.

Acknowledgements

First and foremost, I thank God for paving this way for me to make this goal come true. I would love to thank my parents particularly, my dear father, Ahmad Ahmadvand, and my lovely sister, Sanaz Ahmadvand, for their encouragements and efforts to become the person I am today. All the support and the unlimited love they have provided for me over the years have been the invaluable gift I have ever could have. I would also like to thank my brother-in-law, Dr. Mahmood Salehi, because of all his helpful and valuable input during my master study.

I need to express my sincere gratitude to my sophisticated supervisor, Professor Azzedine Boukerche, for the continuous support of my master study and research, for his patience, motivation, enthusiasm, immense knowledge, and financial support. He provided his guidance all the time of my research and writing of this thesis. I am so appreciate for studying and researching under his expertise supervising.

I wish to thank for many discussion with Dr. Abdelhamid Mammeri, as a member of the PARADISE research laboratory.

I would truly like to thank my friends and colleagues at the PARADISE Research Laboratory, University of Ottawa. They always keep supporting and assisting me the past two years to achieve a productive M.Sc. work. Also special thanks to Ehsan Karami for his willingness to share thoughts.

Table of Contents

List of Tables

List of Figures

Nomenclature

AV	Autonomous Vehicle
ADAS	Advanced Driver Assistance System
LIDAR	Light Imaging Detection and Ranging
PMD	Photonic Mixer Device
DAS	Driver Assistance System
CIE	International Commission on Illumination
FVES	Fog Vision Enhancement System
SNR	Signal-to-Noise Ratio
ICA	Independent Component Analysis
DCP	Dark Channel Prior
WLS	Weighted Least Square
NIR	Near-Infrared
NBPC	No-Black-Pixel Constraint
NBPC+PA	No-Black-Pixel Constraint + Planar scene Assumption
FSS	Free-Space Segmentation
PA	Planar scene Assumption
FMRF	Factorial Markov Random Field
MDF	Multiscale Depth Fusion
DOG	Difference-of-Gaussian
SSR	Single Scale Retinex
MSR	Multiscale Retinex
MSRCR	Multiscale Retinex with Color Restoration
HE	Histogram Equalization
GHE	Global Histogram Equalization
LHE	Local Histogram Equalization

Nomenclature

POSHE	Partially Overlapped Sub-block Histogram Equalization
RSWHE	Recursively Separated and Weighted Histogram Equalization
BPDFHE	Brightness Preserving Dynamic Fuzzy Histogram Equalization
CLAHE	Contrast-Limited Adaptive Histogram Equalization
RGB	Red Green Blue
VL	Visible Light
CLAHE	Contrast-Limited Adaptive Histogram Equalization
DE	Depth Estimation
VR	Visibility Restoration
RF	Recursive Filtering
1D	one-Dimensional
3D	three-Dimensional
5D	five-Dimensional
NC	Normalized Convolution
IC	Interpolated Convolution
BF	Bilateral Filter
AD	Anisotropic Diffusion
ASV	Advanced Safety Vehicle
MPE	Media Processing Engine
VLIW	Very Long Instruction Word
SIMD	Single Instruction Stream, Multiple Data Stream
SSIM	Structural Similarity Index
HVS	Human Visual System
NSS	Natural Scene Statistics
HCC	Histogram Correlation Coefficient
PSNR	Peak Signal-to-Noise Ratio

Nomenclature

VCM	Visual Contrast Measure
IVM	Image Visibility Measurement
MSE	Mean Squared Error
ITS	Intelligent Transportation System
EMS	Electronic Management System

Chapter 1

Introduction

Recently, in order to reduce the costs of mobility and infrastructure and increase safety, mobility, customer satisfaction and reduce crime, Autonomous Vehicles (AV) have become a favoured research field [129], [199], and [39]. Because of the ability of autonomous vehicles to reduce the traffic collisions; the resulting injuries; reduce the need for parking, increase traffic flow and compliment transportation services, they have vast disruptive potential for academic research and automotive industry to industrialize the production [79], [203], [127], [128], citeren2010monitoring, and [188]. This technology was proposed to reduce the number of injuries and deaths caused by road accidents but unfortunately, there have been some failures in this technology which can be solved by investigation into related technologies in depth. In this context, camera-based Advanced Driver Assistance System (ADAS) has been proposed, which are able to increase the safety by restoring the video or images degraded from the road surface under bad weather conditions [207] and [161]. ADAS can be easily improved by restoration and enhancement algorithms and be applied in autonomous vehicles [164] and [28].

1.1 Background and Problems of Advanced Driver Assistance Systems (ADAS)

Advanced Driver Assistance Systems (ADAS) provide assistance, safety and satisfaction to the driver which have been integrated with the vehicle to automate, adapt and enhance vehicle systems [31] and [27]. Reducing the road death rate by providing safer vehicles and roads is caused to demand for advanced driver assistance systems with respect to legislation in the industrialized countries [37], [19], and [21]. Therefore, ADAS was designed to ensure safety of the vehicle, the driver, and the pedestrians. A vehicle which is equipped with ADAS is able to monitor near and far areas in each direction, because of using the physical sensors, such as radar, LIDAR, ultrasonic, photonic mixer device (PMD), cameras, and night vision devices, Figure. 1.1, [32]. ADAS can be improved by advanced and efficient sensor fusion algorithms. Safety with ADAS is provided based on data collected via traffic, weather, dangerous conditions, etc. Acting in real time plays a main role in

ADAS system that delivers adequate warning to driver in dangerous situations [59], [208], and [16]. Modern real-time ADAS systems can control systems directly which means they can integrated with autonomous vehicles in the future [209] and [11].

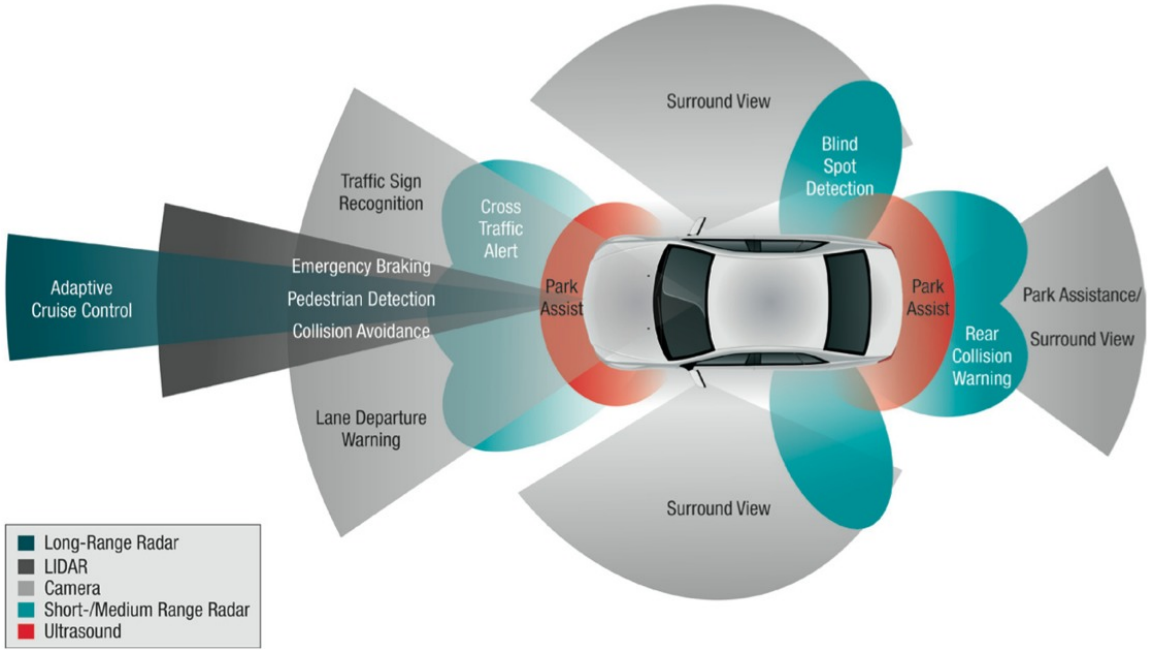

Figure 1.1: Set of ADAS sensors to enable sensor fusion and actions (https://medium.com).

ADAS system is considered as a advanced version of Driver Assistance System (DAS), by increasing the use of complex processing algorithms to detect and assess the vehicle's environment. In case of danger, DAS system will inform the driver by delivering adequate warnings and based on the actions they will provide the corresponding response. It also by considering the vehicle's stabilizing or maneuvering, reduce the workload. The set of DAS capabilities is illustrated in Figure. 1.2 in which the capabilities in production today considered as ADAS are specified with stars [209] and [52].

ADAS systems like any other advanced systems suffer from some short comings in their design, implementation, deploying, and operation. To overcome these problems, incredible amounts of research and study have been conducted in academic institutions and research and development industries. In terms of providing data via ADAS systems, the collected input which can be as images or videos must be accurate and their process should have high performance [43]. The system is expected to predict context correctly, and has a real-time response. Therefore, having a system with the above mentioned features must also be robust, reliable, and maintain a significant level of accuracy [209], [20], and [13].

The potential threats or failures for different parts of ADAS systems are illustrated in Figure. 1.3 in which the exposed interfaces are specified as main attack surfaces and are demonstrated by vulnerable internal or external assets.

Some data features, such as syntax, semantics, timing, availability, and correlation are demonstrated in Figure. 1.3 as vulnerable features particularly, when they are manipulated

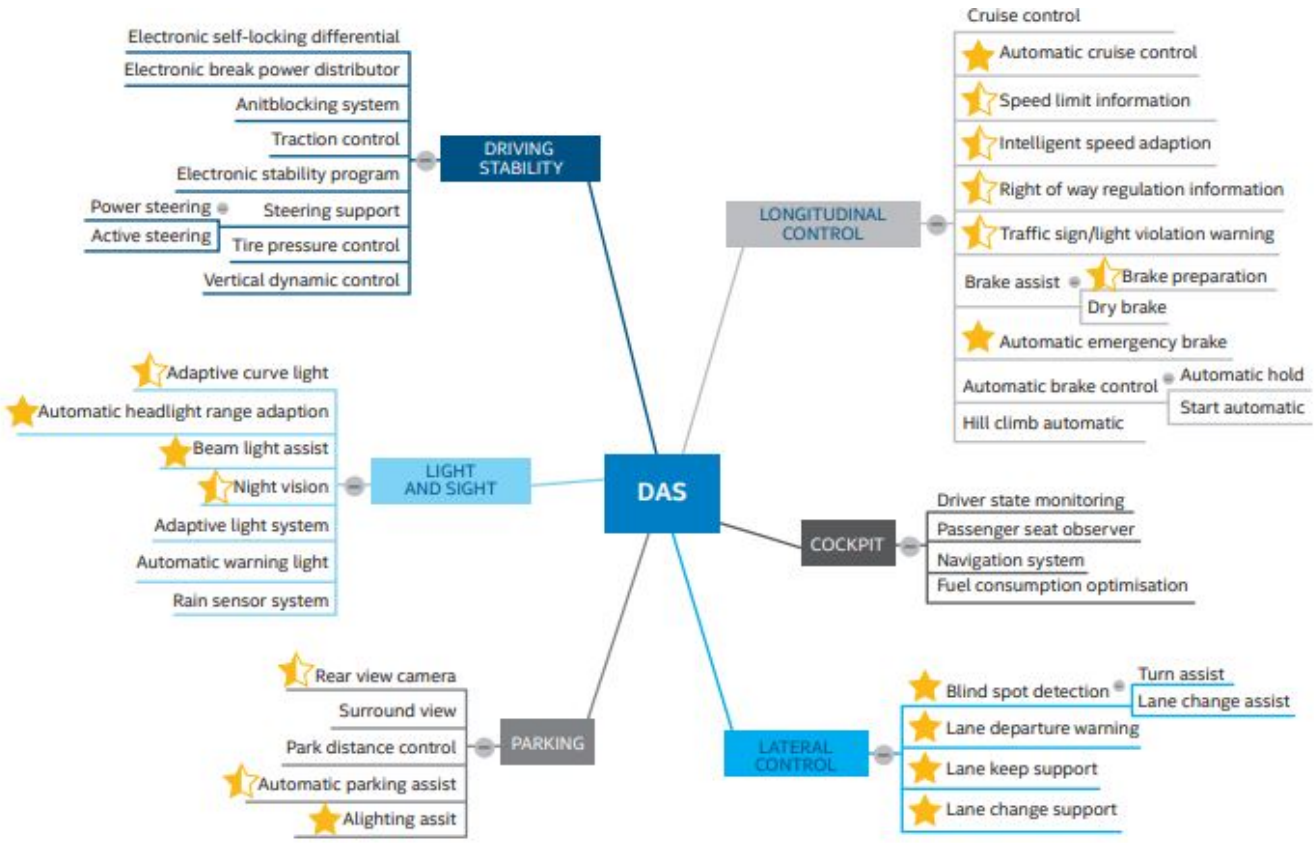

Figure 1.2: Different ADAS functions and spectrum of DAS [209].

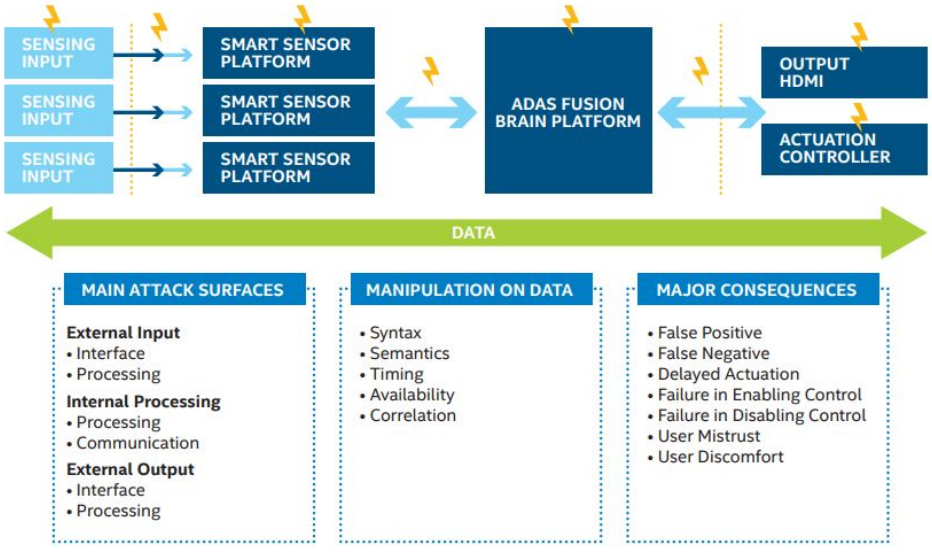

Figure 1.3: Different possible threats to ADAS assets and interfaces [209].

[57]. Also the compromised ADAS system can inform and warn the driver via false positive or false negative which is considered as disadvantages of this system and it can even lead to dangerous situations. In the main "brain" of ADAS the data is processed by applying the considered algorithms or software, the algorithm is expected to have simple performance functionality, because the algorithm should process the large amount of data in real time, and also precise models should be obtained from multiple data streams by these algorithms. It is important for ADAS systems to retain its simplicity even by using different algorithms with any goals, such as detection, recognition, restoration, and etc [148]. In terms of being real-time, the real-time operating system and software are supposed to be applied for ADAS to meet real-time reaction requirement [29]. With regarding the ADAS computing platform it must be connected to every parts of vehicles Electronic Management System (EMS), such as user interface and physical sensing, it is crucial to keep the system integrity by isolation solution, such as "Trusted Execution Environment + Protected Data Path" which is expected to meet real-time requirement as well [209], [30], and [15].

Although ADAS system has the potential to be applied to the automotive industry, independent audits suggest that the potential revenues could be from $5 billion to $8 billion annually which is rather low in comparison to other automotive systems. There are also two problems corresponding to this technology. One problem is that many of the required ADAS applications are still in development and testing stages while others which have hit the market are still expensive and only available on luxury brand cars. The main problem which is discouraging demand for ADAS is that many consumers are still unaware of ADAS technology. An online survey newly has collected information regarding to the consumer awareness about ADAS, this includes more than 4,500 car buyers in five countries by McKinsey which is illustrated in Figure. 1.4. Based on this survey, it is determined that consumers will be more inclined to purchase vehicles with the ADAS features if they get familiar with this technology [46], [34], [3], and [26].

In terms of growth prospects for ADAS, the market experts anticipate more than 10 percent growth annually from 2015 to 2020, for example, one leading analyst, Strategy Analytic, anticipates 16 percent rise during this era, and TechNavio anticipates 29 percent rise Figure. 1.5. In 2015 only 8 % of cars were equipped with advanced driver assistance systems; in 2025, it predicts to be 62% by VisionGain.

1.2 Thesis Objective and Contribution

Fog and haze are two natural phenomena that are common on land and ocean. Every year the presence of fog increases the risk of accidents and has been a factor in thousands of deaths. Fog reduces visibility, limits contrast, distorts perception and fades color [170]. In essence, commuters ability to see other vehicles and objects on the road is reduced, therefore greater precautions must be taken. The huge number of very fine suspended moisture droplets in the air produce fog. Fog and haze not only absorbs and scatters reflected light of the scene, but also scatter some atmospheric light to the camera which leads to a reduction in contrast and a dense white background. Fog will get more dense

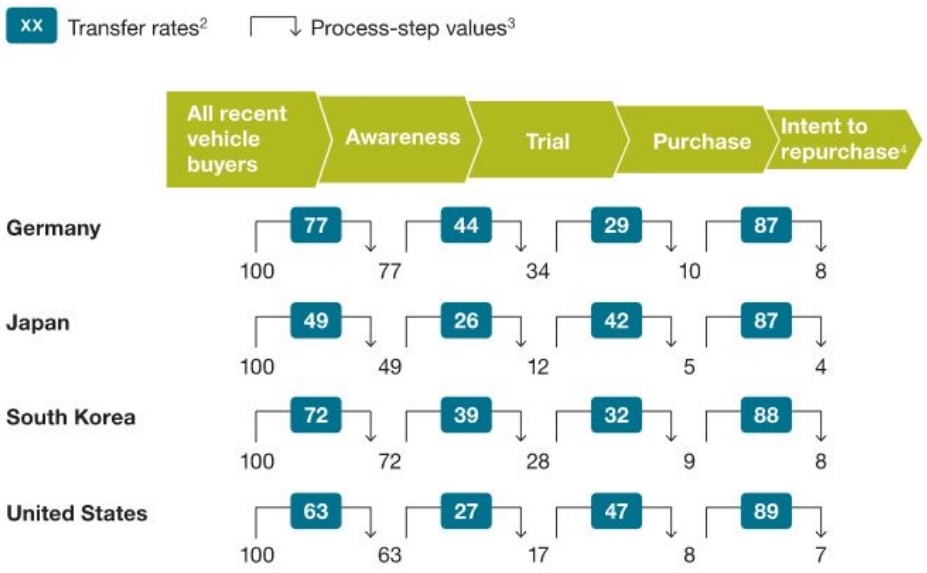

Figure 1.4: The rate of consumers unfamiliar with ADAS applications and purchased cars with this technology (McKinsey survey on connected cars, 2015).

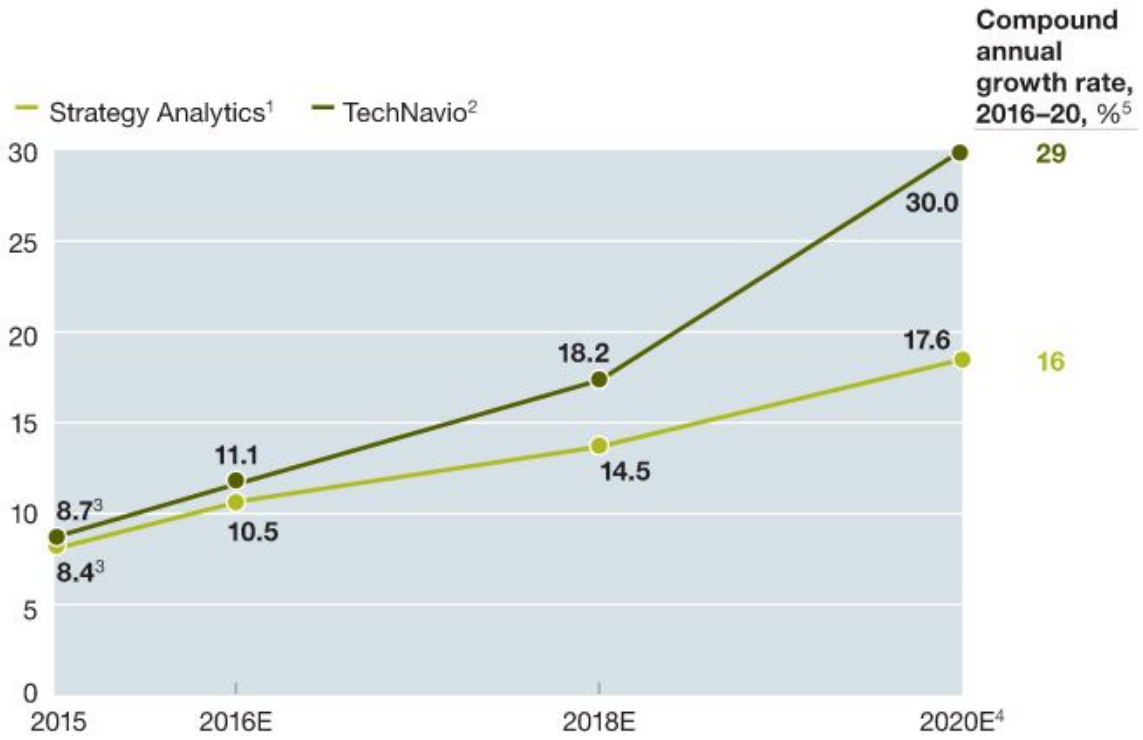

Figure 1.5: Global revenue of advanced driver assistance system projections from 2015 to 2020 (IHS, SBD, Strategy Analytics, TechNavio, McKinsey Analysis).

when droplets get smaller and it will cover the roadways. Therefore, vehicle collisions occur due to poor visibility limiting drivers ability to see potential hazards ahead [133], [135].

Visual systems based on the visible light spectrum are seriously affected under bad weather conditions. Also captured images via a classical in-vehicle camera in the visible light range are degraded dramatically under poor weather conditions because of the high sensitivity of current in-vehicle camera-based devices. Therefore, it is important to design an image defogging algorithm that the visual system is capable of analyzing in poor environmental conditions. Removing the effects of fog should be performed with high reliability in an in-vehicle surveillance system. Considering the importance of reliability two potential solutions can be applied. In one solutions, the operating thresholds of the system is adapted or deactivated for a moment in case of it has been surpassed. In the second solution, defogging is performed as a pre-processing [84], [175], [193], [15], and [14]. In order to remove fog effects from the foggy image, filtering techniques which are space stable cannot be applied directly because haze or fog effects are not stable across the scene and these effects changed exponentially when considering the depth of scene points. Therefore, a reasonable approach is that the degradation in the image is measured by detecting the relative weather conditions to enhance the original capture image [84]. An algorithm with above mentioned features can enhance the visibility and contrast in foggy images and will be used for various camera based Advanced Driver Assistance Systems (ADAS). Table. 1.6 illustrates the serious traffic problems in cities, such as China and Swedish and high influence of bad weather conditions on it. Based on table. 1.6 it can be perceived the important role of camera based ADAS with defogging ability to overcome this issue by increasing the traffic flow.

The defogging process can be performed by using specific sensors, such as scatterometer, and transmissometer to measure the visibility distance, while the most of effective sensors that are suited for this purpose have high operating cost and their installation and calibration have been found to be problematic in this dynamic application. There remains challenges when trying to combine the ADAS platform with these types of devices. Unlike the sensor, using a camera does not have these types of issues. Based on this, Bush and Kwon measured the visibility distances by placing a fixed camera above the roadway [44], [112]. Although, systems with this features with an on-board camera are not used mostly. Pomerleau proposed a system to estimate visibility by measuring the attenuation of contrast between constant road features like road markings at various distances ahead of the a moving vehicle [153]. In order to measure the visibility distances and detect the presence of fog under foggy weather during the day Hautire et al. presented a technique using a camera placed onboard a moving vehicle in which visibility distance is defined by the International Commission on Illumination (CIE) as the distance further than it a black object is found out with a contrast of less than 5% [88]. The improved version of their method by applying stereovision is proposed in [82].

Restoration methods which improve the contrast of image under foggy conditions have not yet hit the market [46].

Methods which restore image contrast under bad weather conditions are encountered more often in the literature. However, all these methods suffers from some serious limi-

Problems	Often	Occasionally	Never
1. Advanced weather conditions, slippery	0%	67%	33%
2. Bad visibility (fog, rain and darkness)	**17%**	**62%**	**27%**
3. Blind spot visibility	0%	55%	45%
4. Punctured tire	0%	39%	61%
5. Driving on hard shoulder	33%	50%	17%
6. Pedestrians not crossing road at crosswalk	73%	27%	0%
7. Bicycle do not cross road at crosswalk	71%	29%	0%
8. Drinking and driving	6%	33%	61%
9. Fatigue	0%	39%	61%
10. Illegal overtaking	17%	50%	33%
11. Driver distraction (e.g. cellphone)	85%	15%	0%
12. Speeding	57%	26%	17%
13. Difficulties detection obstacles on the road	3%	23%	74%
14. Congestion	87%	13%	0%

Figure 1.6: The various reasons of traffic problems encountered by drivers [121].

tation when combined with the ADAS platform [84]. Some methods for restoration need more information about the scene, like the proposed method in [142] which reduces the effects of fog by determining the landscape geometry. Other methods estimate the weather conditions via specific hardware [198]. The proposed method in [136] describes the appearance of the scene based on the changes of scene points intensity under different weather conditions to restore the contrast by estimating the range map of the scene. However, in this method the scene should be under uniform foggy condition. Polarization techniques are another way to reduce the effects of fog which was proposed in [168], although two different filtered images of the scene are required in this technique. The image enhancement method in [141] estimates visual motion by using navigational information, the camera specifications, and a database of terrain elevation to restore the contrast with respect to the relationship between depth and the brightness which is obtained via the sum of the light scattered from the terrain and that scattered from the atmospheric particles. However, radiance distribution is estimated via a simple Gaussian with known variance. To solve the visibility enhancement problem, [137] estimated geometrical depth-map of the scene from a single image to obtain non-foggy luminance map [48]. However, computing geometrical depth-map of the scene by camera-based ADAS is complicated from the driver's viewing angle along the road. To refine the idea of estimating the geometrical depth-map of the scene, captured imagery from in front of the vehicle are modeled by several simple geometrical models [84]. However, the proposed geometrical models do not have enough flexibility to be applied for all road types. Local spatial regularization is another technique to enhance the visibility from a single image and it is able to handle both gray level and color images which is used and introduced in [176], [173], and [89]. However, two proposed algorithms, [173] and [89], have a high processing time which are not very appropriate to in real-time application or to restore the road portion of the image correctly. In order to restore the contrast of road portion of the image properly, the planar assumption was first introduced in [80] in which the road way is assumed to be planar. However, in this method, the visibility of objects out of the road plane are restored incorrectly. Finally, a visibility enhancement algorithm devoted to road images and based on planar assumption was proposed in [86]. The proposed algorithm is not only able to restore contrast of the road part of the image and also able to restore contrast of the objects out of the road plane correctly however, it cannot have a satisfied performance when the fog is heterogeneous.

In this thesis, we propose a restoration algorithm based on the composed physical model of the airlight model and direct transmission model from a single image. The proposed method is based on a key assumption, which is known as a dark channel prior, that there are some pixels with very low intensity in at least one color channel in most local patches of outdoor clear images. Restoration algorithms based on computing the depth map achieve high-quality restored images compared to other techniques. While computing the depth map of the scene from a single image leads to a computational complex analysis and high processing time which have been found an ill posed problem [35], [42], and [38]. To tackle this issue, first, we compute the dark channel prior based on photometric properties of the foggy scene while involving edge preserving smoothing filter in transformed domain. And then the depth map of the scene is computed and refined by applying the obtained dark channel prior from the first step. The applied edge-aware filtering is a new approach based

on a domain transform for performing high-quality edge preserving filtering of images and videos in real time which prevents the presence of halo artifacts in the restored image [69]. The proposed algorithm can thus be seen as the extension of the local visibility enhancement algorithm [176] combined with dark channel prior enhancement algorithm [89]. We also apply a detailed manipulation function based on domain transfer to let the objects of the image, to ensure they can be seen clearly and with more detail, such as traffic signs. The proposed algorithm is appropriate for camera based ADAS system, such as FVES since it is able to process both gray-level and color images and runs in almost real time.

The most challenging parts of the defogging procedure that we have encountered are:

- Computing the depth map of the scene from a single image tends to increase the complexity and processing time of the system.
- Computing a refined transmission map without the presence of block artifacts, to achieve a high quality restored image without the presence of halo and block artifacts.
- Defining a defogging algorithm which is fast enough to can be applied in real-time ADAS systems.
- Applying an edge preserving smoothing filter which is able to preserve all edges as well as corners with obtuse angle while smoothing the image.
- Obtaining a restored image without the presence of any halo artifacts and block artifacts in the sky region of the image.
- Removing fog from the image without losing the edge and texture information.
- Defining a defogging method which has no difficulties to restore image under heterogeneous fog.

1.3 Thesis Outline

The contents of this thesis are organized in the following chapters: In Chapter 2, a literature review of different defogging algorithms can be studied. In this chapter defogging algorithms based on image restoration, image contrast enhancement, and fusion-based techniques form a single image or multiple images have been covered. As the focus of proposed work is about image restoration from a single image under foggy condition, this subject will cover an adequate proportion of this chapter.

In Chapter 3, a depth-based image defogging method based on image restoration from a single image with high-efficiency integrated solution is denoted. The main idea of the proposed method is the estimation of the refined transmission map by applying the advantages of Recursive Filtering in the transformed domain as an edge preserving filtering and using the estimated depth information in the dark channel prior (DCP) in the defogging process to have high efficient, fast and accurate restored image.

Chapter 4 presents the methodology and results of experiments of the proposed algorithm. Synthetic and real or camera images have been used to illustrate the restored images. The synthetic images have been made by using the SiVICTM software to generate a moving vehicle with a physically-driven model of dynamic behavior with having an environment based on the physics of the road [75], and virtual embedded sensors. Theses images have been generated from a virtual inboard camera by simulating a moving vehicle on a road path while considering three realistic and complex structure models (urban, highway and mounts) [175]. 66 synthetic images from various viewpoints with 640×480 size and also 400 real images with arbitrary sizes have been applied in this chapter. The program built with Matlab software.

In Chapter 5, the proposed algorithm is summarized with a detailed description of its potential benefits and hindrance. In the meantime, some possible improvements and methods of enhancement were discussed in the future work.

Chapter 2

Literature Review

2.1 Image Defogging Algorithms

In some articles, considering the incorporation of the physical model of fog, the image defogging algorithms have been classified into two groups [118], [189], [181], [195], and [105]. Image restoration algorithm based on the physics of fog [176], [136], [73], [93], [63], and image enhancement algorithm [182], [1], [119], [154], [184], [210] are considered as the first and second model respectively. In order to restore images under foggy conditions, a physical imaging model is created in restoration methods with respect to the factors that decay foggy images. In this group of algorithms, parameters such as the atmospheric light (atmospheric veil) and transmission map (depth map) are required to be estimated as parameters of the physical model. Therefore, by inversing the physical model, the image can be restored. The goal of image restoration algorithms is to obtain a natural and defogged image with good visibility while in which color restoration is performed appropriately. However, the physical model of fog is not considered in the second group in which defogging procedure is based on image enhancement. In the second group, therefore, to increase the contrast and visibility of the image under foggy conditions, different kinds of image enhancement methods have been applied. The third group of defogging algorithms are fusion-based algorithms in which image enhancement is performed by merging multiple input images [9], [78], [66], [166]. Figure 2.1 illustrates the classification of image defogging algorithms.

2.2 Image Defogging Based on Image Restoration

In bad weather conditions such as fog, haze or smoke, scattering can be regarded as the main cause of image degradation. The physical model of atmospheric scattering was proposed by McCartney in 1976 [124] and is based on the Mie scattering theory. The airlight and direct transmission models are the components of physical model of scattering which is illustrated in Figure 2.2. The attenuation of edge information and object textures of the foggy image is caused by the degradation of light in direct transmission model because of

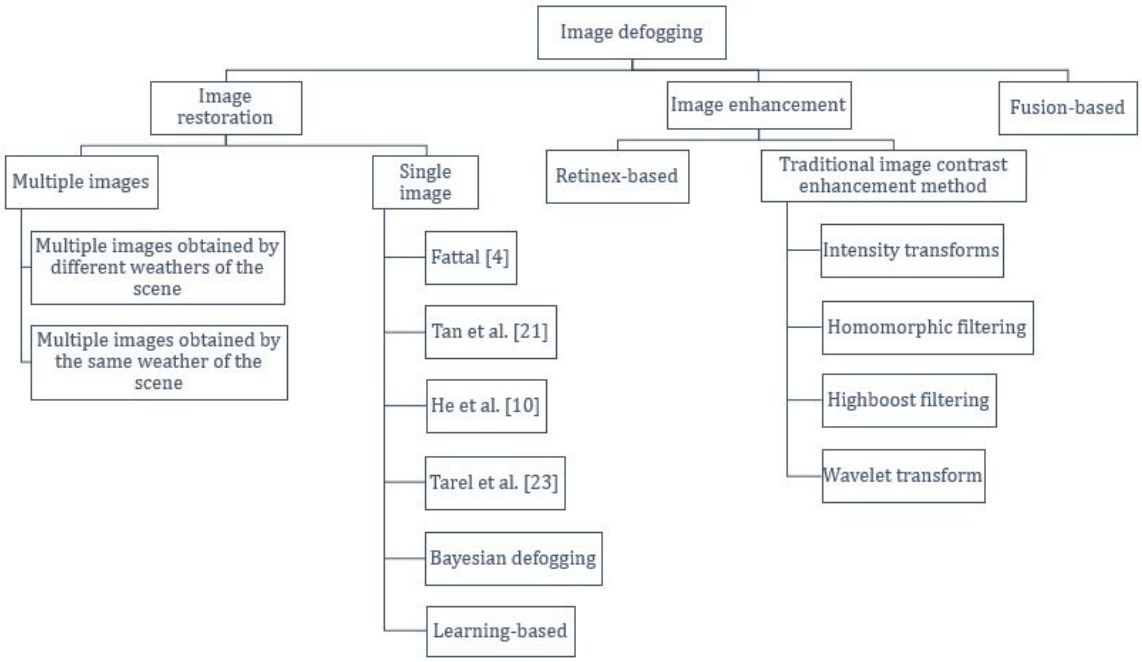

Figure 2.1: The classification of image defogging algorithms [193].

the scattering phenomenon. In the airlight model, the atmosphere scatters some sunlight which are not the scene lights; thus, this light scattering can be seen as a veil which fades the colors and reduces the contrast of the image. In images under foggy conditions, fog will reduce the part of the direct transmission model. However, the direct transmission model will create a large part of the imaging model for images in good visibility conditions. In addition, fog will increase the part of the airlight model which reduces the visibility of the image. Therefore, attenuated contrast and visibility in foggy images are resulted from the airlight model. To restore the image under the homogenous foggy condition, a physical model has been proposed by Narasimhan and Nayar in [134], [137], and [139] with respect to the wavelength of visible light which does not effect the scattering coefficient:

$$I(x) = I_{\infty} p(x) e^{-\beta d(x)} + I_{\infty}(1 - e^{-\beta d(x)}) \tag{2.1}$$

where I_{∞} is the intensity of the sky, the normalized radiance of a scene in pixel x is represented by $p(x)$, β is extinction coefficient of the atmosphere, and the distance between the pixel x and the camera or observer is denoted by $d(x)$. The first term of Eq. 2.1 denotes an exponential decay with respect to the distance between the object and observer in the direct transmission model and the second term represents the airlight model. Eq. 2.1 can be simplified [89], where J represents the restored image or intrinsic intensity, t is the transmission, and the intensity of an object which is placed in so far distance is indicated by A_{∞}, on the other hand, A_{∞} can represent the atmospheric light value of the sky so Eq. 2.1 can be rewritten as follows:

$$I(x) = J(x)t(x) + A_{\infty}(1 - t(x)) \tag{2.2}$$

To obtain the restored image (J) by Eq. 2.2 two parameters transmission t and atmospheric light value A_∞ should be estimated. By estimating these two parameters correctly the restoration procedure will be performed perfectly. The defogged image in the defogging algorithms based on the physical model is specified by the parameters directly. The physical model is only able to be simplified when the atmospheric medium is homogeneous and there is single-scattering. Thus, for some conditions, such as foggy sea or heterogeneous fog, this model is not an appropriate imaging model. Based on the physical model of fog, many restoration algorithms have been introduced recently. These can be classified into two groups with respect to the number of input images: 1) image restoration algorithms based on multiple input images and 2) image restoration algorithms based on a single input image [201], [76].

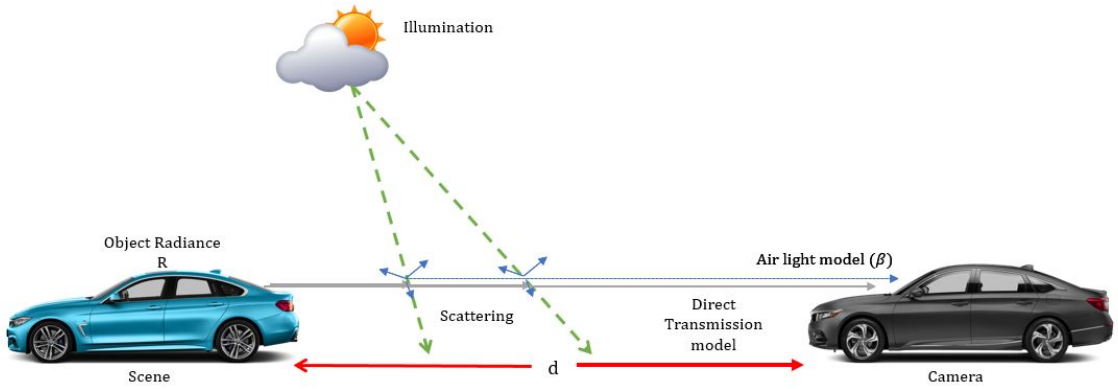

Figure 2.2: Scattering model in foggy weather.

2.2.1 Image Restoration Based on Multiple Foggy Images

Image restoration algorithms that rely on multiple images can be classified into two classes as shown in Figure 2.1. The first class utilizes multiple foggy images which are captured from the same weather condition of the scene with different orientations. The second class utilizes multiple images which are captured from different weather conditions of the scene [25].

- **Multiple Images Obtained Under the Same Weather of the Scene:**

This class of algorithms is based on the fact that the path radiance (airlight) scattered by atmospheric particles is usually partially polarized. In [132], [168], [172], [167], and [130] some novel image defogging methods have been proposed which work under a wide range of atmospheric and viewing conditions with taking into account polarization effects of atmospheric scattering by applying multiple polarization images. In [179] a comparison has been performed between using a polarizer or a dehazing process while taking into account the change of Signal-to-Noise Ratio (SNR). It has demonstrated that to discriminate signal from noise in the image under foggy condition, applying one polarized image or two polarized images will be unnecessary [24]. However, to restore foggy images the comparison

between one or two polarization images has demonstrated that applying two polarization images reduces the noise. Utilizing a polarization filter with different direction provides the polarization images of the same situation of the scene with different brightness. In order to estimate the parameters of the physical model of fog by this restoration algorithm, at least two polarization images are required. Therefore, by having these parameters, the restored image can be obtained by reversing the physical model. For the first time, a restoration algorithm which is able to restore image by applying two polarization images has been proposed by Schechner et al. in [167]. A plane of incidence is defined in this work with taking into account the light ray from the source to a scatterer and the line of sight from the camera to the scatterer Figure 2.3, [167]. To provide two polarization images, the airlight intensity is divided into two components, that are parallel $A_{\infty}^{\perp}$ and perpendicular $A_{\infty}^{\parallel}$ to this plane [17]. In image defogging algorithms based on polarization images, direction is assumed not to have an effect on the direct transmission,and the two polarization images can be written as follow:

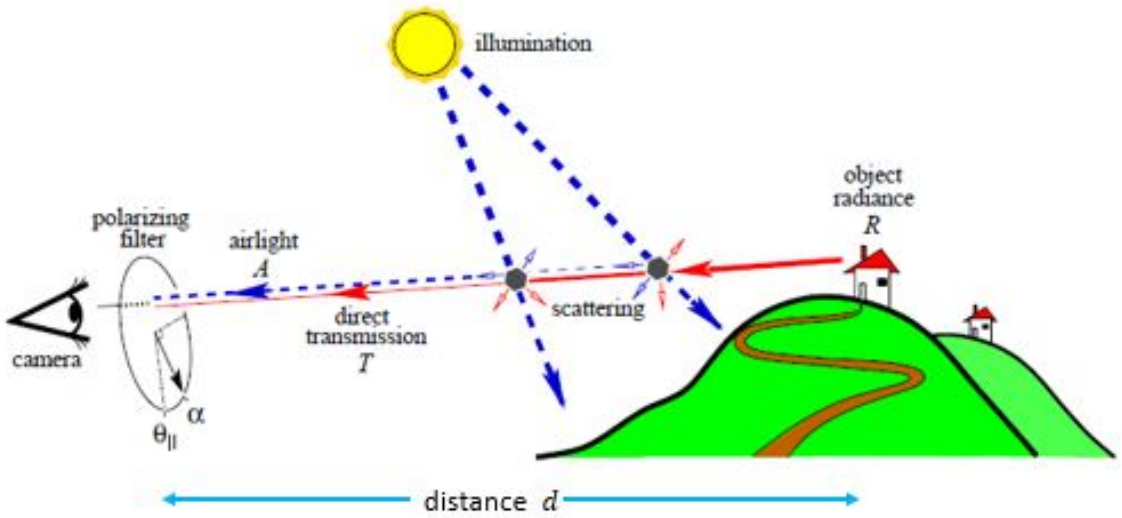

Figure 2.3: Dashed ray illustrates airlight A which is coming from the source of illuminant (sun) and scattered by particles in the atmospheric towards the camera and it has a direct relationship with distance d. Solid ray illustrates the direct transmission T which is resulted from the attenuation of intrinsic luminance of the object R along the line of sight by scattering. The direct transmission would be attenuated with increasing the distance d. A polarizing filter at angle α images the scene [167].

$$I^{\perp} = \frac{D(x)}{2} + V^{\perp}(x) \tag{2.3}$$

$$I^{\parallel} = \frac{D(x)}{2} + V^{\parallel}(x) \tag{2.4}$$

where $D(x)$ is the direct transmission model. $V^{\parallel}$ is the airlight which is modeled by parallel polarization image and $V^{\perp}$ is the airlight which is modeled by perpendicular polarization image.

$$V^{\perp}(x) = A_{\infty}^{\perp}(1 - t(x)) \tag{2.5}$$

$$V^{\parallel}(x) = A_{\infty}^{\parallel}(1 - t(x)) \tag{2.6}$$

the values of the atmospheric light of the two parallel and perpendicular polarization images has been demonstrated by $A_{\infty}^{\parallel}$ and $A_{\infty}^{\perp}$. The degree of polarization can be as follow:

$$p \equiv \frac{V^{\perp} - V^{\parallel}}{V^{\perp} + V^{\parallel}} \tag{2.7}$$

In order to obtain the restored image J , the estimation of two parameters degree of polarization p and atmospheric light A_{∞} of each polarization images are required.The degree of polarization can be estimated as

$$\hat{p} = \frac{A_{\infty}^{\perp} - A_{\infty}^{\parallel}}{A_{\infty}^{\perp} + A_{\infty}^{\parallel}} \tag{2.8}$$

So from Eq.2.3 and Eq. 2.8 the airlight model and transmission can be estimated.

$$\hat{V}(x) = \frac{V^{\perp}(x) - V^{\parallel}(x)}{\hat{p}} \tag{2.9}$$

$$t(x) = 1 - \frac{\hat{V}(x)}{A_{\infty}^{\perp} + A_{\infty}^{\parallel}} \tag{2.10}$$

Therefore, by putting two parameters t and $\hat{V}(x)$ in the inverse physical model Eq. 2.2, the restored image can be obtained. The problem such as natural image which is captured under a clear day also encounters airlights scattering having no effect on image restoration algorithms based on polarization images.

Schechner et al. in [168] presented an improved restoration algorithm based on polarization images with respect to this idea that by preserving part of airlights, it is feasible that the image is restored more natural. This improvement is limited by multiplying a coefficient to the polarization degree $\hat{p} = \varepsilon p$ where $1 \leq \varepsilon \leq \frac{1}{p}$.

Miyazaki et al. in [130] applied the polarization information of two objects under foggy and clear condition of the scene at different distances to estimate the optical density and maximum scattered light. This method is supposed to be applied in moving vehicles under foggy condition; hence, traffic signs are supposed to be used as the reference objects. Figure 2.4 illustrates the condition to estimate two parameters: the optical density and the maximum scattered light. This proposed method by Miyazaki et al. requires to set up a traffic sign database to find the two traffic signs, which means it is not suitable to be utilized in realtime applications [130] and [41].

Regarding image restoration algorithms, image restoration requires estimated parameters of the airlight. Shwartz et al. in [172] introduced a novel approach to recover blindly

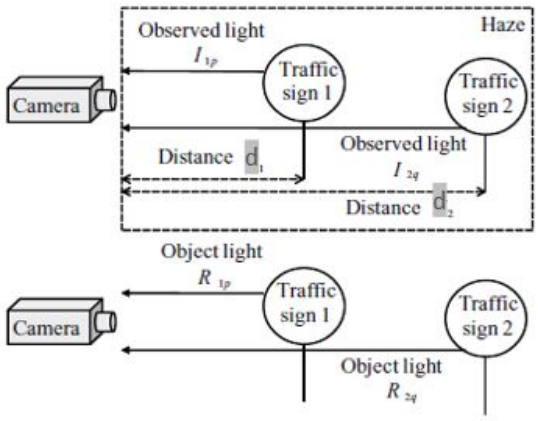

Figure 2.4: Polarization database for two reference traffic signs [130].

the required parameters without having the airlight measurement, hence contrast can be recovered, without user interaction or existence of the sky in the image. Therefore, $A\infty$ will be obtained by selecting two similar features in the scene. The changes in quantity of SNR is related to visibility changes [180]. Thus, a method was proposed in [179] to avoid noise amplification in restored image based on polarization images only by using a single polarized or unpolarized frame, polarization to optimize the restored image better.

Image defogging algorithms based on polarization has more satisfied results in comparison with defogging algorithms based on optical filtering. However, the value of $A\infty$ is obtained manually in polarization-based algorithms which means it is not acceptable to remove the fog automatically. The polarization-based defogging algorithm is based on the partial polarization of airlight. Therefore, if the polarization degree reduces, it leads to the reduction of its effect. Furthermore, dense foggy weather leads to some failures in these algorithms. In addition, for some situations like a moving camera obtaining two polarization images when scenes are changing more rapidly is hard for the filter rotation which means applying these defogging algorithms in vehicles will not be helpful [193] and [5]. Also polarization hardly ever improves the SNR over an average of unpolarized images obtained under the same acquisition time.

- **Multiple Images Obtained Under Different Weather Conditions of the Scene:**

In some algorithms in order to restore the image under bad weather condition, two or more images are utilized which are supposed to be captured under different weather conditions. Therefore, Narasimhan et al. in [138], [135], [134], [133], [136], and [137] proposed the restoration algorithm based on this idea. The visual manifestations of different weather conditions, and then a color model from atmospheric scattering were obtained by Nayar and Narasimhan in [139]. Based on this model which is called the dichromatic atmospheric scattering model, the color of a scene point under foggy condition is a linear combination of the direct transmission color and airlight color. The dichromatic model is illustrated by Figure 2.5 in R-G-B color space, where vector E is the observed color of a scene point (P)

under foggy condition and vector $\hat{D}$ is the direction of direct transmission color of P. The direction of airlight color is represented by vector $\hat{A}$. Therefore, this model can be written as follow:

$$E = p\hat{D} + q\hat{A} \tag{2.11}$$

In [133] a geometric framework for foggy scene based on this proposed model was represented. Also in this paper the 3D structure and color of the scene were calculated by using two or more foggy images. However, there is a limitation to using this defogging model when the color of the object in the scene is similar to fog or haze as it makes it unstable. To solve this limitation, a physical model was presented to estimate the structure of scenes under homogeneous bad weather conditions [136]. Therefore, a monochrome atmospheric scattering model was applied to distinguish intensity changes in scene points under different weather conditions by which the recognition of depth discontinuities in the scene and also computation of scene structure can be provided. As well, a fast algorithm based on this model was proposed by Narasimhan et al. to restore the contrast of the foggy image [136]. The proposed method was able to handle both gray level and color images and can be extended to restore the contrast of scenes with moving objects.

As mentioned above, these image restoration algorithms are only appropriate for surveillance scenes. However, there will be failures in these algorithms when scenes are dynamic, particularly for vehicle cameras, since it is difficult to provide the above two images simultaneously. In addition, the monochrome atmospheric scattering model is only limited to define how scene intensities are influenced by homogeneous weather conditions, hence it is not able to deal with heterogeneous fog or haze.

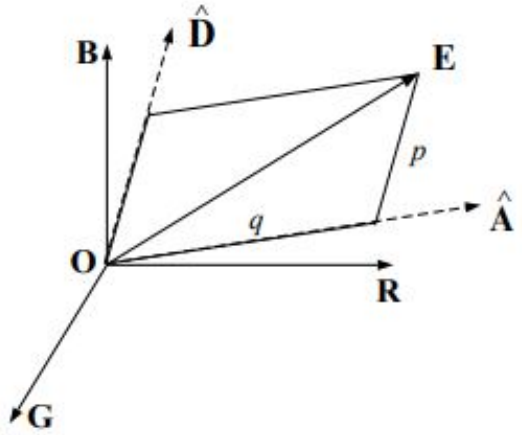

Figure 2.5: Dichromatic atmospheric scattering model in R-G-B color space. A linear combination of direct transmission color, vector $\hat{D}$, and airlight color, vector $\hat{A}$, defines the color of a scene point under foggy condition, vector E [139].

2.2.2 Image Restoration Based on a Single Foggy Image

Single image restoration algorithms have many advantages in comparison with image restoration algorithms using multiple images and they have been attracting much attention in the last few years [176], [89], [93], [111], [60], [77], and [116]. Single image defogging algorithms are able to restore foggy images in arbitrary sizes with different conditions. As mentioned in previous sections, two parameters transmission t and atmospheric light A_∞ are the key factors to restore foggy image by inversely solving the physical model Eq. 2.2. However, this physical model is not a fulfillment equation, thus to obtain these two key parameters some prior science should be used.

- **Restoration Algorithm of Fattal:**

In [63] a refined physical model based on ICA was proposed by Fattal to obtain the transmission and atmospheric light. Based on the assumption that surface shading and transmission are locally uncorrelated, the proposed model estimates these two parameters. The refined physical model was defined in two steps. Firstly, the clear image J was broken into the product of surface albedo coefficients R and shading factor l ($J = Rl$). Then R was broken into two components. One component was parallel to the atmospheric light A_∞ and the other was a residual component $\acute{R}$. Finally, To compute transmission t the independent component analysis (ICA) algorithm [96] and to infer the color of the entire image, a Gauss-Markov random field model [151] was used. To estimate atmospheric light A_∞ by the ICA algorithm, the surface shading and transmission in a small square are assumed to be independent, and the shading direction can be estimated by ICA. In Fetal restoration method, the defogged image is obtained by estimating parameters statistically. There will be some failures in this method when the image is heavily foggy and signal-to-noise ratio is not adequate. In addition, the method is not able to handle gray scale images because it is based on the color statistic [91].

- **Restoration Algorithm of Tan et al. :**

An automated restoration algorithm based on a single image was proposed by Tan et al. [173]. In the proposed algorithm two observations were considered. First, a haze-free image must have a higher contrast ratio in comparison with input hazy image. As a result, fog and haze can be removed by maximizing the local contrast of the restored image. The second observation considered that in a small local area, the airlight is changed smoothly. Then, Tan et al. used the Markov random field following the white balance operation to further normalize the results. Based on this model, the maximum local contrast in the restored image can be considered as the airlight. The image details and structure can be maximized after restoration by this method and user interaction is not required. However, there will be distortion and color saturation in the restored image because this method disconnects from the physical model and does not take into account color restoration. In addition, the results show halo artifacts in the area of the local depth discontinuity.

- **Restoration Algorithm of He et al. and Their Improved Algorithm:**

To overcome the mentioned drawbacks in previous sections, a simple but efficient image prior which is called dark channel prior was introduced by He et al [89] to remove fog from a single foggy image. The proposed method has proven to be effective to restore outdoor foggy or hazy images. This method is based on the key observation, in most regions of a clear image except sky region that there are pixels with low intensity values at least in one channel of RGB color channel Eq. 2.12. In dark channel equation size of square window which is centered at pixel x is denoted by Ω and the color channels are specified by r,g,b.

$$J^{dark}(x) = \min_{c\in r,g,b}\{\min_{y\in\Omega(x)}(J^c(y))\} \tag{2.12}$$

The value of dark channel J^{dark} is approximately zero ($J^{dark} \approx 0$) for a clear or defogged image except for the sky region. In foggy image, dark channel intensity values are mainly composed of airlight. In regard to that observation, He et al. [89] estimated the transmission to restore image with respect to the proposed dark channel prior (DCP) theory by taking the following min operation locally on Eq. 2.2. Therefore, transmission map in this method is estimated directly by applying dark channel.

$$\min_{c\in r,g,b}\{\min_{y\in\Omega(x)}\frac{J^c(y)}{A^c_\infty}\} = t(x)\min_{c\in r,g,b}\{\min_{y\in\Omega(x)}\frac{J^c(y)}{A^c_\infty}\} + (1-t(x)) \tag{2.13}$$

Thus from Eq. 2.12 and Eq. 2.13, unrefined transmission ($\tilde{t}$) can be written as follows:

$$\tilde{t}(x) = 1 - \min_{c\in r,g,b}\{\min_{y\in\Omega(x)}\frac{J^c(y)}{A^c_\infty}\} \tag{2.14}$$

There will be some artifacts in the dark channel image which can be seen as halo. The presence of these artifacts are resulted from taking the min filtering locally on dark channel image. This also leads to the presence of block artifacts in the restored image. Therefore, a soft matting operation was used in the original dark channel prior restoration algorithm to solve the block artifacts and refine the transmission. To compute the value of atmospheric light A_∞ in this algorithm, DCP theory was applied. Therefore, atmospheric light A_∞ was estimated firstly, by selecting a region in the dark channel image which have pixels that are of the top 0.1% brightest, and then by selecting the pixel with the highest intensity in the original foggy image. Eventually, restored image J was resulted by

$$J = \frac{I(x) - A_\infty}{max(t(x), t_0)} + A_\infty \tag{2.15}$$

where t is the transmission $\tilde{t}$ after refining by using soft matting, and t_0 is a small constant to restrict the refined transmission. The scene luminance is not as bright as the atmospheric light, thus the value of t_0 can be considered to be 0.1. [89]. In order to prove the efficiency of dark channel prior algorithm to remove fog from a single outdoor image, Gibson et al. provided a mathematical explanation [71]. This method has better performance for

foggy images with more various color information, such that images with these features will be restored very well. However, there will be some failures when the large part of the image is sky or white area. The DCP theory also cannot deal with images with heavy and heterogeneous fog. Furthermore, the optimization of transmission by the soft matting algorithm takes up a great deal of time and cannot be employed for real-time applications. Also, there will be halo artifacts in the restored image by undefined transmission which is a result of performing min filtering locally. Therefore, as mentioned, the original DCP defogging algorithm suffers from three outstanding problems: 1) generation of halo effects, 2) inadequate transmission map estimation and 3) high time consuming. In order to solve the mentioned problems, Zhang et al. represented a novel fast method to compute the refined transmission map by using guided filter [205]. Firstly, they decreased the processing time of guided filter and zoomed out on the input images of this filter in order to estimate the transmission map and guidance image by using nearest neighbor interpolation down-sampling. Then the refined transmission map is obtained by applying bilinear interpolation up-sampling on the resultant image from guided filter. In order to estimate the refined transmission, first, the nearest neighbor interpolation down-sampling is performed on gray level input (J^{gray}) image and the obtained transmission map to obtain two parameters the guidance image J^{gs} and $\tilde{t}^s$.

$$J^{gs} = nearest(J^{gray}, down) \tag{2.16}$$

$$\tilde{t}^s(x) = nearest(\tilde{t}(x), down) \tag{2.17}$$

In order to refine $\tilde{t}^s(x)$, guided filter is applied to add a guidance image to smoothed image.

$$t^s(x) = \sum_y W(x,y)(J^{gs})\tilde{t}^s(y) \tag{2.18}$$

$$W(x,y)(J^{gs}) = \frac{1}{|\omega|^2} \sum_{k:\,(x,y)\in\omega_k} \left(1 + \frac{(J^{gs}(x) - \mu_k)(J^{gs}(y) - \mu_k)}{\sigma_k^2 + \varepsilon}\right) \tag{2.19}$$

where ω_k and $|\omega|$ are a window centered at pixel k and the number of pixels in this window, respectively. The mean and variance of pixels in the window are showed respectively by μ_k and σ_k^2. ε is set to 0.001. Eventually, the refined transmission map is obtained by performing bilinear interpolation up-sampling on $t^s(x)$ as follow:

$$t_r(x) = bilinear(t^s(x), up) \tag{2.20}$$

Huang et al. proposed a novel DCP-based visibility restoration approach which utilizes a combination of three main modules: 1) a depth estimation module 2) a color analysis module and 3) a visibility restoration module [93]. In other words, the proposed method

combines the applying of the median filter operation, the adaptive gamma correction technique, the gray world assumption, and the dark channel prior method [93] to restore foggy image. This method is also able to handle images with sandstorms. Thus Huang et al. computed the refined transmission $t_r(x)$ by preserving the edge information as follows:

$$t_r(x) = \tilde{t}(x) - D(x) \tag{2.21}$$

where $D(x)$ is the detailed edge information obtained by median filter and $\tilde{t}$ is the transmission. In order to solve the difficulties to restore sky and white regions based on the dark channel prior technique, Zhang et al. employed the tolerance mechanism [204]. Including the tolerance mechanism gets rid of color distortion completely in the bright areas of the image. Their proposed algorithm also can be applied in real-time image defogging applications by decreasing the resolution of transmission map wisely. Xie et al. represented a technique to estimate the transmission which was based on multiscale Retinex algorithm. This proposed method was able to increase the efficiency of original DCP theory [191]. In order to avoid halo effects in the restored image, the transmission was refined by median filter in [73], [70]. Also the proposed method by Gibson et al. was a fast method because of its use of a single median filter operation [73]. Moreover, this work analytically showed that performing the defogging algorithm before JPEG compression had fewer blocking artifacts in the resulting image and that performing the defogging algorithm after JPEG compression leads to lower signal-to-noise ratio [73], [70]. However, the edge information may be lost by applying the median filter. To overcome the above drawback, some edge-preserving smoothing filters with better performance were studied to replace the soft matting algorithm. For instance, Park et al. proposed a method to improve the contrast, color and detail for the entire image domain effectively by applying the Weighted Least Square (WLS) based edge-preserving smoothing method [145]. Gibson et al. proposed a fast method to estimate noise parameters for the filter by using locally adaptive Wiener filter [72]. A fast scheme was introduced by Yu et al. to derive the atmospheric veil of an outdoor foggy image based on a fast bilateral filtering method which leads to the defogged image with high contrast. The proposed edge-preserving smoothing filter is also able to preserve edges with large depth jumps [200]. Joint bilateral filtering was represented by Xiao et al. to obtain a new atmosphere veil in which plenty of texture information is removed but the edge information is preserved [190]. He et al. presented a guided image filtering method as an edge-preserving smoothing operator which had a better performance. The proposed guided filter is faster than bilateral filtering and joint bilateral filtering. Furthermore, the filtering size did not have effects on computational procedure [90]. Following the introduction of guided image filtering, many algorithms were improved based on this technique. For instance, Pei et al. in [150] introduced a defogging algorithm based on DCP theory to restore night-time foggy image by using guided image filtering. Because near-infrared (NIR) light is scattered less than visible light caused by the long wavelengths of near-infrared, Chen in [65] proposed a restoration algorithm to improve the performance of the detail recovering and the color distribution. Chen improved DCP restoration algorithm by using a pair of color and NIR images, in which the airlight color and transfers details from near-infrared can be estimated. Lin and Wang in [120] utilized an edge-preserving filter as opposed to soft matting algorithm in image

restoration algorithm to improve the efficiency of defogging algorithm which is resulted by preserving the edge information. Therefore, they applied the down-sampling algorithm to resize the transmission, and then the resulted transmission is optimized by using guided image filtering. In order to refine the transmission, an inherent boundary limitation on the transmission and the weighted L_1-norm based contextual regularization were considered in [125]. Thus, by applying the mentioned process, Meng et al. could improved DCP defogging algorithm. In this proposed algorithm, the boundary of restored image is limited as $C_0 \leq J(x) \leq C_1$ that C_0 and C_1 are two mentioned boundaries. Thus the unrefined transmission map can be written as follows:

$$\tilde{t}(x) = \max_{y \in \omega(x)} \left\{ min \left[\max_{c \in r,g,b} \left(\frac{A^c - I^c(y)}{A^c - C_0^c}, \frac{A^c - I^c(y)}{A^c - C_1^c} \right), 1 \right] \right\} \tag{2.22}$$

where A is the atmospheric light, which is estimated as the highest value of intensity in each channel after taking minimum and maximum filtering. Transmission function was refined with the weighted L_1-norm based contextual regularization. So Meng et al. [125] defined the optimized transmission map by Eq. 2.23.

$$\frac{\lambda}{2} \left\| t - \tilde{t} \right\|_2^2 + \sum_{j \in \omega} \left\| W_j \circ (D_j \otimes t) \right\|_1 \tag{2.23}$$

The regularization parameter λ is applied to keep balance in the two terms of the above function. W and D are a weighting matrix and a first-order differential operator, respectively. Element-wise multiplication and convolution operators are demonstrated by $\circ$ and $\otimes$, respectively. To obtain refined transmission t the above objective function should be minimized. The restored foggy image resulted from this optimized transmission has a high efficiency, yet time-consuming is high in refined transmission due to iteration computation. The number of iterations and the two boundary restrictions cannot adaptively modify [125]. The restored outdoor images which are achieved by DCP defogging algorithm have good efficiency, however there will be failure in the resulted image for foggy images with some light areas. Moreover, computing the dark channel leads to inability to preserve the edge information due to applying erosion filter. In addition, the optimization of the transmission and soft matting algorithm can consume large amounts of memory and time. Therefore, this method cannot be suitable for real-time applications.

- **Restoration Algorithm of Tarel et al. :**

Hautiere and Tarel et al. proposed an algorithm which is able to detect the presence of daytime fog by estimating the meteorological visibility distance [88]. The proposed algorithm is directly related to the β in Eq. 2.1. In order to extract the image contours, the Canny-Deriche filter was used first in order to highlight the edges of roadways. Then the road surface was obtained by the region growing algorithm. This algorithm, which is also known as the inflection point algorithm, is mainly based on three conditions: fog is supposed to be homogeneous, the road surface should be the main part the image which is assumed to be planar and a homogeneous surface [88], [115]. Finally, Hautiere and Tarel et

al. obtained the visibility distance of the image by using a horizontal line. Thus, knowing the approximate camera calibration by taking into account the road, a visible distance d with each line y of the image is:

$$d = \frac{\lambda}{y - y_h} \text{if } y > y_h \tag{2.24}$$

where y_h is the vertical position of the horizontal line in the image and parameter λ depends on the camera. Thus, the restored image can be achieved by using transmission d to inversely solve the physical model of Eq. 2.2. Concidering that meteorological visibility distance of an image is widely used in vehicle visual system to detect foggy image [83], the proposed algorithm can be applied in-vehicles applications. However, only the road portion of the image is restored correctly. This means that the region above the horizontal line is usually foggy and invisible. In order to solve this issue, Hautiere and Tarel et al. proposed a solution based on contrast restoration approach [175]. The proposed method is able to restore not only the road part of the image, but also the vertical objects. In this method, once again, the road was assumed to be planar with a clipping plane. As mentioned previously, the intensity of vertical objects after restoration is zero and will be seen as black pixels in the restored image. In this proposed method, the set of all these black pixels were supposed to segment the image in two regions, one inside the road surface in three-dimensional and the other outside of the road surface Figure. 2.6, [85]. Therefore, based on this segmentation, each pixel that belongs to the road part of the scene will be restored correctly by using Eq. 2.24 and each pixel outside of the road plane (red regions Figure. 2.6) will be restored correctly by using geometric model Eq. 2.25 [86].

$$d_c(x, y) = \begin{cases} \frac{\lambda}{y - y_h} & \text{if } y > c \\ \frac{\lambda}{c - y_h} & \text{if } y \leq c \end{cases} \tag{2.25}$$

Considering that the derivation of depth map form a single image and soft matting algorithm is complicated. Therefore, Tarel et al. [176] proposed a fast visibility restoration algorithm by using median filtering as opposed to the soft matting algorithm. The main advantages of the proposed algorithm, which is named NBPC, are its speed, due to having a linear complexity of the number of image pixels only, and its ability to process both color or gray level images. In this algorithm, after performing the white balance algorithm, the atmospheric light value A_∞ can be set to $(1, 1, 1)$. To estimate the atmospheric veil $V(x)$, the dark channel prior theory was only used, because taking minimum filtering operator leads to the presence of artifacts in the restored image. In the proposed algorithm by Tarel et al., the atmospheric veil $V(x)$ was assumed to be less than the minimal component of the original foggy image $W(x)$. In order to obtain the maximum atmospheric veil V, they smoothed the most regions of the image except along the edges. Thus, they introduced an original filter named Median of Median Along Lines to preserve edges, as well as corners, which leads to improved efficiency of the restored image.

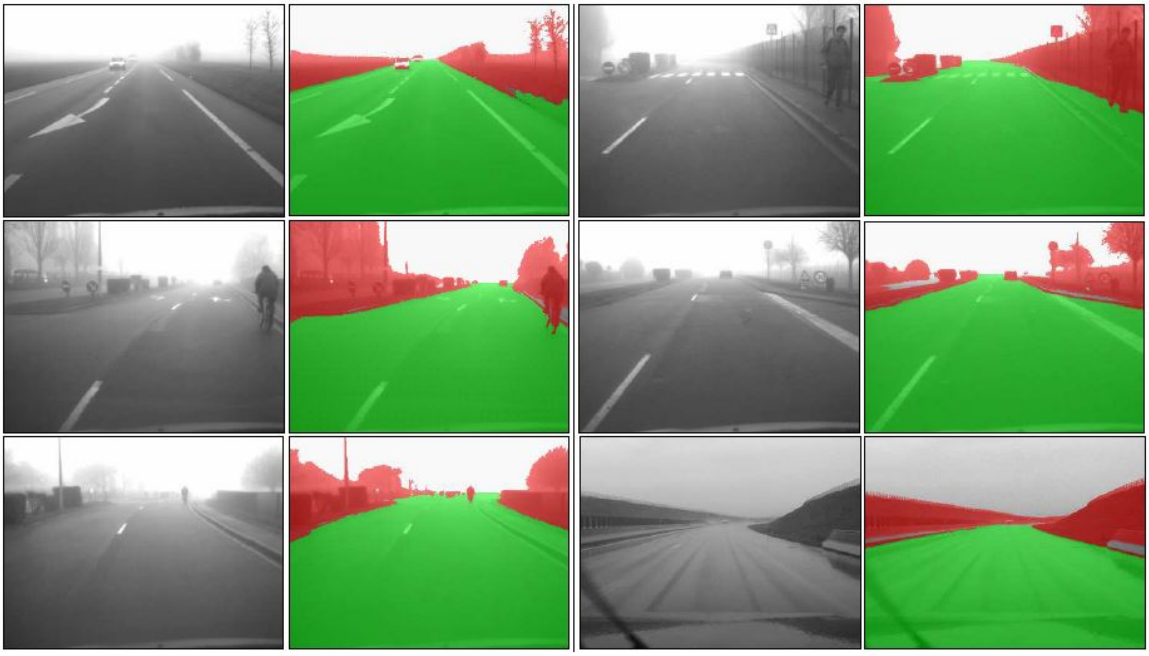

Figure 2.6: First and third columns are original foggy images. Second and fourth columns are the results of vertical objects segmentation and road plain area which can be seen as red and green colors, respectively [85].

$$
\begin{aligned}
& & V(x) &= max(min(pB(x), W(x)), 0) \\
& with & B(x) &= C(x) - \underset{y\in\Omega(x)}{\text{median}}\ (|W - C|)(y) \\
& and & C(x) &= \underset{y\in\Omega(x)}{\text{median}}\ (W)(y)
\end{aligned}
$$

where $W(x)$ is the minimal component of the original foggy image $I(x)$, $W(x) = \min\limits_{c\in r,g,b}\ (I^c(x))$ and p is the restoration degree which usually set in the range of [0.9,0.95], for example, when $p = 0.95$ it means that 95% of the fog will be removed, and Ω gives the median filter diameter.

The proposed algorithm by Tarel et al. will restore the image by Eq. 2.2. after obtaining the atmospheric veil $V(x)$. In order to apply NBPC algorithm for vehicle applications, Hautiere and Tarel et al. considered a constraint based on planar assumption which is able to restore road images [175]. NBPC and DCP restoration algorithms have difficulty restoring images with presence of a large uniform gray region, such as a road surface [177]. In fact, the atmospheric veil is over-estimated in the bottom part of the image which leads to the over-restoration of the road part of the restored image. To avoid over-estimation in the bottom part of the image, Hautiere and Tarel et al. considered an extra constraint for NBPC during the derivation of the atmospheric veil $V(x)$ by taking into account that a large part of the image can be assumed to be a planar road. Because of this constraint, they decreased the distance between the camera and the road. Therefore, the atmospheric

veil was defined by assuming that the minimum meteorological visibility distance is sixty meters and the road is a plane up to a specific distance and that, with respect to the road, the camera calibration is known [175], [88], and [115].

- **Bayesian Defogging:**

Kratz and Nishino proposed a probabilistic defogging method from a single image to restore color of foggy images correctly [111], [140]. In their algorithm, the image was modeled with a factorial Markov random field in which the scene albedo p and depth d are two statistically independent components. Thus first factorized the image into the scene albedo and depth as

$$\ln(1 - \frac{I(x)}{I_\infty}) = \ln(p(x) - 1) - \beta d(x) \tag{2.26}$$

the above equation demonstrates the factorized image into the scene albedo and depth, where $\ln(1-\frac{I(x)}{I_\infty})$ was assigned to parameter $\tilde{I}(x)$, the scene albedo $\ln(p(x)-1)$ was assigned to $C(x)$, and depth $-\beta d(x)$ was assigned to parameter $D(x)$. Then the dependence between two parameters $C(x)$ and $D(x)$,and the input image $I(x)$ was modeled by applying a Factorial Markov Random Field (FMRF) as follow:

$$p(C, D|\tilde{I}) \propto p(\tilde{I}|C, D)p(C)p(D) \tag{2.27}$$

By maximizing Eq. 2.27 two parameters scene albedo and depth were obtained. Thus by inversely solving the Eg. 2.2 the restored image was resulted. Another depth map based on Bayesian theory and Markov regularization was proposed by Wang et al [184]. The proposed depth map was obtained by Multiscale Depth Fusion (MDF). Firstly, each prior depth map p_i is the correct depth map t which is effected by noise ϵ_i

$$p_i(x) = H_i(x)t(x) + \epsilon_i(x), i = 1, ..., m, \tag{2.28}$$

where H_i is the degree of the pure depth map to the prior map. The noise was performed by the Gaussian function. Therefore, by maximizing Eq. 2.28 the correct depth map t was written as

$$t = arg \quad max P(D|_{p1,...,pm}) \tag{2.29}$$

where $P(D)$ was obtained by the Gibbs distribution and for an energy function Eq. 2.29 was defined as

$$t = arg \quad \max_i E(t) \tag{2.30}$$

where $E(t) = U(t) + \sum_i \sigma^{-2}(p_i - t)^T(p_i - t)$. The first term $(U(t))$ is the edge preserving smoothing imitations, and the second term is dedicated to noise part. Finally, the correct depth map and restored image can be obtained after computing the energy function

iteratively. The amount of halo artifacts will be decreased in the restored image by using this proposed algorithm , while the iteration takes time, and the parameters need to be set manually [193] and [10].

- **Learning-based Restoration Algorithm:**

In order to recognize the best feature combination for image defogging, different features of fog were investigated in a learning-based framework by Tang et al. [174]. The dark channel is one of the most informative features in this process. Therefore, in order to obtain the relation between the fog features and their refined transmission of image patches, the Random Forest was used to achieve a regression model. To obtain the transmission of the unknown foggy image, first, the different features related to the fog must be obtained after dividing the image into small patches, and then the transmission of each patch is extracted by using the learned Random Forest model. Eventually, the addition of obtained transmissions from each image patch provides the unrefined transmission. In this proposed algorithm, the optimization of transmission is performed by utilizing the guided image filtering. The learning framework is able to restore images with homogeneous and heterogeneous fog, and adaptive regression models can be obtained under different weather conditions. However, to learn the regression model, many fog-free and foggy image pairs are required for training data although providing a large number of training data is difficult. The accurate depth information cannot be obtained in this method, particularly along the edges. In addition, the regression model does not provide an accurate, unrefined transmission of the image. This model cannot reveal the true depth information of the image, especially for edge areas.

2.3 Image Defogging Based on Image Contrast Enhancement

Image contrast enhancement algorithms increase the contrast of the image and are frequently applied in image defogging area.

2.3.1 Image Defogging Based on the Retinex Theory

Color constancy is a main feature of computer vision. In order to consider this component in image defogging, Edwin Land proposed the Retinex theory [114]. The proposed algorithms based on Retinex theory estimate the reflectances of each pixel by receiving the value of each pixel of the input image in three color channels. This theory has been widely used in image defogging, dark image enhancement, and Mars Express image enhancement areas [99], [211], [157], and [158].

In the Retinex theory, an image is supposed to be composed of two components: incident and reflection Figure 2.7. The luminance information which is also called luminance image

is indicated by incident component. The internal information of an image, which is also called the reflection image, is represented by the reflection.

For the original foggy image S, the Retinex theory with two components reflection R and incident L can be written as follows:

$$S(x, y) = L(x, y).R(x, y) \tag{2.31}$$

where (x, y) are the pixel coordination of the image.

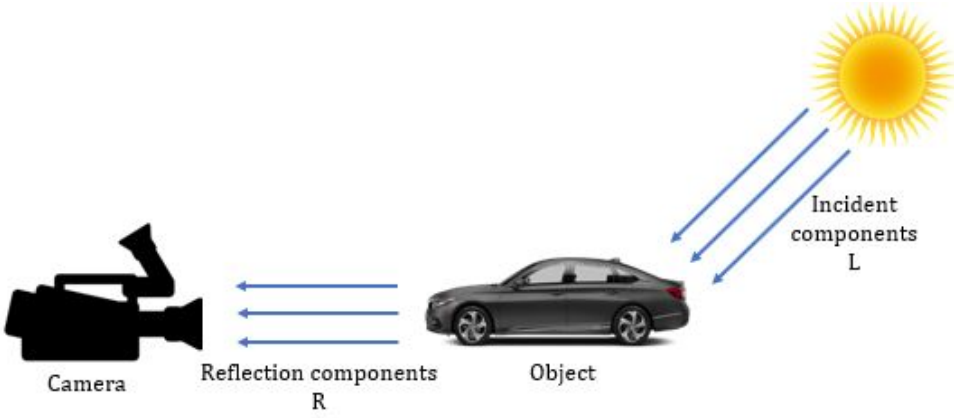

Figure 2.7: Retinex model.

In defogging algorithms based on Retinex theory, by solving the Retinex model the reflection image is obtained. Thus by applying the logarithm both sides of Eq. 2.31, the reflection component R from original foggy image S is defined as

$$\log S(x, y) = \log L(x, y) + \log R(x, y) \tag{2.32}$$

R can be resulted from Eq. 2.32 after obtaining L. Thus to estimate the incident component, Edwin Land proposed the random path-based algorithm [113]. The passion equation-based iteration algorithm was used to estimate this component. Also, the multiple-scale algorithm based on the Difference-of-Gaussian (DOG) operator was another proposed approach to obtain the incident component. The summary of all proposed methods to compute the incident component can be found in [94]. Based on the multi-resolution pyramid, two Retinex algorithms were proposed by McCann et al.: 1) the McCann Retinex algorithm and 2) the Frankle-McCann Retinex algorithm [123], [67]. Retinex algorithm is also able to realize the dynamic range compression, color constancy, and lightness in image enhancement algorithms at the same time [101]. In order to solve the complexity and unsatisfactory resulted color constancy of proposed estimation algorithms, the Gaussian function was recommended to be utilized by Jobson et al. to estimate the incident component [101], [103]. In the original Single Scale Retinex (SSR) algorithm, the incident component is resulted from the convolution of Gaussian function $G(x, y)$ and original foggy image $S(x, y)$. Thus for $G(x, y) = k. \exp(-\frac{x^2+y^2}{\sigma^2})$, where σ and k are the scale controlling

of the Gaussian function and a unit normalization respectively, the incident component is computed by

$$L(x,y) = S(x,y) * G(x,y) \tag{2.33}$$

where $*$ is the convolution operation. By applying values of $L(x,y)$, which is obtained from Eq. 2.33, in Eq. 2.32, the reflection component for a RGB image is resulted:

$$r_{i\in r,g,b}(x,y) = \log(S_{i\in r,g,b}(x,y)) - \log(S_{i\in r,g,b}(x,y) * G(x,y)) \tag{2.34}$$

where i is one of the RGB channels, and $r(x,y) = \log R(x,y)$. The value of parameter σ in the SSR algorithm, defines the performance of image enhancement. The large value of σ leads to the high preservation of color/lightness rendition in the enhanced image. However, the large value of σ is not able to restore the details of enhanced image properly. Although the small value of σ cannot preserve the color/lightness rendition in the resulted image, the details will be restored very well. This means that dynamic range compression and color/lightness rendition cannot be performed at the same time in this algorithm.

In order to solve the above problem, two algorithms, the Multiscale Retinex (MSR) and the Multiscale Retinex with Color Restoration (MSRCR) were represented [99], [156], [101], [155], and [100]. The MSR algorithm, compared with the SSR algorithm consists of three scales representing narrow, medium, and wide surroundings in each channel that are adequate to provide both dynamic range compression and tonal rendition: $\sigma_1 = 15$,$\sigma_2 = 80$,$\sigma_3 = 250$ and the three weights are all equal to 1/3 ($\omega_j = 1/3$) [100]. The MSR output is the weighted sum of the outputs of three SSR algorithms at different scales and is achieved as

$$r_i(x,y) = \sum_{j=1}^{3} \omega_j \Big[\log S_i(x,y) - \log(S_i(x,y) * G_j(x,y)) \Big] \tag{2.35}$$

where ω_i is the weight of each scale associated to normalized Gaussian G. Eventually, the reflection component is transformed into the representation domain [0, 255] by applying a gain/offset algorithm.

As mentioned before, the MSR algorithm has the ability to perform the small scale dynamic range compression, details preservation of image edges and big scale color balance. However, the MSR algorithm is not able to restore color properly. In regards to this issue, the MSRCR algorithm is proposed in which a color restoration C_i function is used to control the saturation as

$$r_i(x,y) = C_i(x,y) \sum_{j=1}^{3} \omega_j \times \Big[\log S_i(x,y) - \log(S_i(x,y) * G_j(x,y)) \Big] \tag{2.36}$$

The achieved reflection component from Eq. 2.36 is also required to be transformed into the representation domain. Thus, in order to transform the output into the representation domain, a "canonical gain/offset" algorithm was presented by Jobson et al. [100].

Furthermore, a normalization approach was presented by Moore et al. to automatically transform the output of the algorithms based on Retinex [131].

There is a possibility that the restored color in the resulted image will be inverted when using SSR, MSR, and MSRCR algorithms. Therefore, to overcome this problem, Petro et al. proposed a color restoration approach based on the intensity channel [152].

The fog consists of components with the low-frequency in the image. In order to restrain the information with low-frequency, Wang et al. applied the wavelet transform. To obtain the defogging image, they improved the brightness by applying the SSR-based color constancy algorithm which properly enhanced the scene information through a nonlinear transformation [182]. The logarithm function in the Multiscale Retinex algorithm (MSR) was replaced by the nonlinear sigmoid function by Zhao et al. [210]. The Gaussian filter is not able to preserve edges appropriately. As a result, the edges in the resulted image after enhancement by the original SSR, MSR, and MSRCR algorithms will be degraded due to applying Gaussian filtering to compute the incident component. To solve this issue, Hu et al. estimated the incident component by applying the bilateral filter, instead of Gaussian filter, which is able to preserve the edges appropriately. In addition to this, Hu et al. utilized the Gamma adjustment and sigmoid function to better enhance the reflection component [92]. In order to enhance the contrast perfectly for each local area and increase the visibility, a variable filter Retinex algorithm was presented by Yang et al. in which the scale parameters were selected in every local area of the foggy image adaptively [187].

2.3.2 Image Defogging Based on the Traditional Image Contrast Enhancement Method

In order to defog image, some approaches rely on image contrast enhancement, such as the intensity transforms, homomorphic filtering, high-boost filtering, and wavelet, which are covered briefly in this section.

- **Intensity Transforms:**

There are two parameters, contrast and dynamic range, which are low in hazy and foggy images. This is caused by the large values of color or gray pixels in the images, leading to the histogram of these images to be centrally distributed. Redistributing the histogram of foggy images is effective to enhance these images. Therefore, intensity transforms were proposed as a solution to enhance the images [74]. In order to enhance night, X-ray, and defog images, some contrast enhancement algorithms such as the power-law gamma transformation, piecewise-linear transformation, and Histogram Equalization (HE) are widely applied. To brighten up the resulted image by the MSR algorithm, the power-law gamma transformation and piecewise-linear transformation are applied to each channel of the enhanced image at the end [68]. Not only can the gain/offset step in the algorithms based on Retinex be used to transform the reflection component to the certain domain, but it can also be considered as a specific piecewise-linear transformation. Also, to improve the

visibility of the achieved image by the SSR algorithm, the piecewise-linear transformation was utilized by Ma et al. [211].

Histogram Equalization (HE) algorithm is widely used to enhance the contrast because of its effectiveness and simplicity. The HE method improves the dynamic range of the image by redistributing the image histogram. It can be classified into two categories according to the transformation function used: 1) Global Histogram Equalization (GHE) and 2) Local Histogram Equalization (LHE) [154], [106]. Global histogram equalization is simple and fast; it can only enhance the global contrast of a foggy image, not the local contrast; and in total, its contrast-enhancement performance is relatively low. Images with a heterogeneous fog cannot be enhanced very well by the GHE algorithm. In addition, there will be some artifacts in the enhanced image by the GHE algorithm, particularly where the depth is discontinuous. Contrarily, power is relatively high for local histogram equalization; however, it requires a complex computation since the sub-blocks are overlapped completely [106]. In order to decrease the presence of artifacts and noise in the achieved image by the GHE algorithm, the wavelet transform was used after enhancing the foggy image by Jun and Rong [104].

Local histogram equalization method (LHE) is a popular enhancement algorithm to increase the information of image locally, so different LHE algorithms and some methods to tackle its problems have been presented [106], [107], and [108]. In order to avoid overlapping sub-block histogram-equalization function and obtain a sub-region probability density function, a low-pass filter-type mask was applied by Kim which leads to an enhanced image with high contrast associated with local histogram equalization [106]. The proposed Partially Overlapped Sub-block Histogram Equalization (POSHE) derived from local histogram equalization, gives an enhanced image which is much faster and more efficient compared with local histogram equalization. Also, there are no blocking effects in the resulted image by the POSHE algorithm. In order to preserve the brightness and enhance the contrast of the foggy image with high accuracy, Kim et al. proposed a Recursively Separated and Weighted Histogram Equalization (RSWHE) [107]. In this method, the input histogram is segmented into two or more sub-histograms recursively, then these sub-histograms are modified by means of a weighting process based on a normalized power law function, and to perform histogram equalization on the weighted sub-histograms independently [107]. Patel et al. in [146] evaluated various local histogram equalization algorithms in terms of their performance to preserve brightness and enhance contrast. To enhance the degraded video sequences under foggy condition, Ramya et al. presented a method by using a Brightness Preserving Dynamic Fuzzy Histogram Equalization (BPDFHE) [159]. BPDFHE algorithm not only enhances visibility, it also maintains the color fidelity. To avoid amplifying noise or unwelcome structures by the histogram equalization (HE) algorithm, Contrast-Limited Adaptive Histogram Equalization (CLAHE) was proposed in [213] to enhance the contrast of the foggy image. CLAHE operates on 8×8 regions called tile in the image and then the contrast of each tile is enhanced, so that the histogram of the obtained region approximately matches a flat histogram. In this algorithm to remove artificially resulted boundaries, bilinear interpolation is used to combine neighboring tiles [213]. Xu et al. presented a method based on Contrast Limited Adaptive Histogram Equalization(CLAHE) to reduce the noise while enhancing the contrast [194]. In the first

step, they obtained the background image from the video sequence. And then foreground images were achieved by estimating and bounding the moving pixels. In the second step, CLAHE algorithm was applied to defog the foreground and background images. Combining the foreground and background images to generate new frames was considered as the third step. Eventually, the defogged video sequence was resulted [194].

As mentioned in the above paragraph, histogram equalization enhances the image contrast by stretching the histogram, which leads to an unrealistic resulted image. For images with remarkable depth changes or under heterogeneous fog, there will be some failures in the achieved image by this technique. The color structure will be changed in the enhanced image, if the HE algorithm is performed directly on each channel, which means a color distortion can be considered as a weakness of the HE algorithm. In order to decrease the color distortion, the HE algorithm can only be applied to the intensity channel but it leads to color degradation in the enhanced image which is caused by the effects of the intensity on all channels of foggy image. On the other hand, algorithms based on HE have better performance to enhance visibility for foggy images with heavy fog in comparison with algorithms based on the Retinex and physical model.

- **Homomorphic Filtering:**

In the frequency domain, the edge of the image has the high-frequency components, since in this area the intensity dramatically is changed. The flat area of an image has the low-frequency components such as the sky area. In the physical model, the airlight component can be considered as a component with low-frequency. The presence of fog in the image will decrease the edge information. In other words, in images under foggy condition, fog will decrease the high-frequency components while it increases the low-frequency components. Therefore, the visibility of foggy image can be enhanced by improving the high-frequency components and reducing the low-frequency components of an image. To enhance the image, the homomorphic filtering has been applied in some methods. The homomorphic filtering can decrease low frequencies and increase high frequencies by using high-pass filtering. A method based on a homomorphic processing and a novel Ratio rule learning algorithm was proposed in [169] to improve the dynamic range and carry out the natural color rendition process, simultaneously. The proposed method is almost like Retinex theory, however the incident component is not required to be estimated. This algorithm is simple and fast, but it is not able to enhance images with heavy or heterogeneous fog.

- **High-boost Filtering:**

In order to enhance foggy images, the high-boost filtering can also be used as it is able to improve high frequency component while still preserving the low frequency components [74]. Due to the similarity of high-boost filtering and Retinex theory in some ways, the reflection image of the Retinex-based algorithm can be considered as the mask image of high-boost filtering. Merging the obtained mask image and original image by high-boost filtering can enhance the high frequency component which leads to visibility enhancement

due to improving the edge information of the image. This algorithm is efficient in terms of time consumption and computational cost. However, the enhanced image by this algorithm suffers from color distortion and noise amplification.

- **Wavelet Transform:**

The wavelet transform is similar to homomorphic filtering in terms of amplifying the high frequency component and suppressing the low frequency component. The wavelet transform can be used to enhance image by preserving the edge of the image while reducing the noise of the image [192], [53]. To obtain the measure of visibility distance for a traffic control system, Busch et al. presented a fog visibility analysis method based on a B-spline wavelet transform with improved signal-analysis techniques. The proposed wavelet-based approach can inform the driver of the presence of fog in real time [44]. To ascertain the degradation factors of foggy image, after transferring the original image into YUV color space, the wavelet transform was used by Jia and Yue to decompose the luminance component into low frequency and high frequency of the YUV space. In the low frequency sub-bands, the airlight model was first estimated and then removed by applying Gaussian filtering, then the image information in the high frequency sub-bands were improved by using high-pass filter. Eventually, by the inverse wavelet transform, the enhanced image was achieved [98]. Toward this objective, Rong et al. in [163] first applied unsharp masking algorithm for the low frequency domain to enhance image contrast. Then to improve the details and contrast, a high pass filter was used for high frequency domain. Finally, via informing the inverse wavelet transform the primary defogging image was reconstructed, at this time the Retinex-based algorithm and color restoration algorithm were applied to rectify the color degradation of the processed image. While the enhanced imaged via wavelet-based algorithm with minimal effects of artifact or noise, this algorithm is not able to enhance visibility for images with dense or heterogeneous fog. This problem is caused by applying the simple filter, which does not consider scene information as it cannot estimate the fog component and edge information. An image defogging algorithm with combination of the wavelet transformation and physical model based on dark channel prior was proposed by Yang et al. [197]. In this proposed algorithm, Haar wavelet transform was used to obtain the low-frequency component of foggy image, and then guided image filtering was applied instead of soft matting algorithm to optimize the transmission map. The proposed algorithm can be used in real time application.

2.4 Image Defogging Based on the Fusion Strategy

In near-infrared (NIR) image, the phenomenon, atmospheric haze or scattering, is almost absent. Therefore, under foggy or hazy condition, NIR image in comparison with visible light (VL) image has more detailed information and higher contrast. Considering this fact, in order to collect information from an environment for applications, such as surveillance systems, security, face recognition, target detection, target tracking, and recognition visible

and infrared technology have typically been utilized via fusion algorithms of the near-infrared and visible light images [122], [212], and [206]. Schaul et al. proposed an algorithm to increase the contrast of fog-degraded color images in which the fog or airlight detection or depth maps information were not required [166]. Their algorithm proposed that fusing a visible light (VL) image and a near-infrared (NIR) image of the same scene can obtain the high contrast enhanced image with minimum halo artifacts through a multiresolution approach by applying edge-preserving filtering. Recently, NIR image defogging and VL image defogging have been attracting more attention in defogging, detection, tracking, and recognition research directions.

Ancuti et al. represented a defogging algorithm from a single image by fusion of several images obtained from the initial foggy image [6]. In this fusion-based algorithm, firstly foggy regions in a foggy image is detected in a pixel-wise manner automatically. It has been observed that on the dark channel, patches indicating sky and hazy areas have high values and these values change smoothly, except at depth discontinuities. Based on these assumptions, a semi-inversed image $L_{si}(x) = [L^r_{si}, L^g_{si}, L^b_{si}]$ was created to detect fog. Finally, foggy regions were estimated by computing the difference between the hue channels of the original image I and L_{si}. This image was obtained as follows:

$$
\begin{aligned}
L^r_{si}(x) &= \max_{x \in I} \left[I^r(x), 1 - I^r(x) \right] \\
L^g_{si}(x) &= \max_{x \in I} \left[I^g(x), 1 - I^g(x) \right] \\
L^b_{si}(x) &= \max_{x \in I} \left[I^b(x), 1 - I^b(x) \right]
\end{aligned}
$$

where $I^r(x)$, $I^g(x)$ and $I^b(x)$ are the RGB channels of the image for pixel x. Then the atmospheric value A_∞ in fog-free areas was estimated. In this proposed algorithm, after a per-pixel recognition of foggy areas, a layer-based method was proposed to preserve a maximum amount of detail. Then several new images L_i with $i \in [1, k]$ are achieved by using

$$
L_i = I - a_i . A_\infty \tag{2.37}
$$

where a_i is a constant value in the range [0, 1] and its value depends on the number of layers, and the number of images used for fusion was indicated by k. Then on each obtained image L_i identification of foggy region is performed and the region with low hue disparity of the corresponding image L_i is considered as the final input image for fusion. Eventually, the defogged image was obtained by a simple weighted fusion of these layers.

Because haze detection is based on the semi-inverse method in this algorithm, it will fail for scenes with the little difference between the original image and the inverse image, such as sea. Therefore, if foggy areas are not detected correctly, the desired restored image will not be resulted.

To tackle the above issue, another single image defogging algorithm based on fusion strategy was introduced by Ancuti et al. that took as inputs two adapted versions of

the original image [8], [7]. In this method, the implementation was computed in a per-pixel. To obtain the accurate defogged images, these two images are weighted by specific maps: luminance, chromaticity, and saliency. The first input image is achieved via the white balance operation of the original foggy image. The obtained image by the white balance leads to the resulted images with natural rendition, by removing chromatic casts. The second input image is achieved by subtracting the average luminance value of the entire image from the original foggy image. By this step they enhanced the contrast of the foggy image. Eventually, to fuse these two input images, the fusion based method was used which applies three weight maps to enhance the visibility. This single image fusion-based strategy was also extended to enhance the contrast of underwater image [9] and [49]. The obtained results by these fusion-based defogging algorithm are similar to the obtained results by physical-based defogging algorithms. Moreover, they are also efficient in terms of time consumption and computational cost [2]. However, these algorithms did not consider the depth information of a foggy image which leads to some failures when the fog is heterogeneous.

Fu et al. also proposed an enhancement method that focuses on single sandstorm image based on the fusion strategy. In this proposed approach, first, a statistical strategy was applied to perform color correction of degraded sandstorm image. Then two input images with different brightness were exploited from the color corrected by gamma correction with different scales for sandstorm image enhancement [66]. Guo et al. presented an improved fusion-based algorithm with different input images for single image to display color corrected and contrast enhanced versions of the original foggy image. To increase the visibility, they applied sharpness weight map, chromaticity weight map and prominence weight map for enhancement of the foggy image [78].

Defogging algorithms based on fusion strategy from a single image are novel and efficient. In this strategy, in order to increase the contrast of the degraded image, the second input image is used which leads to the presence of noise. In regards to this, the first input image is used to decrease the effects of noise and artifacts and also to perform color correction. In other words, color restoration and noise reduction are performed via the fist image, and the visibility enhancement of foggy image is performed via the second image. Fusion-based algorithms are fast and simple; however, if the visibility enhancement is not performed appropriately by the second input image, the desired result will not be obtained [193] . Tables 2.2, 2.3, and 2.4 summarize some main features of the mentioned image defogging algorithms.

	Defogging method	Advantages	Disadvantages
Image restoration	Multiple images obtained by different weathers of the scene	Good color restoration.	1) Hard to acquired the source images. 2) Fail to restore image with dense fog. 3) Fail to restore heterogeneous foggy image.
	Multiple images obtained by the same weather of the scene	1) Natural restored image is obtained for thin foggy image. 2) Good visibility enhancement for thin foggy image.	1) The value of atmospheric light is obtained manually. 2) Hard to acquired the source images with a moving camera.
	Fattal	1) Good visibility enhancement for thin foggy image. 2) Ability to restore image with heterogeneous fog.	1) Fail to restore image with dense fog. 2) Fail to restore image with low signal-to-noise ratio.
	Tan et al.	Obtain a restored image with high contrast.	1) Color distortion and the presence of halo artifacts. 3) The resultant image may be over restored.
	He et al.	Natural restored image with good color restoration is obtained for thin foggy image.	1) Fail to restore image with dense fog. 2) Fail to restore image with large sky or white areas. 3) The presence of halo artifacts and high processing time.
	Tarel et al.	1) Fast 2) Good visibility enhancement for thin foggy image.	1) The presence of halo and artifacts. 2) Color distortion in the restored image. 3) Fail to process the image with discontinuous depth.
Image enhancement	Bayesian defogging	1) Good visibility enhancement. 2) Few halo artifacts in the enhanced image.	1) The parameters need to be set manually. 2) Color distortion and edge degradation. 3) High computational complexity.
	Learning-based	Ability to restore foggy image with dense or heterogeneous fog.	1) Hard to obtain the source images. 2) Fail to estimate the depth information. 3) The lack of a good learning model.
	Retinex-based	Greatly enhance the visibility for foggy image with low intensity, simple and fast.	1) Inefficient color restoration. 2) Fail to enhance heterogeneous foggy image.
	Intensity transforms	Greatly enhance the contrast of the foggy image.	1) Color distortion and edge degradation. 2) Increase halo artifacts and noise .
	Wavelet transform	Greatly prevent the generation of noise.	1) Fail to enhance heterogeneous foggy image. 2) The enhanced image can be too dark or too bright.
Fusion-based	Fusion-based algorithms	Better performance than single image defogging algorithms.	High complexity and low accuracy.

Table 2.1: The comparison of some defogging algorithms.

Defogging method	Fast	simple	Color restoration	Visibility enhancement
Multiple images obtained under different weather conditions of the scene			√	
Multiple images obtained under the same weather of the scene			√	√
Fattal [63]				√
Tan et al. [173]				√
He et al. [89],[90]			√	
Tarel et al. [176]	√			√
Bayesian defogging [184]				√
Learning-based [114]			√	
Retinex-based	√	√	√	
Intensity transforms			√	
Wavelet transform				
Fusion-based algorithms	√		√	
Our proposed algorithm	√	√		√

Table 2.2: A comparison between some main features of image defogging algorithms.

Defogging method	Input foggy image	Halo artifacts	Vehicle applications
Multiple images obtained under different weather conditions of the scene	Multiple color/gray images		
Multiple images obtained under the same weather of the scene	Multiple color images		
Fattal [63]	Single color image		√
Tan et al. [173]	Single color/gray image	√	√
He et al. [89], [90]	Single color image		√
Tarel et al. [176]	Single color/gray image	√	√
Bayesian defogging [184]	Single color image	√	√
Learning-based [114]	Color image		
Retinex-based	Single color/gray image		
Intensity transforms	Single color/gray image	√	
Wavelet transform	Single color/gray image		√
Fusion-based algorithms	Single color/gray image		√
Our proposed algorithm	Single color/gray image		√

Table 2.3: A comparison between some main features of image defogging algorithms.

Chapter 3

Our Proposed Visibility Restoration Algorithm

3.1 Visibility Restoration Algorithm

3.1.1 Fog Modeling

- **Definition**

Fog is an accumulation of visible cloud water droplets or ice crystal very small particles accompanied by hygroscopic, water-saturated fine particles in the air or close to the Earth's surface. Whenever horizontal visibility has been reduced to less than one kilometer, the term fog is applied. The term would be mist properly with respect to the level of visibility reach or surpass this threshold. Visibility in fog can limit from the appearance of haze, to almost zero visibility, rely on the density of the water droplets.

- **Propagation of light through fog**

The presence of fog leads to the propagation of light (with a wavelength placed between 400 and 700 nanometers) within a large number of water droplets [88]. The two phenomena, absorption and diffusion make the headlight's light weak, which leads to specifying fog by defining of an extinction coefficient β which is equal to the sum of the absorption and diffusion coefficients. The absorption phenomenon is not significant in reality which means it can be unconsidered. Therefore, diffusion can be considered as a predominant phenomenon. Daytime fog is the main source of fog illumination, or haze luminance. Dumont has described these effects in [54]. Jaruwatanadilok in [97] has covered the general problem of optical imaging captured in foggy condition. Many people are lost their lives every year all around the word from accidents that caused by fog conditions on the roadways, it also leads to multiple-vehicle collisions.

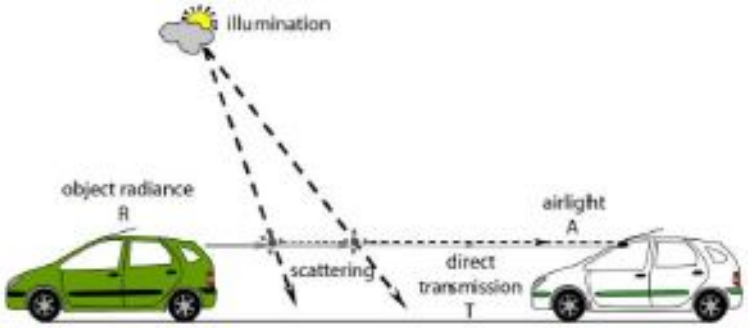

Figure 3.1: Diffusion of light by daytime fog.

- **Koschmieders model**

The model of the effects of the fog is established by Koschmieder in 1924 [126], this theory which is known as Koschmieder's law is a simple relationship between the distance of an object with intrinsic luminance L_0 and its apparent luminance L with respecting to a object placed in distance winds up blending in with the sky, on gray level image Koschmieder's law can be written as follow:

$$L(x,y) = L_0(x,y)e^{-\beta d(x,y)} + L_s(1 - e^{-\beta d(x,y)}) \tag{3.1}$$

where $L(x,y)$ is the observed luminance with the presence of fog and $L_0(x,y)$ is the intrinsic luminance at pixel (x,y), $d(x,y)$ is the distance of the object from the observer and it is also known as the scene depth, L_s is the luminance of the sky and β indicates the scattering coefficient of the atmosphere. This model can be directly applied to a color image as well by extending the same model on each RGB channel, assuming a camera with a linear response. In Eq. 3.1, an exponential decay $e^{-\beta d(x,y)}$ on the intrinsic luminance $L_0(x,y)$ (right-hand term), which is called direct attenuation, leads to contrast reduction of the object and also visibility reduction of the scene [173]. In the second term, which is called airlight, a white atmospheric veil $L_s(1e^{\beta d(x,y)})$ is added, white atmospheric veil will be increased by increasing the distance of the object $d(x,y)$ [110], [173]. Direct attenuation and airlight are considered as the effects of fog on the scene. Regarding to the physics of fog, in order to restore image under foggy conditions the estimation of both the scene luminance without fog and the scene depth-map are required. By assuming the camera response is linear, image intensity I is substituted to luminance L [175], so Eq. 3.1 is rewritten in Eq. 3.2 that by obtaining I_0 the foggy image will be restored.

$$I(x,y) = I_0(x,y)e^{-\beta d(x,y)} + I_s(1 - e^{-\beta d(x,y)}) \tag{3.2}$$

Based on Koschmieder's theory an attenuation law of atmospheric contrasts has been derived as follow:

$$C = C_0 e^{-\beta d(x,y)} \tag{3.3}$$

where C and C_0 indicate the apparent contrast at distance d and the intrinsic contrast of the object against its background respectively. When the atmosphere has uniform illumination this law can be applied. The value of C is equal to the contrast threshold ϵ for the objects can be seen hardly. An average value of $\epsilon = 0.05$ has been assigned to the contrast threshold, practically by the International Commission on Illumination (CIE) [165]. Therefore, a conventional distance which is called the "meteorological visibility distance" d_{met} is defined as the greatest distance that a black object ($C_0 = 1$) can be observed in the sky on the horizon and computed as follow [88]:

$$d_{met} = -\frac{1}{\beta}\ln(0.05) \simeq \frac{3}{\beta} \tag{3.4}$$

As mentioned in the last chapter, there have been different methods to remove fog from foggy images. Some of them can restore image by using multiple images, while some of them restore image by using only a single image. Some algorithms have been introduced as image enhancement algorithms that can be applied to increase the contrast of the image by using retinex-based or traditional image contrast enhancement methods. Fusion-based algorithms have been also introduced as an another technique for defogging and has considered as a complex method.

In this section, a restoration algorithm using only a single image and based on the physical model has been introduced. Using a single image leads to obtaining a real-time and inexpensive algorithm. Regarding to this issue that computing the depth map from a single image is known as a ill-posed problem, we have propssed an efficient technique relies on a local spatial regularization to estimate the transmission map/depth map from a single image without requiring any geometric models of the scene. Being local, makes these algorithms able to cope with homogeneous and heterogeneous fog. The proposed algorithm can thus be seen as the extension of the local visibility enhancement algorithm [176] combined with the restoration method in [183].

3.2 Proposed Fog Removal Approach

Our proposed approach is defined by two main modules: a Depth Estimation (DE) module and a Visibility Restoration (VR) module. First, the proposed DE module estimates an efficient refined transmission procedure that takes advantage of the Recursive Filtering (RF) in the transformed domain to preserve edge information and thereby avoid generation of halo artifacts in the restored image [69]. In addition, using recursive filtering in the transformed domain leads to considerable speedups and memory savings [12]. The VR module restores a high-quality haze-free image by applying the obtained depth information from DE module to remove the presence of the atmospheric particles in original foggy image. In this section, we present a high-quality edge preserving smoothing filter in real time [149]. Before the transmission is estimated, the white balance approach is described, which is considered as a first step to obtain the refined transmission map. Depth estimation (DE) and Visibility Restoration (VR) modules are described in details after covering all required information, respectively.

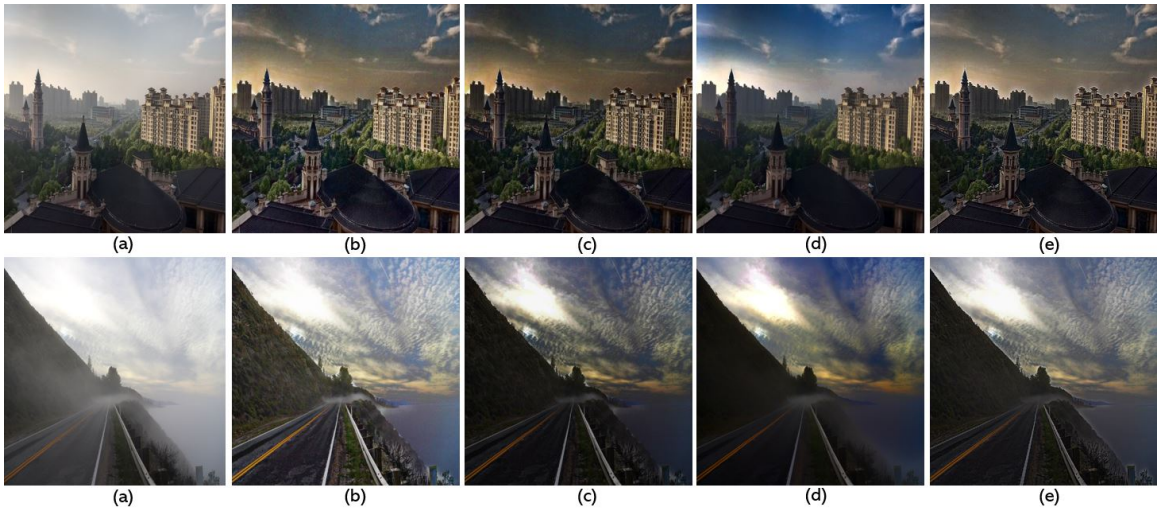

Figure 3.2: From left to right, the original image and the restored images by Tarel and Hautiere [176], Tarel and Hautiere [175], He et al. [89] and our result.

3.2.1 Depth Estimation Module

- **White balance**

In order to restore the visibility of foggy image, performing the white balance is assumed prior. By normalizing the input image $I(x, y)$ between 0 and 1 and performing the white balance accurately, the fog gets white purely so the intensity of the sky I_s can be set to (1, 1, 1). By biasing the average color of the image towards pure white the white balance can be obtained that is resulted from the presence of fog in the image. A local white balance is recommended for images in which light color changes along the image by biasing the average color of the image towards local image averages Figure 3.2.

- **Edge preserving filtering**

In order to achieve a real-time defogging algorithm with high performance that the restored image does not suffer from the presence of block artifacts, an edge preserving filtering of image and video based on a domain transform has been applied in this work to estimate and refine the transmission map. The proposed filter generates high-quality 2D edge-preserving filtering by iterating 1D-filtering operations. The efficiency of this edge preserving filtering is derived from a key assumption that a color image, which has 2D space, can be manifolded in a 5D space, so an edge preserving filter can be specified as a 5D spatially-invariant kernel, whose response decreases as the distances among pixels increase in 5D [69]. In comparison with other existing edge preserving filters, such as median filter, median of median along lines filter, bilateral filter and anisotropic diffusion filters [95], [117], [109], [176], [144], [196], [4], [64], [51], and [61], the recommended filter leads to remarkable speedups and memory saving which is due to use of 1D operations. In this approach, the filter parameters do not have effects on its computational cost. Furthermore, this edge preserving filter is able to

work on color images at arbitrary sizes in real time, without restoring to subsampling or quantization [69].

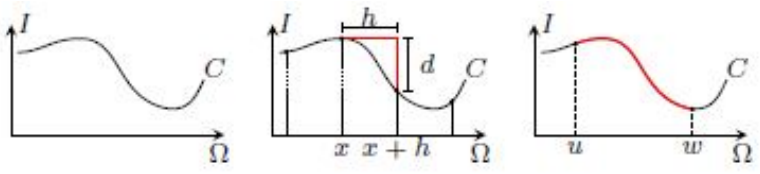

Figure 3.3: From left to right, curve C is specified in $\mathbb{R}^2$ into $\mathbb{R}s$ by graph $(x, I(x))$, the proper transform for being isometric (in ℓ_1 norm), the arc length between two points u and w [69].

In domain transform, to derive an isometric 1D transform which is inspired by the multi dimentional interpretation of edge preserving filtering [55], let $I\colon \Omega \to \mathbb{R}, \Omega = [0, +\infty) \subset \mathbb{R}$, be a 1D signal, which defines a curve C in $\mathbb{R}^2$ by the graph $(x, I(x))$, for $x \in \Omega$ (Figure 3.3, left). Therefore, to preserve the original distances between points on a curve C, a transform $t\colon \mathbb{R}^2 \to \mathbb{R}$ must be informed, in $\mathbb{R}$, by some metric. $S = \{x_0, x_1, ..., x_n\}$ is a sampling of Ω, where $x_{i+1} = x_i + h$, for some sampling interval h. To transform t we will have s where $x_i, x_j \in S$, $|.|$ and $||.||$ are the absolute value and some metrics have been chosen respectively. Proper transform with respect to be isometric can be written as follow:

$$ct(x + h) - ct(x) = h + |I(x + h) - I(x)| \tag{3.5}$$

where $ct(x) = t(\widehat{x}) = t(x, I(x))$, thus by dividing both sides of Eq. 3.5 by h and integrating from the resulted equation to preserve the geodesic distance between all points on the curve we will have:

$$ct(u) = \int_0^u 1 + |\acute{I}(x)|\, dx, \quad u \in \Omega \tag{3.6}$$

Therefore, to preserve distance in the new domain between two points u and w which is the arc length of C between these two points,(Figure 3.3, right) we will have:

$$ct(w) - ct(u) = \int_u^w 1 + |\acute{I}(x)|\, dx, \quad u\,, w \in \Omega, \quad w \geq u \tag{3.7}$$

Performing edge preserving filtering on each channel of input image separately leads to the presence of halo artifacts around the edges of the restored image [178]. To tackle this issue, the proposed edge preserving filtering [69] processes all channels of input image I_k at once which avoid the presence of artifacts in the restored image. By reducing the evaluation domain of the filter from $\mathbb{R}^{c+1}$ to $\mathbb{R}$ Eq. 3.6, a domain transform ct for color image is defined by Eq.3.9.

$$ct(u) = \int_0^u 1 + \sum_{k=1}^{c} |\acute{I}_k(x)|\, dx, \tag{3.8}$$

Regarding the transformation is isometric, any filter H, whose response reductions with distance at least as fast as Fs, will be edge-preserving. In order to preserve the filter's support over the signal's space and range that may be seemed to be lost due to reduction of the filter's dimension, the values of σ_s and σ_r in the transformation can be encoded. The final domain transform is rewritten as follow:

$$ct(u) = \int_0^u 1 + \frac{\sigma_s}{\sigma_r} \sum_{k=1}^{c} |\acute{I}_k(x)| \, dx, \tag{3.9}$$

Three realizations for this 1D edge preserving filter based on normalized convolution, interpolated convolution, and recursion have been defined. Each of these three filters has very well-defined response to different impulse which make each of them more proper for specific applications. In this thesis, we have applied 1D edge preserving filter based on recursion realization. Recursive filtering for the transformed signal $I_\omega(ct(x)) = I(x)$ in a transformed domain $ct\,\Omega \rightarrow \Omega_\omega$ is defined by using the 1D kernel H between two adjacent samples x_n and x_{n-1} as:

$$J[n] = (1 - a^d)I[n] + a^d J[n-1] \tag{3.10}$$

where $d = ct(x_n) - ct(x_{n-1})$ is the distance between two points x_n and x_{n-1} that is defined in the transformed domain, Figure 3.4 illustrates the applied recursive filter on flower images with different values for σ_s and σ_r. As can be seen in Figure 3.4, recursive filtering is able to smooth the color images while preserve the edge information without generating any artifacts in the resulted images.

Figure 3.4: From left to right, the original image, the obtained recursive filter by using parameters $\sigma_s = 20$ and $\sigma_r = 0.5$, $\sigma_s = 50$ and $\sigma_r = 0.8$, $\sigma_s = 100$ and $\sigma_r = 1$.

A comparison of the impulse response between three filters NC, IC, RF and BF, AD, WLS has been illustrated in Figure 3.6. As can be seen in this figure the NC and IC filters

have similar response to AD and BF filters, these filters have response like Gaussian. The IC filter has similar behavior to AD in the presence of strong edges. Strong edges attenuate the exponential impulse response of recursive filter (RF), like the WLSs response [69]. In order to stylize and abstract, the NC filter is highly recommended because of its ability to smooth similar parts of the image correctly and preserve and sharp the considered edges, simultaneously. However, two filters IC and RF are ideal for applications where sharpening of edges is not appropriate, the obtained results by these two filters IC and RF have same quality compared to other the state-of-the-art methods [62], [64]. Regarding infinite impulse response of the RF filter which leads to the information is propagated across the whole image lattice, this filter is able to obtain the satisfied results with aim of edge-aware interpolation, such as colorization and recoloring. Figure 3.5 shows the high performance of the domain transform recursive filter, which is applied in this thesis, to preserve and restore edges in the obtained image.

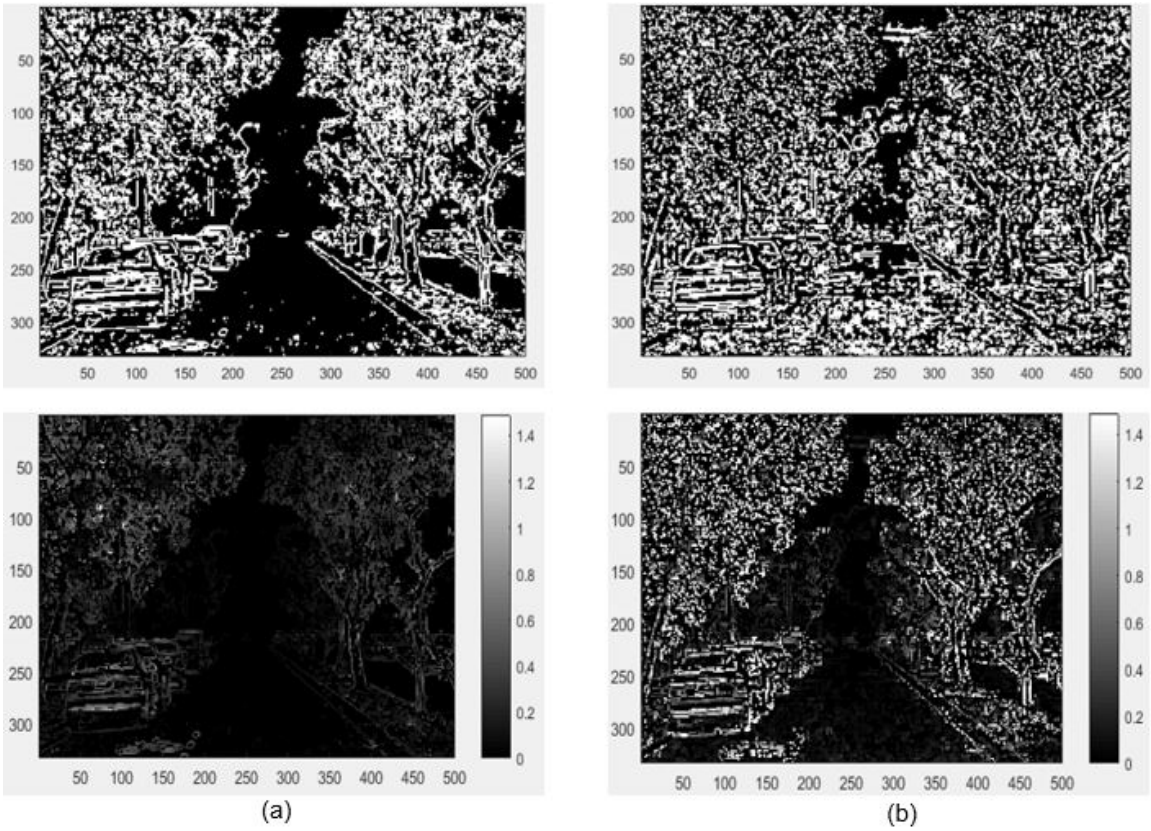

Figure 3.5: The comparison of visible edge between the original foggy image and the restored image by RF. (a)Visible edge in the original foggy image (56392 edges). (b) Visible edge in the restored image by our work (62114 edges).

- **Depth map inference**

In order to restore the visibility of fogy image which is known as an ill-posed problem for estimating depth map from a single image, an appropriate solution is maximizing the

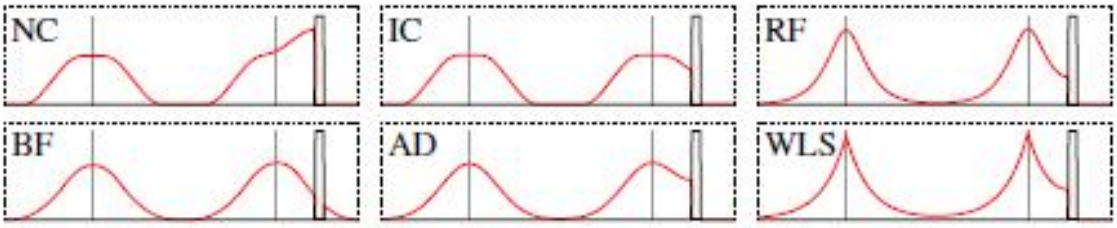

Figure 3.6: From left to right, impulse response of different filters at neighborhoods without and with strong edges, respectively. NC: Normal. Convolution; IC: Interp. Convolution; RF: Recursive Filter; BF: Bilateral Filter; AD: Anisotropic Diffusion; WLS: Weighted Least Squares [69].

contrast of the image. The restored image with high contrast is achieved by obtaining a depth map that must be smooth except along edges with large depth jumps [173], [176]. Regarding this subject, therefore, it is essential that possible large jump edges are preserved appropriately to restore visibility such as the one in Figure 3.7. In fact, this figure shows the difference results from informing different methods for smoothness and edge preserving. In the first row of this figure, it can be seen that the restored image by He et al. [89] algorithm is over-smoothed and edges are not preserved correctly, in the second row, there are halo artifacts along edges of buildings with large jumps in the restored image by Tarel and Hautiere [175] algorithm which means the applied edge preserving filter in this algorithm is not able to preserve all edges as well as corners with obtuse angle, and the last row in this figure proves that the applied filter is able to smooth image while preserve all edges with large depth jumps.

Indeed, if the edge preserving smoothing is not performed appropriately to estimate depth map, an incorrect halo artifacts appear in the restored image. To preserve large jumps along edges, a smoothing algorithm which is able to preserve edges with large jumps is required to be applied on input image after performing the white balance. Robust bilateral filters, anisotropic diffusion filters or faster the median filter can be used to perform an edge preserving smoothing. In summary, the refined transmission map t_r is inferred as:

$$
\begin{aligned}
&A(x,y) = domainTransform_{RF}(N(x,y), \sigma_S, \sigma_R) \\
&B(x,y) = A(x,y) - domainTransform_{RF}(|N - A|(x,y), \sigma_S, \sigma_R) \\
&B^{dark}(x) = darkChannel(B) \\
&\widetilde{t}(x) = 1 - \omega(B^{dark}(x)) \\
&M = domainTransform_{RF}(B^{dark}, \sigma_S, \sigma_R) \\
&D(x) = \omega(\min(M, min(B(x,y)))) - \min(B^{dark}) \\
&t_r(x) = \widetilde{t}(x) - D(x)
\end{aligned}
$$

where N is the mean value of input image after performing white balance, σ_S and σ_R are the scaling factors of edge preserving filter and our results have obtained with σ_S=5 and σ_R=0.3. The value of ω is defined based on the application. It has been fixed to 0.95

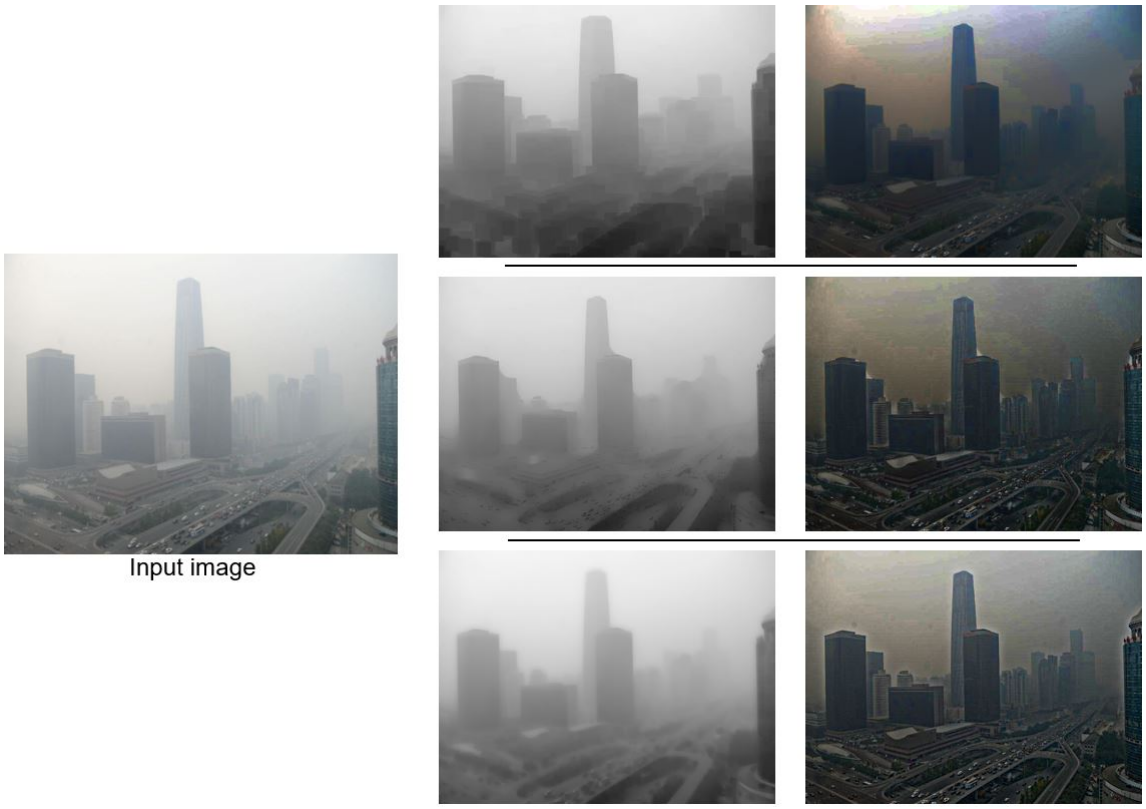

Figure 3.7: From up to down, the edge preserving smoothing and the obtained restored images by He et al. [89] algorithm, the edge preserving smoothing and the obtained restored images by Tarel and Hautiere [175] algorithm and the edge preserving smoothing and the obtained restored images by our work.

for all results reported in this thesis. $\widetilde{t}(x)$ and $t_r(x)$ are transmission map and refined transmission map, respectively. where $B^{dark}(x)$ is defined as follow:

$$B^{dark}(x) = \min_{y \in \Omega(x)} \{ \min_{c \in r,g,b} B^c(y) \} \tag{3.11}$$

A dark channel is resulted from two minimum operators: $\min_{c \in r,g,b}$ which is performed on each pixel, and $\min_{y \in \Omega(x)}$ is a minimum filter. Where B^c is a color channel of B and $\Omega(x)$ is a local patch centered at x, Figure 3.8.

Figure 3.8: Estimation of a dark channel. (a) An arbitrary image B. (b) Calculation of minimum value of each pixel. (c) A minimum filter is performed on (b). This is the dark channel of B. The patch size of Ω is 15×15 [89].

3.2.2 Visibility Restoration Module

After computing the depth map (DE module), the scene visibility R(x) (I_0 in Eq. 3.2) can be restored via the proposed refined transmission map as follows:

$$R^c(x) = \frac{I^c(x) - I_s^c}{\max(t_r(x), t_0)} + I_s^c, forc \in (r, g, b) \tag{3.12}$$

where $I(x)$ is the observed image intensity with the presence of fog (gray level or RGB), $R(x)$ is the intensity of restored image, I_s is the intensity of the sky which is set to (1, 1, 1), t_r (x) is the proposed refined transmission map, and t_0 is generally set to 0.1.

Therefore, the density of the haze which is resulted from atmospheric particles can be estimated correctly by Eq. 3.12. The flowchart of the proposed visibility restoration algorithm is illustrated in Figure 3.9.

- **Smoothing adapted to contrast magnification**

As a result of the image visibility restoration, the contrast of the restored image will increase as well. Due to increasing the image contrast, noise and image compression artifacts will

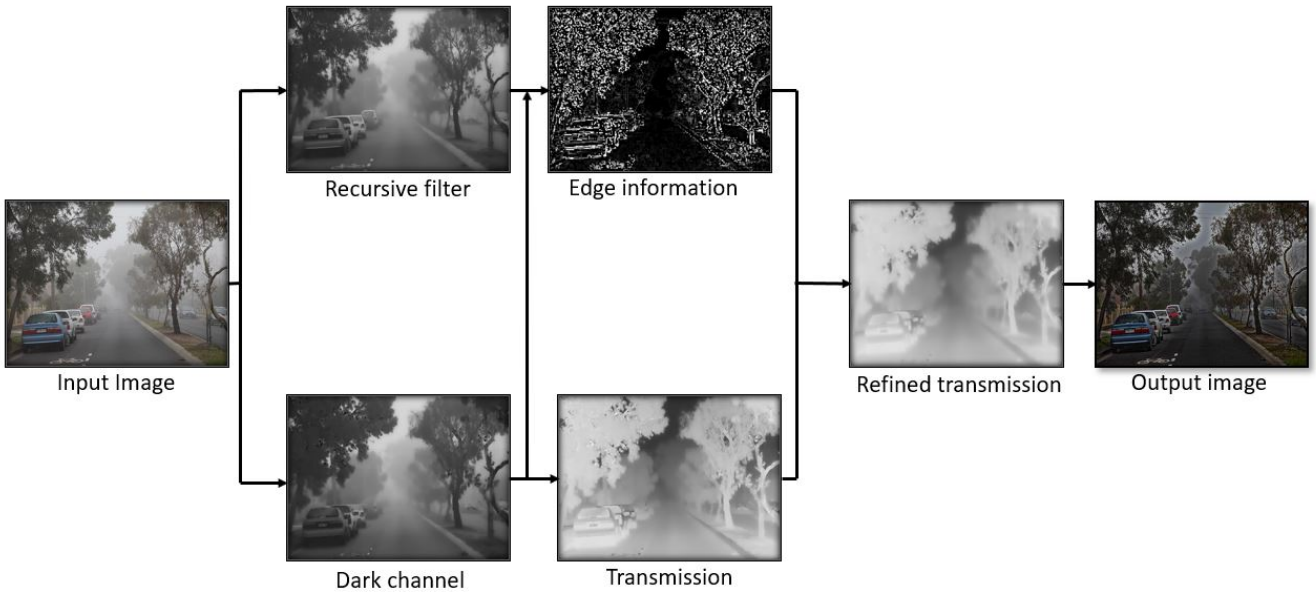

Figure 3.9: Flowchart of the procedure of our proposed refined transmission map.

increase and become more visually clear in the restored image in comparison with the original image which is compressed using jpeg. To tackle this problem a local smoothing should be performed to soften the resulted noise and artifacts.

- **Dedicated tone mapping**

The different steps of the visibility restoration regarding the image is in float format were described in previous sections. The restored images usually suffer from a high dynamic range which is more than the dynamic range of original one. To tackle this issue, the tone mapping is performed in the last step, which is hardly ever described in visibility restoration procedures but it plays a significant role for visualization. In order to have a restored image very similar to the original image, a linear mapping on the log original image and log resulting image have been applied which persuades that the related images have similar mean and std in the bottom third part of the image. Regarding to this fact that the bottom third of the image has less fog (road part of the image), it is used. If a_I and d_I are the mean and standard deviation of the log original image $\log(I(x,y))$ in the bottom third part of foggy input image, and a_R and d_R are the mean and standard deviation of the log restored image $\log(R(x,y))$ also in the bottom third part. The tone mapped image $T(x,y)$ is computed by non-linear mapping as follow:

$$T(x,y) = \frac{U(x,y)}{1 + (\frac{1}{255} - \frac{1}{M_G})G(x,y)} \tag{3.13}$$

where $U(x,y) = R(x,y)^{\frac{d_I}{d_R}} e^{a_I - a_R \frac{d_I}{d_R}}$, $G(x,y)$ is the gray level of $U(x,y)$ and M_G is the maximum of G. The obtained image T is always in [0, 255] [176]. Figure 3.10 shows the restored image by different depth maps.

Figure 3.10: (a) Input foggy images. (b) Estimated depth map by He et al. [89]. (c) Restored images using (b). (d) Estimated depth map by our work, (e) Restored images using (d).

Chapter 4

Experimental Results

This chapter is organized into 3 sections: introducing the camera-based Advanced Driver Assistance Systems (ADAS) as applications that can be improved via efficient algorithms to enhance the visibility in road images, performance evaluation methodology, and defogging results performance for real and synthetic images under homogeneous and heterogeneous fog, respectively [18]. The concentration will be on the last section for demonstrating the performance evaluation on the proposed method.

4.1 Applications of the Proposed Thesis in Camera-based Advanced Driver Assistance Systems (ADAS); and Overview

Advanced Driver Assistant System (ADAS) is considered as the advancement from driver assistant system (DAS) to help the driver in the driving process [209], [33], and [50]. Camera-based advanced driver assistance systems are widely applied in Advanced Safety Vehicles (ASVs). Regarding to the collecting data from sensor inputs, ADAS uses one or multiple automotive cameras which are monocular or stereo cameras (toshiba.com) Figure 4.1, [160].

Two kinds of ADAS can be considered. In one kind of ADAS which is called a Fog Vision Enhancement System (FVES), driver is able to see the enhanced image visibility which is displayed from a frontal camera. In another kind, visibility enhancement as a pre-processing is combined with detection and recognition of stopped or moving vehicles, pedestrians, traffic signs and the like around a vehicle, as well as the state of the driver and passengers using image recognition technologies to inform and warn, provide feedback on actions, increase comfort, and decrease workload by actively stabilizing or maneuvering the vehicle Figure 1.2 [147], [175], [**?**], [40], citeboukerche1994static, and [36]. High image data processing performance can be achieved via paralleling Media Processing Engines (MPEs) architectures at three granularity levels, multi core processing, Very Long Instruction Word (VLIW) and Single Instruction Stream, Multiple Data Stream (SIMD) for task-level parallelism, instruction-level parallelism and data-level parallelism, respectively (toshiba.com)

Figure 4.1: Camera based ADAS front camera system.

[23] and [22]. For ADAS based on the use of a single camera in the vehicle, the contrast enhancement algorithm must be able to robustly process each image in a sequence in real time. Figure 4.2 illustrates what the ADAS hardware might look like conceptually.

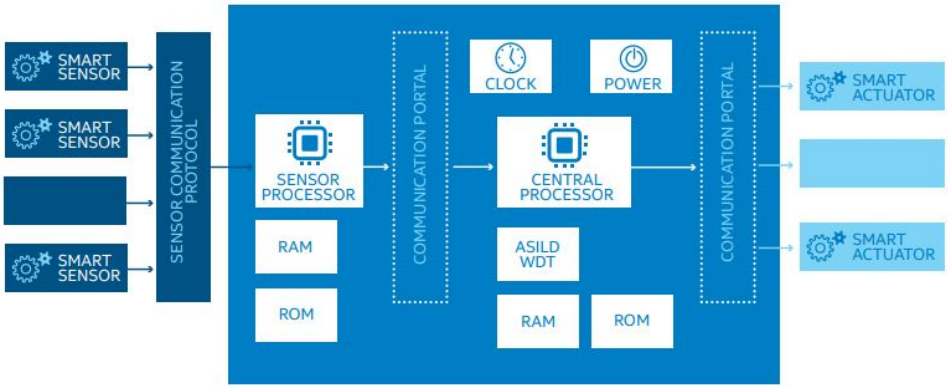

Figure 4.2: ADAS hardware block diagram [209].

4.2 Objective Quality Assessment Criterion of the Image Defogging Algorithm

In image-processing algorithms, such as acquisition, compression, restoration, enhancement, and reproduction the criteria, such as visibility, color restoration and structural similarity are applied to assess the quality of the resulted image. The image quality evaluation criterion can be categorized into three classes: full-reference image quality assessment, reduced-reference image quality assessment, and no-reference image quality assessment.

Wang et al. introduced a full-reference image quality assessment based on the degradation of structural information [186]. Their method, Structural Similarity Index (SSIM), evaluates the structural similarity between the resulted image and original clear image. A reduced-reference image quality assessment based on a rather elaborate model of the Human Visual System (HVS), C4, was proposed in [45]. [171] proposed Natural Scene Statistics (NSS) method to predict image quality without the reference image, it blindly assess the quality of images compressed by JPEG2000. A no-reference image quality assessment was proposed by Yu et al. to assess the color restoration performance of the enhanced image. In their work, Histogram distributions was supposed to be similar in the original foggy image and enhanced image for a good defogging algorithm [201]. Thus, the Histogram Correlation Coefficient (HCC) was used of the two color images as the criterion to evaluate the color restoration performance [58]. Providing a clear image related to the foggy image as a reference image is difficult in real applications unless there is a synthetic foggy image for the full-reference and reduced-reference image quality assessments.

In this work the quality of the defogged image is evaluated by the full-reference metric, such as Peak Signal-to-Noise Ratio (PSNR) [162], structural similarity (SSIM) [186] and no-reference metric, such as color restoration [87], enhanced degree of image edges [87], [81], enhanced degree of image gradients [87], and the presence of the halo artifacts.

An appropriate defogging algorithm should achieve a restored image with high visibility without the presence of halo-artifacts. Also these algorithms should enhance and preserve the image edges, texture information, structure and colors. Edge and texture information is supposed to be seen vividly in the restored image with desirable visibility. Therefore, criteria, such as visibility, color restoration, and image structure similarity are required to be compared via image quality assessment method requires to be compared for different defogging algorithms.

4.2.1 Assessment Criterion of Image Visibility

In this section two indicators $(e, \bar{r})$ of the no-reference assessment are introduced to compare the visibility of images after restoration [87]. To compare image visibility, Visual Contrast Measure (VCM) [102], Image Visibility Measurement (IVM) [202] and image contrast [56] can be used as well.

- **No-reference assessment indicator**

To display the enhanced level of the image visibility, the increased rate of image edges is applied for two indicators $(e, \bar{r})$ of the blind assessment [87]. The indicator e indicates the enhanced degree of visible edges in the defogged image and is computed as follow:

$$e = \frac{n_r - n_o}{n_o} \tag{4.1}$$

where n_r is the cardinal numbers of the set of visible edges in the restored image I_r and n_o is the set of visible edges in original foggy image I_o. The algorithm corresponding to visible

edge segmentation is presented in detail in articles [87], [81]. Visible edges are defined as the set of edges which have a local contrast above 5% regarding to the CIE [47]. The number of the set of visible edges of the original foggy image can be 0 when image has dense fog, so in this case Eq. 4.1 is rewritten by

$$e = \frac{n_r - n_o}{M \times N} \tag{4.2}$$

where M and N indicate image size. Defogged image with the high rate of visibility will have the large the e as well. In order to evaluate the enhanced rate of image visibility, the increased number of the visible edges is used by the indicator e.

The indicator $\bar{r}$ evaluates the enhanced rate of the image edge and texture information in the restored image by applying the enhanced degree of image gradients. A good defogging algorithm has a high performance in terms of better preserving the edges in comparison with others which means these algorithms will have larger $\bar{r}$ and computed as

$$\bar{r} = \exp\left[\frac{1}{n_r}\sum_{i\in\wp_r}\log r_i\right] \tag{4.3}$$

where $r_i = \Delta I_i^r / \Delta I_i^o$ that ΔI^r corresponding to the restored image gradient, ΔI^o corresponding to the original foggy image gradient, and $\wp_r$ indicates the number of visible edges of the restored image. Thus, the amount of the restored edge information is measured by this indicator based on gradient.

4.2.2 Assessment Criterion of Color Restoration

To assess the performance of the color restoration of the enhanced image, index σ is used as the blind indicator assessment [87]. The number of saturated pixels which are seen black or white in the defogged image is indicated by σ and is computed as

$$\sigma = \frac{n_s}{M \times N} \tag{4.4}$$

where n_s is the set of saturated pixels of the restored image which are not absolutely saturated in the original foggy image, where M and N are the size of the image. The smaller the σ, the better result of the defogging algorithm. Evaluating color restoration by indicator σ is not always perfect for the enhanced images via some algorithms based on Retinex, which their domain is transformed into [0, 255] via the gain/offset algorithm. The gain/offset algorithm improves the dynamic range by transforming some pixels to black and white pixels, which means the σ will be high.

4.2.3 Image Structure Similarity

In order to evaluate the structural similarity performance between the original foggy image and the enhanced image, the image Structural Similarity (SSIM) [189] and Universal

Quality Index (UQI) [185] were proposed and applied. A high quality and clear reference image is required for criterion traditional SSIM which calculated as

$$SSIM = [l(a,y)]^{\alpha} \cdot [c(x,y)]^{\beta} \cdot [s(x,y)]^{\gamma} \tag{4.5}$$

where

$$l(x,y) = \frac{2\mu_x\mu_y + C_1}{\mu_x^2 + \mu_y^2 + C_1}$$
$$c(x,y) = \frac{2\sigma_x\sigma_y + C_2}{\sigma_x^2 + \sigma_y^2 + C_2}$$
$$s(x,y) = \frac{\sigma_{xy} + C_3}{\sigma_x\sigma_y + C_3}$$

where μ_x, μ_y are the local means, σ_x, σ_y are standard deviations and σ_{xy} is the cross-covariance for images x, y.

Thus, the higher the SSIM, the better result of the defogging algorithm. Regarding to providing the high quality clear image as a reference image in real-world applications is difficult, thus the original foggy image is always considered as the reference image, in this case small SSIM means the image is restored with high quality. In addition, removing fog from a foggy image will effect on the image structure which leads to small SSIM. Two similar foggy images have a large the SSIM index in comparison with the SSIM index for the foggy and the enhanced image. Therefore, a good visibility enhancement algorithm may lead to the enhanced image with the smallest SSIM.

4.2.4 Peak Signal-to-noise Ratio

In order to assess the affects of different image enhancement algorithms on image quality, peak signal-to-noise ratio (PSNR) was proposed which is an expression for the ratio between the maximum possible value (power) of a signal and the power of distorting noise that affects the quality of its representation [162]. PSNR as a fully-reference image quality assessment criterion needs a clear image as a reference image to evaluate the quality of the enhanced image [143]. The larger PSNR means the defogging algorithm has a good performance to achieve a high quality defogged image and defined via the Mean Squared Error (MSE). MSE for $M \times N$ original clear image I_o and its restored image I_r is computed as follow:

$$MSE = \frac{1}{MN} \sum_{i=0}^{M-1} \sum_{j=0}^{N-1} [I_o(i,j) - I_r(i,j)]^2 \tag{4.6}$$

so with having MSE the PSNR (in dB) can be defined as

$$PSNR = 20 \cdot \log_{10} \left(\frac{MAX_I}{\sqrt{MSE}} \right) \tag{4.7}$$

As mentioned in SSIM index, providing the clear original image corresponding to foggy image as a reference image is difficult, so this index can be considered as a blind image quality assessment criterion by comparing original foggy image as a reference image with the restored image which means a good enhanced image will have small PSNR.

4.3 Defogging Results Performance

In this section our work has been compared with some single visibility restoration algorithms via subjective and objective assessment. The compared algorithms are based on physical model. All images have been assessed by five objective quality assessment indexes (e, $\overline{r}$, σ, SSIM and PASNR). Also, two factors processing time and the presence of artifacts on restored images have been covered in this section. To obtain acceptable and comparable results with other defogging algorithms, blind contrast restoration assessment's source code and stuctural similarity index source code (SSIM) have been obtained from http://perso.lcpc.fr and http://sse.tongji.edu.cn, respectively. In order to evaluate the quality performance of defogging algorithms, having images of the same scene with and without fog are required. In practice providing such pairs of images are so complicated. Therefore, synthetic images without fog and with presence of synthetic fog from the same scene were generated to pave the way to compare restored image with original fog-free image [75]. In producing synthetic images a moving vehicle with considering the physical models of dynamic behavior and physical environment of road was considered [75]. Synthetic images with the mentioned features were generated by using $SiVIC^{TM}$ software and are accessible in (www.lcpc.fr/english/products/image-databases/article/frida-foggyroad-image-database).

In this thesis, the assessment of defogging algorithms has been performed on both synthetic and real images from four realistic and complex structures, such as suburban, highway, urban and mountain areas. The size of applied images for synthetic images is 640 $\times$ 480 and real images is arbitrary.

4.3.1 Comparison on Synthetic Images

Four tested defogging algorithms which are included: Tarel and Hautiere [176], Tarel and Hautiere [175], He et al. [89] and the proposed work have been applied on 66 synthetic images with homogeneous fog and 198 synthetic images with three kinds of heterogeneous fog with different structures. The obtained results on synthetic images with uniform fog and different structures are illustrated in Figures 4.6 and 4.7. The restored images from original images with three kinds of heterogeneous fog are illustrated in Figure 4.5. In these figures, the far away objects in original foggy images have low contrast and can be seen hardly, while the contrast of these objects is increased in the restored images and can be

seen vividly. A visual analysis proves that the farther objects in the restored images by He et al. [89] are more foggy and blurry in comparison with three other algorithms, the road part of the restored image by Tarel and Hautiere [176] is seen over-restored and for entire image looks foggy. The presence of halo artifacts can be seen in the restored images by [176] and [175] which is caused by using the median edge preserving smoothing filter and the way the atmospheric veil is computed in these two algorithms. The far away objects in the restored images by our work appear more clear and defogged which plays a main role in vehicle applications in terms of the ability of the driver to see farther vehicles, pedestrians and other objects on the road surface. In addition, traffic signs can be seen more clear in the enhanced images by our proposed algorithm Figure 4.4 confirms this fact. Figure 4.3 shows the performance of the proposed algorithm in edges with different angles, also it can be noticed that the proposed algorithm is able to restore images without the presence of halo artifacts in the resulted image.

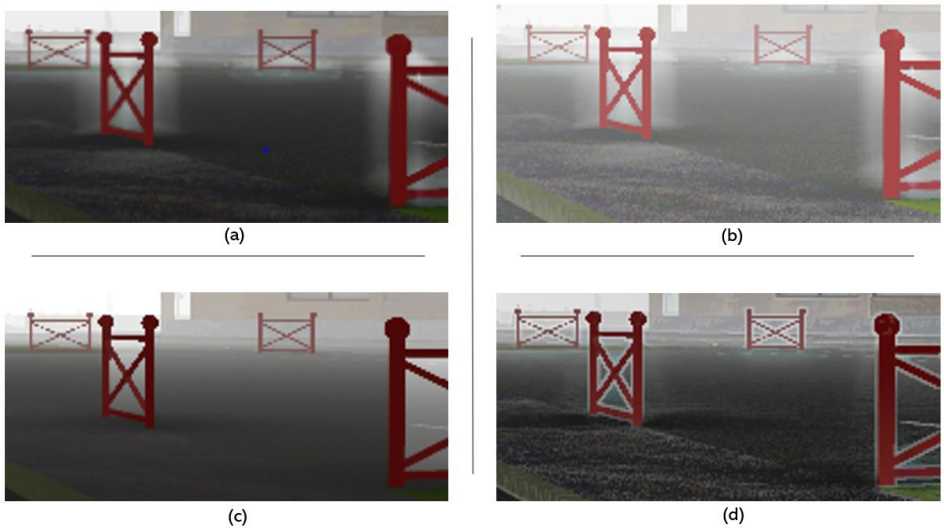

Figure 4.3: Comparisons of some defogging algorithms on synthetic images in terms of the presence of halo artifacts on the restored images. (a) Tarel and Hautiere [176]. (b) Tarel and Hautiere [175]. (c) He et al. [89]. (d) our result.

The same quantitative comparison has been shown in Tables 4.1, 4.2. The tables show that He et al. [89] algorithm obtained smaller values of all visibility assessment criteria in comparison with other defogging algorithms. These tables also prove that the larger e and $\overline{r}$ indexes, the better the defogging result. Regarding this matter that original fog-free images are available for synthetic images, so a good restored image should have large values for two SSIM and PSNR indexes. While some litretures beilive that the procedure of removing fog from a foggy image will change the structure of image. Table 4.1 shows that Tarel and Hautiere [176] algorithm has the largest SSIM index rather than other algorithms. Tables 4.1 and 4.2 show that the proposed work has the largest values for two indicators e and $\overline{r}$ which means there is a high rate of increased visible edges and texture information in the restored images campared to others works. Moreover, based on the obtained values for indicator PSNR, it can be observed that the proposed work has obtained larger values for

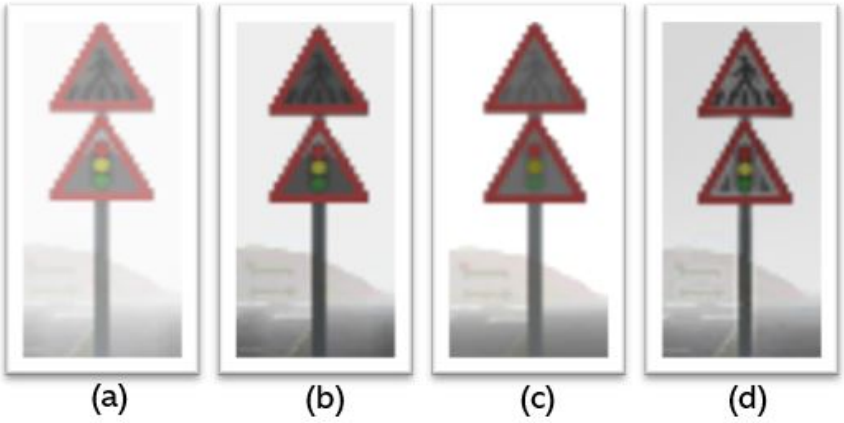

Figure 4.4: Comparisons of the visibility of restored traffic signs by some defogging algorithms on synthetic images. (a) Tarel and Hautiere [176]. (b) Tarel and Hautiere [175]. (c) He et al. [89]. (d) our result.

PSNR than other restoration algorithm, mostly. Regarding the achieved results from these synthetic figures and corresponding tables, we can see that some restored images by Tarel and Hautiere [175] algorithm have better results in comparison with the proposed work. However, we should notice that our proposed algorithm has better restoration performance totally, and reaches a fast algorithm compared to Tarel and Hautiere [175] algorithm. It is noticable that the proposed work has similar approach to He et al. [89] restoration algorithm so it can be seen that our work has greatly improved He et al. [89]. Figure 4.9 illustrates the average PSNR for 66 synthetic images.

4.3.2 Comparison on Real Images

The same algorithms as mentioned in the previous section have been applied on more than 400 real/camera images which are obtained from Flicker.com, Picasaweb.com, Photosig.com and many others websites. The results on 6 images captured from suburban roads, 6 images captured from highways and 7 images captured from urban roads with a uniform fog are presented in Figures 4.8, 4.10 and 4.12. Notice how the contrast is restored for the farther objects. And also, the quantitative comparison is shown in Tables 4.3, 4.4 and 4.5. The results are quite consistent with the obtained results for synthetic images. From Figures 4.8, 4.10, and 4.12 we can see that images after restoration by Tarel and Hautiere [175] look darker rather than other defogging algorithms. Farther objects appear blurry after restoration by He et al. [89] compared to three other algorithms. Moreover, restoration by three algorithms Tarel and Hautiere [176], Tarel and Hautiere [175], and He et al. [89] leads to the presence of halo and block artifacts in the restored image. However, the proposed algorithm can effectively reduce the generation of halo and block artifcts by using the Recursive Filtering (RF) in the transformed domain to preserve edge information of the input image. Also the sky area in the restored images by the proposed work

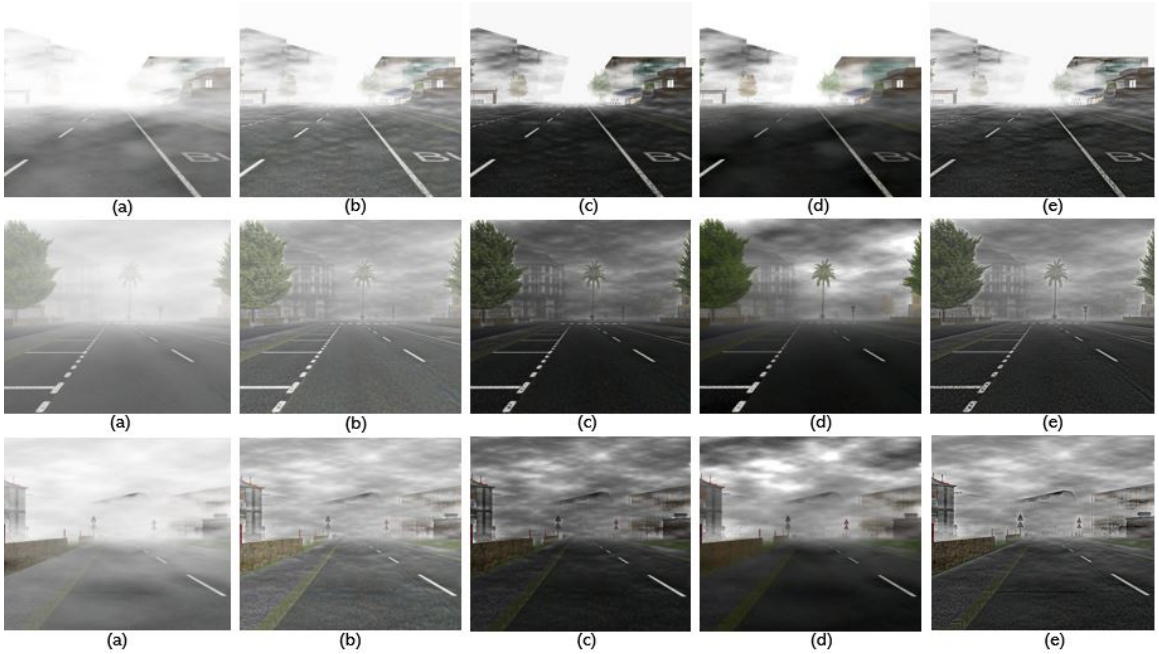

Figure 4.5: Comparisons of some defogging algorithms on synthetic images with three kinds of heterogeneous fog (β, I_∞ and β & I_∞). (a) original images. (b) Tarel and Hautiere [176]. (c) Tarel and Hautiere [175]. (d) He et al. [89]. (e) our results.

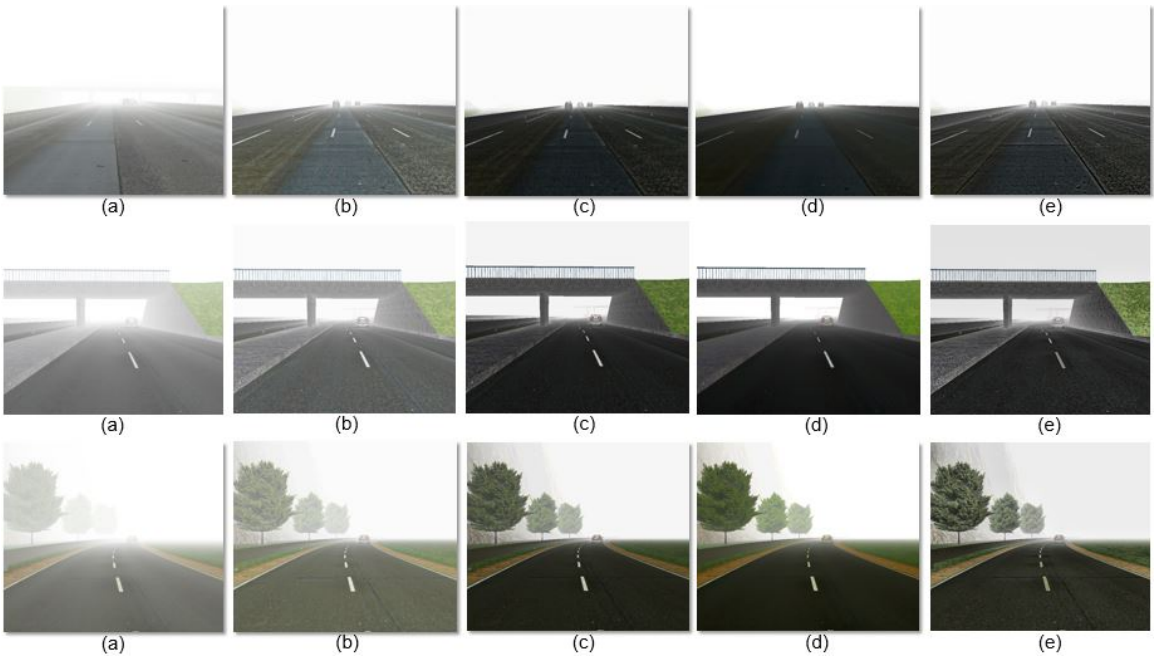

Figure 4.6: Comparisons of some defogging algorithms on less structured synthetic images with a road scene. (a) original images. (b) Tarel and Hautiere [176]. (c) Tarel and Hautiere [175]. (d) He et al. [89]. (e) our results.

Table 4.1: The objective image quality comparison of defogging results of Figure4.6.

	e	$\overline{r}$	σ	SSIM	PSNR
Tarel and Hautiere [176]	4.6253	3.0074	0	**0.8103**	16.2600
	4.1477	2.9525	0	**0.8133**	17.0032
	7.349	2.7206	0	**0.6301**	9.7067

	e	$\overline{r}$	σ	SSIM	PSNR
Tarel and Hautiere [175]	5.6363	1.9961	0	0.7727	15.7258
	5.4934	2.3893	0	0.7309	14.6418
	11.2276	2.3891	0	0.6028	11.0438

	e	$\overline{r}$	σ	SSIM	PSNR
He et al. [89]	2.1127	0.77476	0	0.7599	15.6010
	2.4994	1.2355	0	0.7140	14.6510
	5.6612	1.4471	0	0.5663	10.4095

	e	$\overline{r}$	σ	SSIM	PSNR
Our	**6.3589**	**4.3**	0	0.7597	**16.6250**
	6.6973	**4.4542**	0	0.7041	**15.2539**
	13.4505	**4.856**	0	0.5963	**11.6779**

Table 4.2: The objective image quality comparison of defogging results of Figure 4.7.

	e	$\overline{r}$	σ	SSIM	PSNR
Tarel and Hautiere [176]	3.4899	2.8187	0	**0.6911**	11.42311
	4.4877	2.9703	0	**0.7063**	11.5375
	6.6876	3.0012	0	**0.7291**	10.79209
	5.8271	2.9897	0	**0.7076**	11.25207
	2.1523	2.584	0	0.6295	10.24703
	5.996	2.9147	0	**0.7412**	11.76722
Tarel and Hautiere [175]	4.1764	2.3637	0	0.6896	13.93312
	5.947	2.504	0	0.6891	14.37854
	9.9472	2.3754	0	0.6788	12.22031
	8.2306	2.5115	0	0.6881	14.0761
	2.6616	2.3787	0	**0.6492**	12.73727
	8.1479	2.3951	0	0.6878	13.05169
He et al. [89]	2.4065	1.3348	0	0.6523	12.99128
	3.3172	1.4903	0.0094	0.6526	13.60463
	4.6232	1.3877	0.0019	0.6472	11.61517
	4.1798	1.5574	0.0322	0.6537	13.47711
	1.4202	1.2445	0	0.6392	11.96138
	3.1894	1.1663	0	0.6692	12.48319
Our	**4.8161**	**4.3018**	0	0.6365	**14.11984**
	7.4381	**4.4914**	0	0.6748	**14.92381**
	12.4923	**4.6743**	0	0.6723	**12.99211**
	10.3487	**4.5604**	0	0.6769	**14.6828**
	3.2699	**4.3813**	0	0.5654	**12.92027**
	10.1908	**4.8406**	0	0.6526	**13.79481**

Table 4.3: The objective image quality comparison of defogging results of Figure 4.8.

	e	$\overline{r}$	σ	SSIM	PSNR
Tarel and Hautiere [176]	5.8411	2.7524	0	0.8642	15.4823
	2.6395	4.2111	0.00494	0.6700	15.9287
	5.3698	4.7043	0.00225	0.7559	15.4501
	1.1056	3.3243	0.01921	0.6618	14.8868
	4.6468	3.2166	0	0.8322	15.8140
	4.1352	3.8755	0	0.7761	15.8147
Tarel and Hautiere [175]	11.5279	3.0313	0	0.6696	8.8461
	2.7074	2.9826	0.29235	**0.5041**	11.0579
	4.5952	2.9199	0.01549	**0.5632**	10.1700
	0.6144	2.3462	0.2896	**0.5823**	11.0956
	6.7895	2.387	0.00073	**0.4806**	9.5162
	3.4737	2.7295	0.00206	0.5933	10.0548
He et al. [89]	6.8565	3.1056	0	0.7236	11.2837
	1.2953	1.1622	0	0.7501	9.5653
	0.6377	0.7442	0	0.7825	8.8222
	0	1	0.00442	0.7188	12.2424
	2.996	1.5715	0	0.7963	11.1595
	2.1833	0.94025	0	0.6787	10.7690
Our	**13.1048**	2.3739	0	**0.5620**	**7.1601**
	3.401	2.442	0.02893	0.6089	**8.9665**
	5.8728	2.1486	0.00993	0.6883	**8.0528**
	1.1306	2.0021	0.08569	0.6544	**8.9801**
	8.0893	1.9583	0	0.5268	**7.8125**
	4.4377	2.1856	0	**0.5542**	**8.2852**

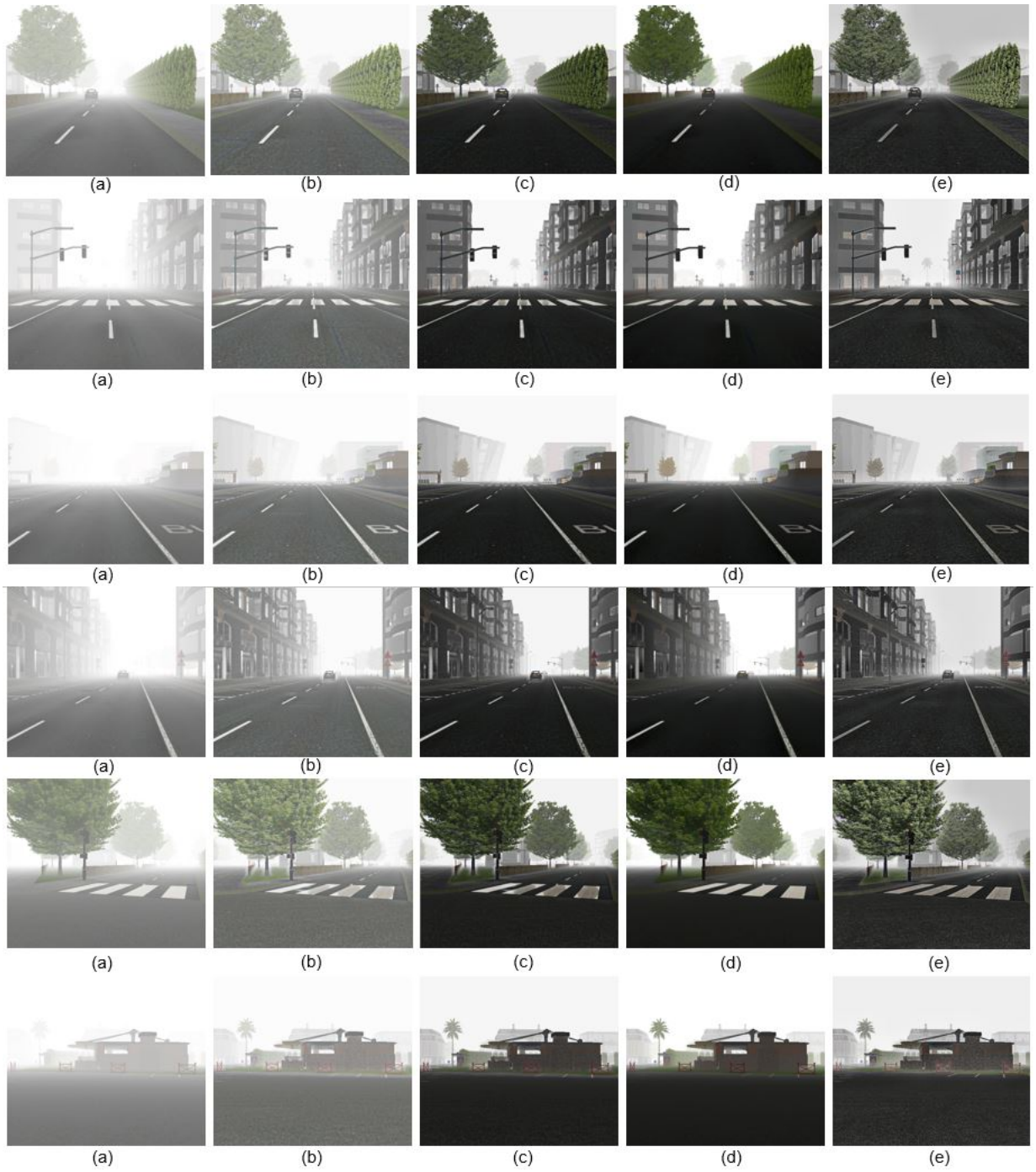

Figure 4.7: Comparisons of some defogging algorithms on more structured synthetic images with a road scene. (a) original images. (b) Tarel and Hautiere [176]. (c) Tarel and Hautiere [175]. (d) He et al. [89]. (e) our results.

appears more correct particularly, in comparison with He et al. [89] algorithm, Figures 4.8, 4.10 and 4.12 confirm all these statements. Obtaining a restored image with high rate

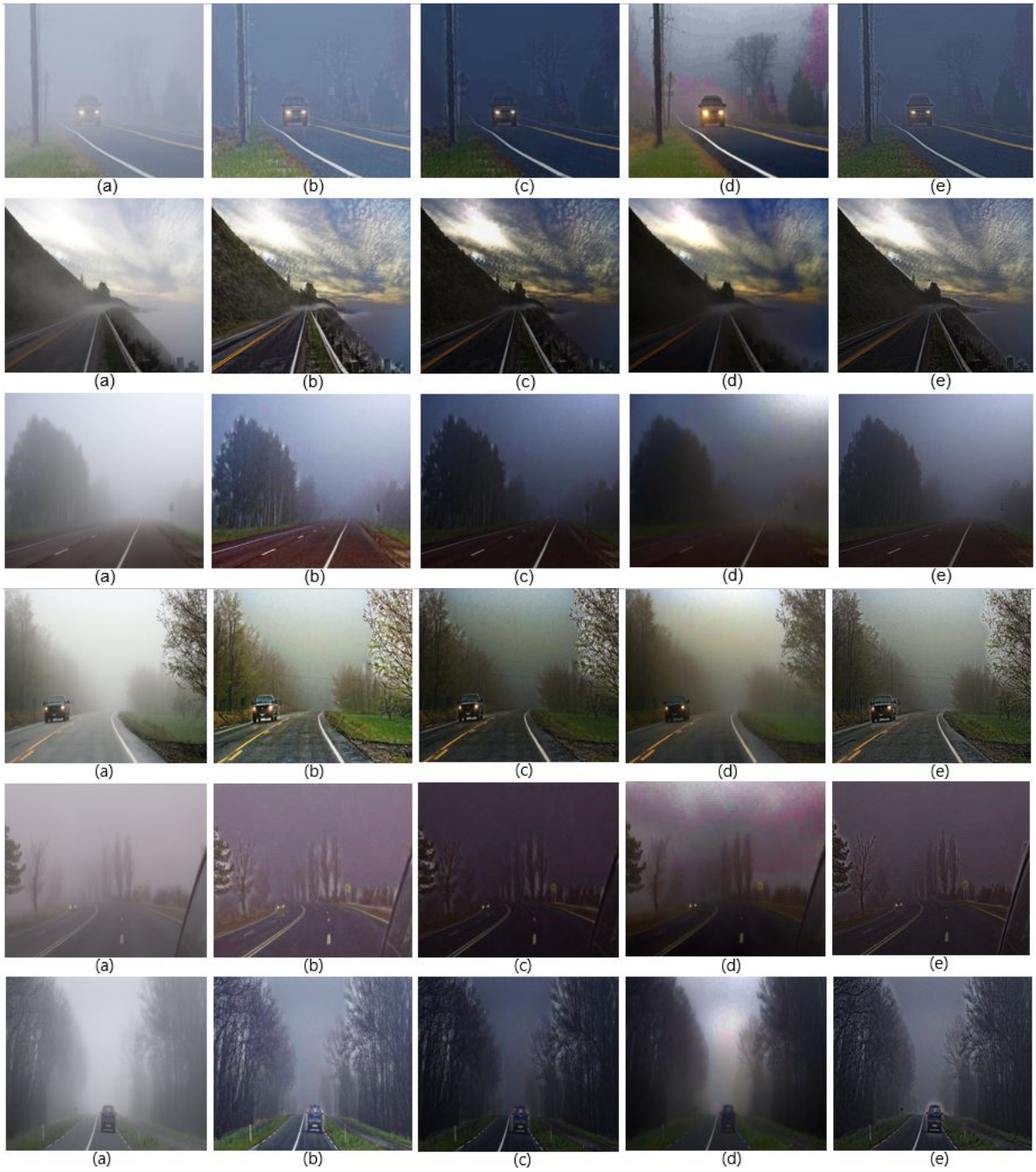

Figure 4.8: Comparisons of some defogging algorithms on real images captured from suburban roads. (a) original images. (b) Tarel and Hautiere [176]. (c) Tarel and Hautiere [175]. (d) He et al. [89]. (e) our results.

of edge and texture preservation leads to high visibility in the enhanced image which can help the traffic signs are observed more clear by the drivers. Figure 4.11 illustrates that

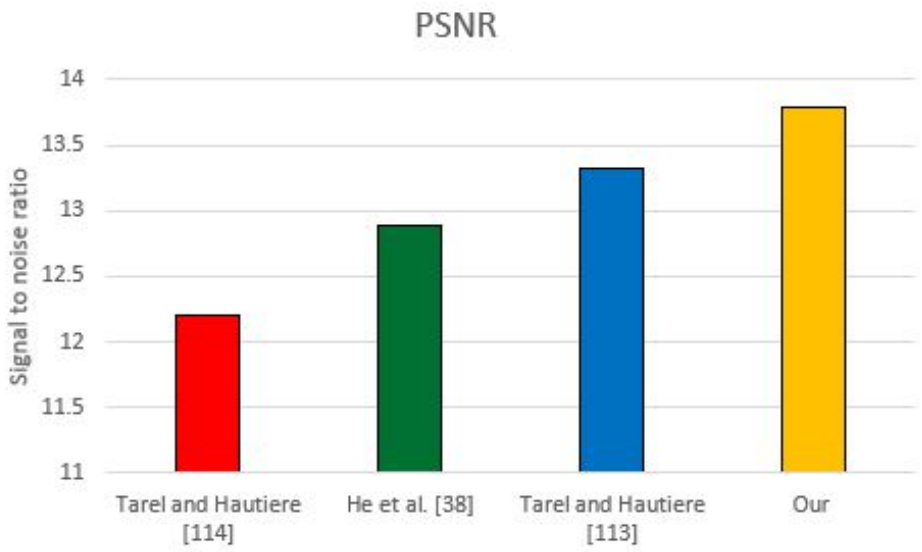

Figure 4.9: Comparisons of the average PSNR index of 66 synthetic images with uniform fog for four defogging algorithms Tarel and Hautiere [176], Tarel and Hautiere [175], He et al. [89] and our work.

the traffic sign appears more visible in the restored image by the proposed algorithm than other algorithms.

Tables 4.3, 4.4, and 4.5 demonstrate the performane of our defogging algorithm to achieve a larger e than other defogging algorithms, which indicates that our proposed algorithm has the best performance in restoring and preserving image edges information. Regarding this issue that the providing of original fog-free images from the same scene of foggy images is not feasible in practice, therefore for real images to compute two parameters PSNR and SSIM, restored images are compared with original foggy images, so the smaller PSNR and SSIM the better the result of the defogging algorithm. Table 4.3 demonstrates that our defogging algorithm achieves a smaller PSNR and Tarel and Hautiere [175] achieved a smaller SSIM than other defogging algorithms but these values are quite close to each other in these two algorithms. The obtained results from the restoration of highway images in Table 4.4 shows that they are quite consistent with the obtained results from suburban road images in which our work has almost similar values for two parameters PSNR and SSIM to Tarel and Hautiere [175] algorithm, but the obtained results by the proposed algorithm for two indexes PSNR and SSIM have remarkable improvement compared to two algorithms Tarel and Hautiere [176] and He et al. [89]. The obtained objective quality assessment indexes from urban road images in Table 4.5 indicate that two defogging algorithms Tarel and Hautiere [175] and our work have rather similar performance in terms of restoring edge and texture information and they also achieve a smaller SSIM and PSNR compared to Tarel and Hautiere [176] and He et al. [89].

It is complicated to specify an algorithm as a best defogging algorithm based on its performance to restore and enhance foggy images, since almost none of defogging algorithm can have high performance under all different conditions. As can be observed from the

Table 4.4: The objective image quality comparison of defogging results of Figure 4.10.

	e	$\overline{r}$	σ	SSIM	PSNR
Tarel and Hautiere [176]	3.5793	2.8523	0	0.7968	16.8906
	13.6721	4.0418	0	0.8511	16.3074
	3.0165	3.4376	0	0.8325	15.1431
	2.5491	2.9786	0	0.7673	14.7890
	1.7398	2.0751	0	0.8554	16.9881
	2.499	3.5198	0	0.7542	14.2706
Tarel and Hautiere [175]	4.2131	2.6389	0.00649	0.5362	**8.7548**
	28.1705	3.2466	0	**0.4322**	7.7797
	3.7835	2.6973	0.03981	0.4924	8.4256
	2.5294	2.812	0.25817	0.4798	**7.4830**
	13.1986	3.1411	0	**0.5130**	6.2207
	2.2785	2.4685	0.00978	0.5339	7.4021
He et al. [89]	0.90263	1.424	0.05818	0.7052	12.1164
	5.7282	1.5036	0	0.7989	11.0984
	0.68247	1.0609	0.006245	0.7728	11.2461
	0.69233	1.1916	0.03862	0.7061	12.5949
	3.4226	2.8746	0	0.8332	7.9874
	1.4483	1.8052	0	0.7796	12.2294
Our	**5.4378**	2.1071	0.00016	**0.5006**	8.8541
	37.8193	2.6614	0	0.5919	**7.2166**
	4.243	2.0112	0.00117	**0.4734**	**8.4126**
	4.0242	2.4177	0.02299	**0.4601**	8.2895
	7.2003	3.4386	0	0.5663	**6.0150**
	3.4835	2.1325	0	**0.5141**	**7.3998**

Table 4.5: The objective image quality comparison of defogging results of Figure 4.12.

	e	$\overline{r}$	σ	SSIM	PSNR
Tarel and Hautiere [176]	**0.53813**	**2.2738**	0.00060	0.8116	17.4715
	0.18093	2.3537	0.01974	0.8032	15.3143
	0.53916	2.0157	0	0.8243	18.2047
	8.6557	3.3057	0	0.7998	18.1428
	7.4232	3.0233	0	0.8345	17.2021
	2.44	**3.7542**	0.00029	0.6952	16.4493
	1.6122	2.5608	0	0.7245	22.5340
Tarel and Hautiere [175]	0.26201	1.7197	0.22763	**0.6998**	**11.6000**
	0.18815	1.6377	0.11255	**0.7550**	**10.6380**
	0.76434	2.0841	0	**0.6082**	9.3494
	23.6482	**3.7306**	0	0.5466	8.2572
	13.5371	2.3426	0	0.6082	8.2712
	2.7312	2.2524	0.00029	0.6845	10.7190
	3.3591	2.2694	0	0.6179	11.0974
He et al. [89]	0.05247	1.0964	0.06946	0.7987	16.0220
	0.0535	0.9381	0.06365	0.7979	14.6699
	0.38914	1.5599	0	0.8044	11.5692
	2.3383	0.97845	0	0.7853	9.2723
	2.9292	1.42	0	0.8301	10.2203
	0.28039	0.9384	0.00254	0.7018	14.2489
	2.3648	2.015	0	0.7099	12.7957
Our	0.27765	2.143	0.0553	0.7043	12.2227
	0.16237	**2.4547**	0.09871	0.7702	11.6606
	0.66981	**2.6279**	0.01333	0.6133	**9.2624**
	20.896	3.5294	0	**0.5417**	**8.1590**
	14.5389	**3.1691**	0	**0.6066**	**8.1276**
	2.5004	2.9883	0.10119	**0.6201**	**10.4001**
	3.6596	**3.0405**	0.00165	**0.6063**	**10.9427**

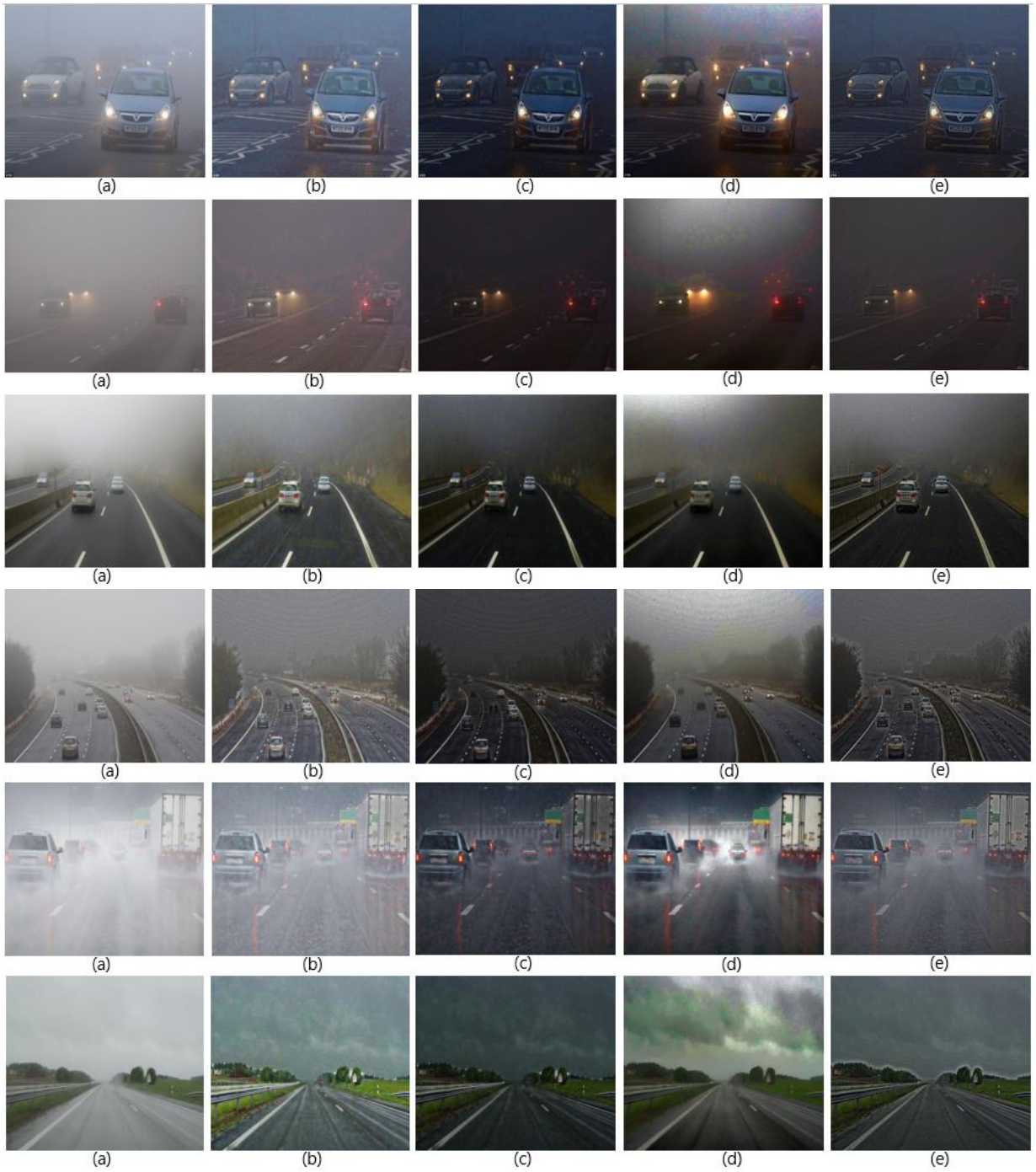

Figure 4.10: Comparisons of some defogging algorithms on real images captured from highways. (a) original images. (b) Tarel and Hautiere [176]. (c) Tarel and Hautiere [175]. (d) He et al. [89]. (e) our results.

above tables and figures, the evaluation of the objective of defogging algorithms by quality assessment indexes are quite inconsistent, however using them as references to compare the

Figure 4.11: Comparisons of the visibility of traffic signs after restoration by some defogging algorithms on real images. (a) Input foggy image. (b) Tarel and Hautiere [176]. (c) He et al. [89]. (d) our result.

performance of different defogging algorithms can be feasible. As a matter of fact the aim of this thesis has been obtaining a simple defogging algorithm from only a single image which can be applied for real time autonomous vehicles' applications such as ADAS systems and simultaneously has a high performance to restore correctly the whole part of the image in which far away objects can be seen clearly by driver. As we have seen from all above figures and tables, our work has very high performance compared to Tarel and Hautiere [176] and He et al. [89] algorithms. In addition, in order to evaluate the processing time of the proposed defogging algorithm, a comparison has been done between the proposed work and two algorithms Tarel and Hautiere [176] and Tarel and Hautiere [175] which have been considered as fast algorithms and can be applied for real time applications. He et al. [89] algorithm is not known as a fast algorithm so for processing time comparison we have not considered this algorithm. Figure 4.13 illustrates the comparison of the average processing time of 70 real images with arbitrary sizes for three Tarel and Hautiere [176], Tarel and Hautiere [175] and our algorithms. Also, a comparison on each image has been done on processing time of the proposed work and the fastet defogging algorithm Tarel and Hautiere [176] for 70 real images with arbitrary sizes in Figure 4.14. Note algorithms are tested on the same computer, the system is Win 10, and the software is MATLAB R2016a, the hardware is Intel(R) Core(TM) i3-370 CPU, and 4.00 GB RAM. Therefore, we can see that the proposed work has met these required features for being good enough as a defogging approach.

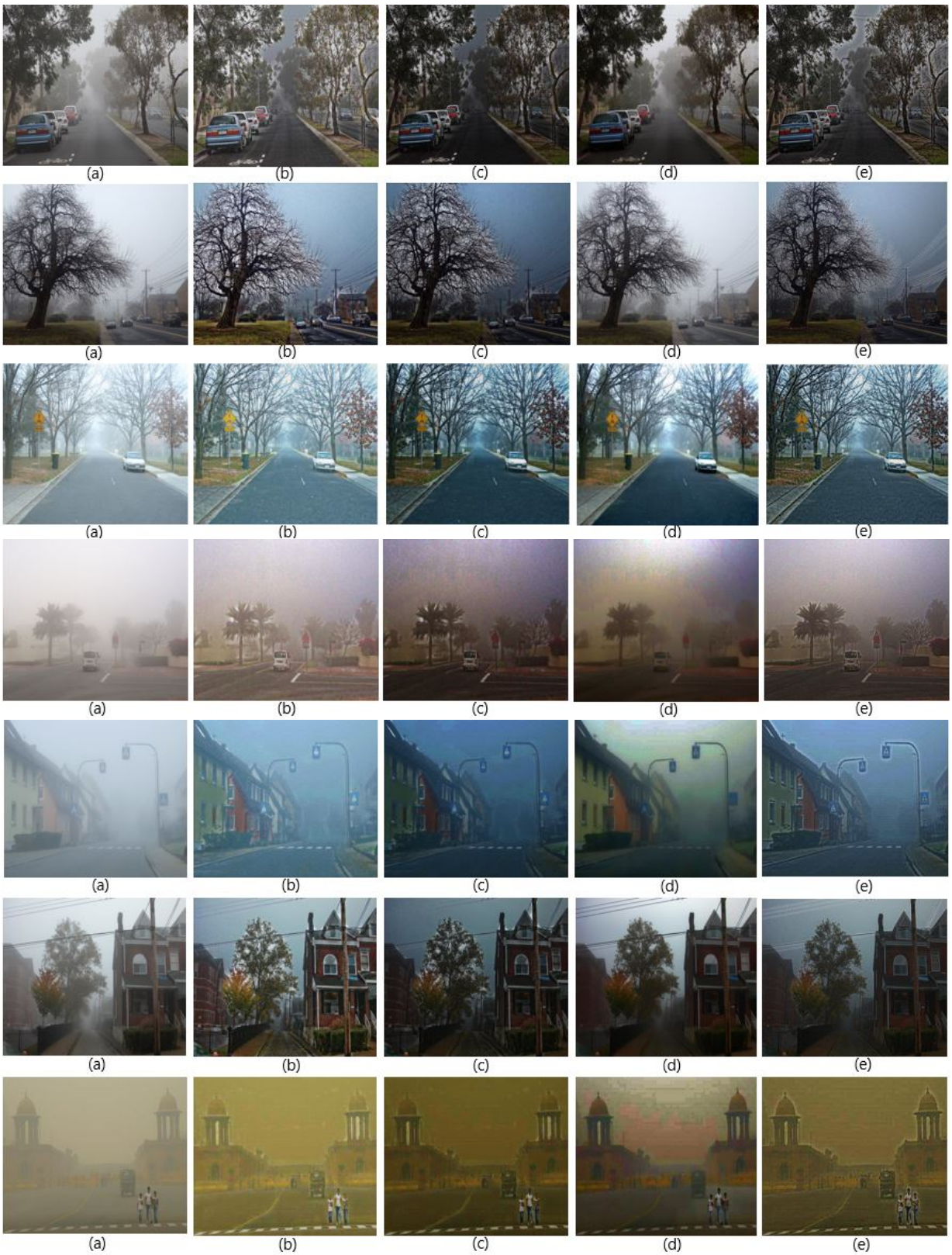

Figure 4.12: Comparisons of some defogging algorithms on real images captured from urban roads. (a) original images. (b) Tarel and Hautiere [176]. (c) Tarel and Hautiere [175]. (d) He et al. [89]. (e) our results.

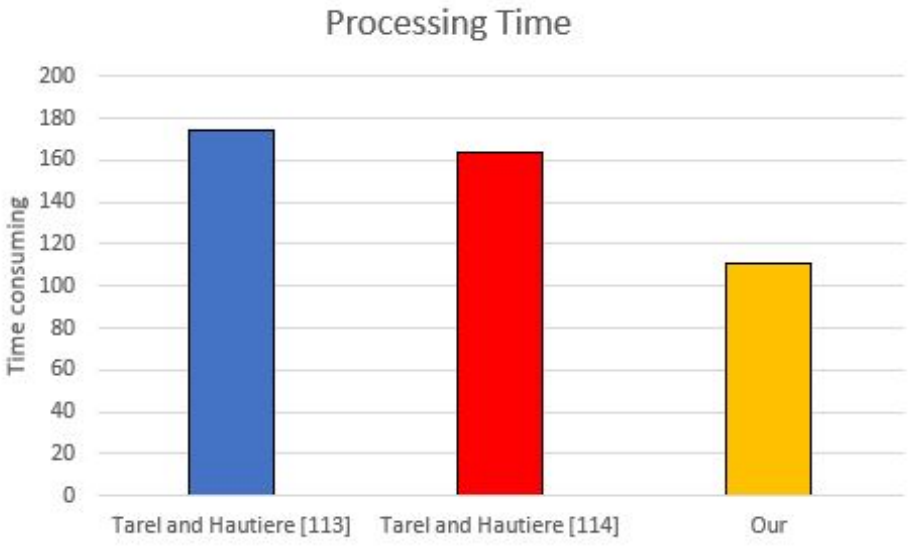

Figure 4.13: The computation time (s) of three defogging algorithms. Tarel and Hautiere [176], Tarel and Hautiere [175] and our work.

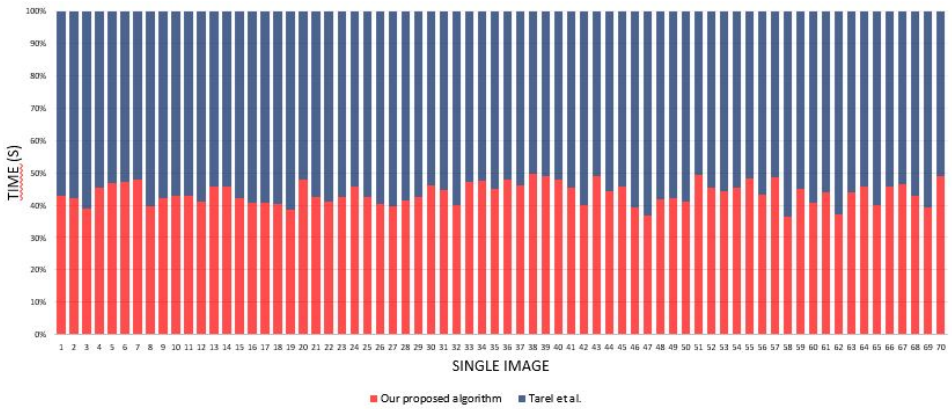

Figure 4.14: The comparison of computation time (s) of two defogging algorithms. Tarel and Hautiere [176]and our work.

Chapter 5

Conclusion and Future Work

5.1 Conclusion

In this thesis, we have proposed a visibility restoration (VR) approach from a single image captured in open air under foggy or hazy conditions. The proposed approach uses a combination of two major modules: 1) a DE module, and 2) a VR module. First, a refined transmission map is applied in the proposed DE module to eliminate the presence of block and halo artifacts in the obtained image by applying RF filter which preserves edge of the image with large jumps and corners with obtuse angle. Finally, the visibility of input foggy image is restored efficiently in the VR module, high-quality defogged results are obtained by the DE module. The proposed approach can be applied for camera-based ADAS systems without using any extra information as a particular filtering problem or inferring scene structure. We thus estimate the depth map of the scene based on recursive filtering in the transformed domain. The desirable feature of the proposed work is its speed which plays a main role in vehicle applications. It is noticable that the achieved results have high performance in achieving a similar or mostly superior results when compared to the state-of-the-art algorithms as illustrated in the experiments. Not only can the proposed approach tackle issues regarding complex structures, but it can also obtain pretty fast high-quality haze-free images compared to the method of He et al. [89]. In addition, the applied edge-preserving filter is a real-time filter with ability to preserve edges with large jumps and corners with obtuse angle. The main advantages of this filter is its speed and potential to save memory due to using of 1D operations, for example, one megapixel color images will be filtered in 0.007 seconds by this filter. Furthermore, filter parameters will not affect its computational cost. The regarding filter is able to work on color images at arbitrary sizes in real time as well [69]. The proposed visibility restoration approach is capable of handling both gray level or color images at arbitrary scales. It does not have any difficulties to restore the visibility of different scenes with highly or less structured such as cities, buildings, mountains and roads scenes.

In Chapter 1, first, ADAS systems with regarding its capabilities and structure and also the development of autonomous cars in academia and industry were reviewed. Since autonomous cars have become a favored research field recently, its potential to increase

safety and decrease the number of deaths and injuries resulted from road accidents every year all around the world was covered. Then some considerable problems corresponding to this technology were mentioned. By analyzing and considering these problems like the the low reliability, high expenses and lack of ability to restore the visibility of the scene under bad weather conditions, these problems are the driving force of our research into a visibility restoration framework for camera-based ADAS. Finally, the main contribution of proposed approach was provided and then the thesis outline was listed.

In Chapter 2, different approaches for removing fog from images captured under foggy or hazy weather conditions were summarized. These defogging methods were classified into three groups: 1) image restoration, 2) image enhancement, and 3) fusion-based. This chapter also specified defogging algorithms based on the required number of input images to remove fog, some methods require two or more images while some of them require only a single image. In addition, it was described that there are failures in algorithms which require two or more input images when scene are dynamic, specially for vehicle cameras. Also it was summarized that the image enhancement algorithms are only able to increase the contrast of the foggy image and can not restore foggy images. Lastly, a comparison between previous defogging approaches with considering different scenarios were performed. Therefore, it can be seen that visibility restoration algorithms from only a single image are the most efficient and appropriate technique to remove fog for vehicle applications.

In Chapter 3, the proposed method to restore the visibility of foggy image from a single image based on the estimation of depth map has been exhibited. Then two main module: 1) a DE module, and 2) a VR module were explained a framework of the proposed work. In DE module, the scene depth was estimated by using a dark channel prior method and RF filter and in VR module, the scene radiance of the scene was computed by the obtained the transmission map.

In Chapter 4, the experiment results were demonstrated and evaluated by full-reference and no-reference metrics. This chapter is organized in three sections, which covers the experimental platform and overview, objective and subjective quality assessment criterion, as well as visibility restoration performance. The proposed approach was compared with three state of the art algorithms 1) Tarel and Hautiere [176], 2) Tarel and Hautiere [175], and 3) He et al. [89] and the obtained results proved that the proposed method is pretty faster than these algorithms and has a high performance to preserve and restore edge of the image and also eliminate the generation of artifacts in the restored image.

5.2 Future Work

Some future work can be considered in order to improve and extend our work.

The proposed method is able to restore the visibility of image under homogeneous and heterogeneous fog which has better performance to restore homogeneous foggy image compared with heterogeneous fog which can be more worked on it. In addition, in order to assess the performance of visibility restoration algorithms, an appropriate dataset which contains adequate number of real and synthetic images with and without the presence

of fog is required. Therefore, experiments can be carried out to collect a dataset under different weather conditions coming with fog, such as rain and snow. Also, the illumination condition can have effect on the performance of visibility restoration algorithm. Therefore, in order to prove the impact of illumination on restoration process, daytime restored images should be compare to nighttime restored images which can be handled by considering captured images in nighttime. Basically, vehicle's application are real-time, which means the applied visibility enhancement algorithm in these applications should be fast enough in terms of time consumption. Therefore, implementing a real-time algorithm can be another consideration in the future work. Visibility restoration can be considered as pre-processing with detection of moving or stopped cars and pedestrians, to deliver adequate warning to driver when the distance is short between the driver and the pedestrian with respect to the driver's speed.

References

[1]

[2] Kaouther Abrougui, Azzedine Boukerche, and Richard Werner Nelem Pazzi. Design and evaluation of context-aware and location-based service discovery protocols for vehicular networks. *IEEE Transactions on Intelligent Transportation Systems*, 12(3):717–735, 2011.

[3] Osama Abumansoor and Azzedine Boukerche. A secure cooperative approach for nonline-of-sight location verification in vanet. *IEEE Transactions on Vehicular Technology*, 61(1):275–285, 2012.

[4] Andrew Adams, Jongmin Baek, and Myers Abraham Davis. Fast high-dimensional filtering using the permutohedral lattice. In *Computer Graphics Forum*, volume 29, pages 753–762. Wiley Online Library, 2010.

[5] Elie El Ajaltouni, Azzedine Boukerche, and Ming Zhang. An efficient dynamic load balancing scheme for distributed simulations on a grid infrastructure. In *Proceedings of the 2008 12th IEEE/ACM International Symposium on Distributed Simulation and Real-Time Applications*, pages 61–68. IEEE Computer Society, 2008.

[6] Codruta O Ancuti, Cosmin Ancuti, Chris Hermans, and Philippe Bekaert. A fast semi-inverse approach to detect and remove the haze from a single image. In *Asian Conference on Computer Vision*, pages 501–514. Springer, 2010.

[7] Codruta Orniana Ancuti and Cosmin Ancuti. Single image dehazing by multi-scale fusion. *IEEE Transactions on Image Processing*, 22(8):3271–3282, 2013.

[8] Codruta Orniana Ancuti, Cosmin Ancuti, and Philippe Bekaert. Effective single image dehazing by fusion. In *Image Processing (ICIP), 2010 17th IEEE International Conference on*, pages 3541–3544. IEEE, 2010.

[9] Cosmin Ancuti, Codruta Orniana Ancuti, Tom Haber, and Philippe Bekaert. Enhancing underwater images and videos by fusion. In *Computer Vision and Pattern Recognition (CVPR), 2012 IEEE Conference on*, pages 81–88. IEEE, 2012.

[10] Thanasis Antoniou, Ioannis Chatzigiannakis, George Mylonas, Sotiris Nikoletseas, and Azzedine Boukerche. A new energy efficient and fault-tolerant protocol for data

propagation in smart dust networks using varying transmission range. In *Proceedings of the 37th annual symposium on Simulation*, page 43. IEEE Computer Society, 2004.

[11] Athanasios Bamis, Azzedine Boukerche, Ioannis Chatzigiannakis, and Sotiris Nikoletseas. A mobility aware protocol synthesis for efficient routing in ad hoc mobile networks. *Computer Networks*, 52(1):130–154, 2008.

[12] Rodolfo Bezerra Batista, Azzedine Boukerche, and Alba Cristina Magalhaes Alves de Melo. A parallel strategy for biological sequence alignment in restricted memory space. *Journal of Parallel and Distributed Computing*, 68(4):548–561, 2008.

[13] A Boukerch, Li Xu, and Khalil El-Khatib. Trust-based security for wireless ad hoc and sensor networks. *Computer Communications*, 30(11-12):2413–2427, 2007.

[14] Azzedine Boukerche. *Handbook of algorithms for wireless networking and mobile computing*. Chapman and Hall/CRC, 2005.

[15] Azzedine Boukerche. *Algorithms and protocols for wireless sensor networks*, volume 62. John Wiley & Sons, 2008.

[16] Azzedine Boukerche, Sajal K Das, and Alessandro Fabbri. Swimnet: a scalable parallel simulation testbed for wireless and mobile networks. *Wireless Networks*, 7(5):467–486, 2001.

[17] Azzedine Boukerche, Sajal K Das, Alessandro Fabbri, and Oktay Yildiz. Exploiting model independence for parallel pcs network simulation. In *Parallel and Distributed Simulation, 1999. Proceedings. Thirteenth Workshop on*, pages 166–173. IEEE, 1999.

[18] Azzedine Boukerche and Caron Dzermajko. Performance evaluation of data distribution management strategies. *Concurrency and Computation: Practice and Experience*, 16(15):1545–1573, 2004.

[19] Azzedine Boukerche, Khalil El-Khatib, Li Xu, and Larry Korba. A novel solution for achieving anonymity in wireless ad hoc networks. In *Proceedings of the 1st ACM international workshop on Performance evaluation of wireless ad hoc, sensor, and ubiquitous networks*, pages 30–38. ACM, 2004.

[20] Azzedine Boukerche, Khalil El-Khatib, Li Xu, and Larry Korba. Sdar: a secure distributed anonymous routing protocol for wireless and mobile ad hoc networks. In *Local Computer Networks, 2004. 29th Annual IEEE International Conference on*, pages 618–624. IEEE, 2004.

[21] Azzedine Boukerche, Khalil El-Khatib, Li Xu, and Larry Korba. An efficient secure distributed anonymous routing protocol for mobile and wireless ad hoc networks. *computer communications*, 28(10):1193–1203, 2005.

[22] Azzedine Boukerche and Xin Fei. A coverage-preserving scheme for wireless sensor network with irregular sensing range. *Ad hoc networks*, 5(8):1303–1316, 2007.

[23] Azzedine Boukerche, Xin Fei, and Regina B Araujo. An optimal coverage-preserving scheme for wireless sensor networks based on local information exchange. *Computer Communications*, 30(14-15):2708–2720, 2007.

[24] Azzedine Boukerche, Sungbum Hong, and Tom Jacob. A distributed algorithm for dynamic channel allocation. *Mobile Networks and Applications*, 7(2):115–126, 2002.

[25] Azzedine Boukerche, Sungbum Hong, and Tom Jacob. An efficient synchronization scheme of multimedia streams in wireless and mobile systems. *IEEE transactions on Parallel and Distributed Systems*, 13(9):911–923, 2002.

[26] Azzedine Boukerche, Kathia Regina Lemos Jucá, João Bosco Sobral, and Mirela Sechi Moretti Annoni Notare. An artificial immune based intrusion detection model for computer and telecommunication systems. *Parallel Computing*, 30(5-6):629–646, 2004.

[27] Azzedine Boukerche, Renato B Machado, Kathia RL Jucá, João Bosco M Sobral, and Mirela SMA Notare. An agent based and biological inspired real-time intrusion detection and security model for computer network operations. *Computer Communications*, 30(13):2649–2660, 2007.

[28] Azzedine Boukerche, Anahit Martirosyan, and Richard Pazzi. An inter-cluster communication based energy aware and fault tolerant protocol for wireless sensor networks. *Mobile Networks and Applications*, 13(6):614–626, 2008.

[29] Azzedine Boukerche and Sotiris Nikoletseas. Protocols for data propagation in wireless sensor networks. In *Wireless communications systems and networks*, pages 23–51. Springer, 2004.

[30] Azzedine Boukerche and Mirela Sechi M Annoni Notare. Behavior-based intrusion detection in mobile phone systems. *Journal of Parallel and Distributed Computing*, 62(9):1476–1490, 2002.

[31] Azzedine Boukerche, Horacio ABF Oliveira, Eduardo F Nakamura, and Antonio AF Loureiro. Secure localization algorithms for wireless sensor networks. *IEEE Communications Magazine*, 46(4), 2008.

[32] Azzedine Boukerche, Richard Werner N Pazzi, and Regina B Araujo. Hpeq a hierarchical periodic, event-driven and query-based wireless sensor network protocol. In *null*, pages 560–567. IEEE, 2005.

[33] Azzedine Boukerche, Richard Werner Nelem Pazzi, and Regina Borges Araujo. A fast and reliable protocol for wireless sensor networks in critical conditions monitoring applications. In *Proceedings of the 7th ACM international symposium on Modeling, analysis and simulation of wireless and mobile systems*, pages 157–164. ACM, 2004.

[34] Azzedine Boukerche, Richard Werner Nelem Pazzi, and Regina Borges Araujo. Fault-tolerant wireless sensor network routing protocols for the supervision of context-aware

physical environments. *Journal of Parallel and Distributed Computing*, 66(4):586–599, 2006.

[35] Azzedine Boukerche and Yonglin Ren. A security management scheme using a novel computational reputation model for wireless and mobile ad hoc networks. In *Proceedings of the 5th ACM symposium on Performance evaluation of wireless ad hoc, sensor, and ubiquitous networks*, pages 88–95. ACM, 2008.

[36] Azzedine Boukerche and Yonglin Ren. A trust-based security system for ubiquitous and pervasive computing environments. *Computer Communications*, 31(18):4343–4351, 2008.

[37] Azzedine Boukerche and Yonglin Ren. A secure mobile healthcare system using trust-based multicast scheme. *IEEE Journal on Selected Areas in Communications*, 27(4), 2009.

[38] Azzedine Boukerche, Cristiano Rezende, and Richard W Pazzi. Improving neighbor localization in vehicular ad hoc networks to avoid overhead from periodic messages. In *Global Telecommunications Conference, 2009. GLOBECOM 2009. IEEE*, pages 1–6. IEEE, 2009.

[39] Azzedine Boukerche and Samer Samarah. A novel algorithm for mining association rules in wireless ad hoc sensor networks. *IEEE Transactions on Parallel and Distributed Systems*, 19(7):865–877, 2008.

[40] Azzedine Boukerche and Carl Tropper. A static partitioning and mapping algorithm for conservative parallel simulations. In *ACM SIGSIM Simulation Digest*, volume 24, pages 164–172. ACM, 1994.

[41] Azzedine Boukerche and Carl Tropper. A distributed graph algorithm for the detection of local cycles and knots. *IEEE Transactions on Parallel and Distributed Systems*, 9(8):748–757, 1998.

[42] Azzedine Boukerche and Damla Turgut. Secure time synchronization protocols for wireless sensor networks. *IEEE Wireless Communications*, 14(5), 2007.

[43] Azzedine Boukerche, Anis Zarrad, and Regina Araujo. A cross-layer approach-based gnutella for collaborative virtual environments over mobile ad hoc networks. *IEEE Transactions on Parallel and Distributed Systems*, 21(7):911–924, 2010.

[44] Christoph Busch and Eric Debes. Wavelet transform for analyzing fog visibility. *IEEE Intelligent Systems and Their Applications*, 13(6):66–71, 1998.

[45] Mathieu Carnec, Patrick Le Callet, and Dominique Barba. Objective quality assessment of color images based on a generic perceptual reduced reference. *Signal Processing: Image Communication*, 23(4):239–256, 2008.

[46] Seunghyuk Choi, Florian Thalmayr, Dominik Wee, and Florian Weig. Advanced driver-assistance systems: Challenges and opportunities ahead, 2016.

[47] CIE CIE. International lighting vocabulary. *Central Bureau of the Commission Internationale de lEclairage, Kegelgasse*, 27, 1989.

[48] Rodolfo WL Coutinho, Azzedine Boukerche, Luiz FM Vieira, and Antonio AF Loureiro. Gedar: geographic and opportunistic routing protocol with depth adjustment for mobile underwater sensor networks. In *Communications (ICC), 2014 IEEE International Conference on*, pages 251–256. IEEE, 2014.

[49] Rodolfo WL Coutinho, Azzedine Boukerche, Luiz FM Vieira, and Antonio AF Loureiro. Design guidelines for opportunistic routing in underwater networks. *IEEE Communications Magazine*, 54(2):40–48, 2016.

[50] Rodolfo WL Coutinho, Azzedine Boukerche, Luiz FM Vieira, and Antonio AF Loureiro. Geographic and opportunistic routing for underwater sensor networks. *IEEE Transactions on Computers*, 65(2):548–561, 2016.

[51] Antonio Criminisi, Toby Sharp, Carsten Rother, and Patrick Pérez. Geodesic image and video editing. *ACM Trans. Graph.*, 29(5):134–1, 2010.

[52] Horacio Antonio Braga Fernandes De Oliveira, Azzedine Boukerche, Eduardo Freire Nakamura, and Antonio Alfredo Ferreira Loureiro. An efficient directed localization recursion protocol for wireless sensor networks. *IEEE Transactions on Computers*, 58(5):677–691, 2009.

[53] Sabine Dippel, Martin Stahl, Rafael Wiemker, and Thomas Blaffert. Multiscale contrast enhancement for radiographies: Laplacian pyramid versus fast wavelet transform. *IEEE Transactions on medical imaging*, 21(4):343–353, 2002.

[54] Eric Dumont and Viola Cavallo. Extended photometric model of fog effects on road vision. *Transportation Research Record: Journal of the Transportation Research Board*, (1862):77–81, 2004.

[55] Frédo Durand and Julie Dorsey. Fast bilateral filtering for the display of high-dynamic-range images. In *ACM Transactions on Graphics (TOG)*, volume 21, pages 257–266. ACM, 2002.

[56] Theodore L Economopoulos, Pantelis A Asvestas, and George K Matsopoulos. Contrast enhancement of images using partitioned iterated function systems. *Image and vision computing*, 28(1):45–54, 2010.

[57] Mourad Elhadef, Azzedine Boukerche, and Hisham Elkadiki. Diagnosing mobile ad-hoc networks: two distributed comparison-based self-diagnosis protocols. In *Proceedings of the 4th ACM international workshop on Mobility management and wireless access*, pages 18–27. ACM, 2006.

[58] Mourad Elhadef, Azzedine Boukerche, and Hisham Elkadiki. Performance analysis of a distributed comparison-based self-diagnosis protocol for wireless ad-hoc networks. In *Proceedings of the 9th ACM international symposium on Modeling analysis and simulation of wireless and mobile systems*, pages 165–172. ACM, 2006.

[59] Mourad Elhadef, Azzedine Boukerche, and Hisham Elkadiki. A distributed fault identification protocol for wireless and mobile ad hoc networks. *Journal of Parallel and Distributed Computing*, 68(3):321–335, 2008.

[60] Shuai Fang, Jiqing Zhan, Yang Cao, and Ruizhong Rao. Improved single image dehazing using segmentation. In *Image Processing (ICIP), 2010 17th IEEE International Conference on*, pages 3589–3592. IEEE, 2010.

[61] Zeev Farbman, Raanan Fattal, and Dani Lischinski. Diffusion maps for edge-aware image editing. In *ACM Transactions on Graphics (TOG)*, volume 29, page 145. ACM, 2010.

[62] Zeev Farbman, Raanan Fattal, Dani Lischinski, and Richard Szeliski. Edge-preserving decompositions for multi-scale tone and detail manipulation. In *ACM Transactions on Graphics (TOG)*, volume 27, page 67. ACM, 2008.

[63] Raanan Fattal. Single image dehazing. *ACM Transactions on Graphics (TOG)*, 27(3):72, 2008.

[64] Raanan Fattal. Edge-avoiding wavelets and their applications. *ACM Transactions on Graphics (TOG)*, 28(3):22, 2009.

[65] Chen Feng, Shaojie Zhuo, Xiaopeng Zhang, Liang Shen, and Sabine Susstrunk. Near-infrared guided color image dehazing. In *Image Processing (ICIP), 2013 20th IEEE International Conference on*, pages 2363–2367. IEEE, 2013.

[66] Xueyang Fu, Yue Huang, Delu Zeng, Xiao-Ping Zhang, and Xinghao Ding. A fusion-based enhancing approach for single sandstorm image. In *Multimedia Signal Processing (MMSP), 2014 IEEE 16th International Workshop on*, pages 1–5. IEEE, 2014.

[67] Brian V Funt, Florian Ciurea, and John J McCann. Retinex in matlab tm. *Journal of electronic imaging*, 13(1):48–58, 2004.

[68] Yin Gao, Lijun Yun, Junsheng Shi, Feiyan Chen, and Liansha Lei. Enhancement msrcr algorithm of color fog image based on the adaptive scale. In *Sixth International Conference on Digital Image Processing (ICDIP 2014)*, volume 9159, page 91591B. International Society for Optics and Photonics, 2014.

[69] Eduardo SL Gastal and Manuel M Oliveira. Domain transform for edge-aware image and video processing. In *ACM Transactions on Graphics (ToG)*, volume 30, page 69. ACM, 2011.

[70] Kristofor Gibson, Dũng Võ, and Truong Nguyen. An investigation in dehazing compressed images and video. In *OCEANS 2010*, pages 1–8. IEEE, 2010.

[71] Kristofor B Gibson and Truong Q Nguyen. On the effectiveness of the dark channel prior for single image dehazing by approximating with minimum volume ellipsoids. In *Acoustics, Speech and Signal Processing (ICASSP), 2011 IEEE International Conference on*, pages 1253–1256. IEEE, 2011.

[72] Kristofor B Gibson and Truong Q Nguyen. Fast single image fog removal using the adaptive wiener filter. In *Image Processing (ICIP), 2013 20th IEEE International Conference on*, pages 714–718. IEEE, 2013.

[73] Kristofor B Gibson, Dung T Vo, and Truong Q Nguyen. An investigation of dehazing effects on image and video coding. *IEEE transactions on image processing*, 21(2):662–673, 2012.

[74] Rafael C Gonzalez and Richard E Woods. Image processing. *Digital image processing*, 2, 2007.

[75] Dominique Gruyer, C Royere, Nicolas du Lac, G Michel, and JM Blosseville. Sivic and rtmaps, interconnected platforms for the conception and the evaluation of driving assistance systems. In *Proceedings of the its world congress*, volume 10, 2006.

[76] Fan Guo, Zi-xing Cai, Bin Xie, and Jin Tang. Review and prospect of image dehazing techniques. *Jisuanji Yingyong/ Journal of Computer Applications*, 30(9):2417–2421, 2010.

[77] Fan Guo, Hui Peng, and Jin Tang. A new restoration algorithm for single image defogging. In *Chinese Conference on Pattern Recognition*, pages 169–178. Springer, 2014.

[78] Fan Guo, Jin Tang, and Zixing Cai. Fusion strategy for single image dehazing. *International Journal of Digital Content Technology and its Applications*, 7(1):19, 2013.

[79] Umar Zakir Abdul Hamid, Konstantin Pushkin, Hairi Zamzuri, Djahid Gueraiche, and Mohd Azizi Abdul Rahman. Current collision mitigation technologies for advanced driver assistance systems : A survey. *PERINTIS eJournal*, 6(2), 2016.

[80] Nicolas Hautiere and Didier Aubert. Contrast restoration of foggy images through use of an onboard camera. In *Intelligent Transportation Systems, 2005. Proceedings. 2005 IEEE*, pages 601–606. IEEE, 2005.

[81] Nicolas Hautière and Didier Aubert. Visible edges thresholding: a hvs based approach. In *Pattern Recognition, 2006. ICPR 2006. 18th International Conference on*, volume 2, pages 155–158. IEEE, 2006.

[82] Nicolas Hautière, Raphaël Labayrade, and Didier Aubert. Real-time disparity contrast combination for onboard estimation of the visibility distance. *IEEE Transactions on Intelligent Transportation Systems*, 7(2):201–212, 2006.

[83] Nicolas Hautière, Raphaël Labayrade, Clément Boussard, Jean-Philippe Tarel, and Didier Aubert. Perception through scattering media for autonomous vehicles. *Autonomous Robots Research Advances*, 8:223–267, 2008.

[84] Nicolas Hautière, Jean-Philippe Tarel, and Didier Aubert. Towards fog-free in-vehicle vision systems through contrast restoration. In *Computer Vision and Pattern Recognition, 2007. CVPR'07. IEEE Conference on*, pages 1–8. IEEE, 2007.

[85] Nicolas Hautière, Jean-Philippe Tarel, and Didier Aubert. Free space detection for autonomous navigation in daytime foggy weather. In *MVA*, pages 501–504, 2009.

[86] Nicolas Hautière, Jean-Philippe Tarel, and Didier Aubert. Mitigation of visibility loss for advanced camera-based driver assistance. *IEEE Transactions on Intelligent Transportation Systems*, 11(2):474–484, 2010.

[87] Nicolas Hautière, Jean-Philippe Tarel, Didier Aubert, and Eric Dumont. Blind contrast enhancement assessment by gradient ratioing at visible edges. *Image Analysis & Stereology*, 27(2):87–95, 2011.

[88] Nicolas Hautiére, Jean-Philippe Tarel, Jean Lavenant, and Didier Aubert. Automatic fog detection and estimation of visibility distance through use of an onboard camera. *Machine Vision and Applications*, 17(1):8–20, 2006.

[89] Kaiming He, Jian Sun, and Xiaoou Tang. Single image haze removal using dark channel prior. *IEEE transactions on pattern analysis and machine intelligence*, 33(12):2341–2353, 2011.

[90] Kaiming He, Jian Sun, and Xiaoou Tang. Guided image filtering. *IEEE transactions on pattern analysis and machine intelligence*, 35(6):1397–1409, 2013.

[91] Xiaoyan He, Jianxu Mao, Zewen Liu, Jiujiang Zhou, and Yajing Hua. A fast algorithm for image defogging. In *Chinese Conference on Pattern Recognition*, pages 149–158. Springer, 2014.

[92] Wei-wei HU, Rong-gui WANG, Shuai Fang, and Qiong HU. Retinex algorithm for image enhancement based on bilateral filtering [j]. *Journal of engineering graphics*, 2:104–109, 2010.

[93] Shih-Chia Huang, Bo-Hao Chen, and Wei-Jheng Wang. Visibility restoration of single hazy images captured in real-world weather conditions. *IEEE Transactions on Circuits and Systems for Video Technology*, 24(10):1814–1824, 2014.

[94] Anya Hurlbert. Formal connections between lightness algorithms. *JOSA A*, 3(10):1684–1693, 1986.

[95] Humor Hwang and Richard A Haddad. Adaptive median filters: new algorithms and results. *IEEE Transactions on image processing*, 4(4):499–502, 1995.

[96] Aapo Hyvärinen and Erkki Oja. Independent component analysis: algorithms and applications. *Neural networks*, 13(4-5):411–430, 2000.

[97] Sermsak Jaruwatanadilok, Akira Ishimaru, and Yasuo Kuga. Optical imaging through clouds and fog. *IEEE Transactions on Geoscience and remote Sensing*, 41(8):1834–1843, 2003.

[98] Jianfang Jia and Hong Yue. A wavelet-based approach to improve foggy image clarity. *IFAC Proceedings Volumes*, 47(3):930–935, 2014.

[99] Daniel J Jobson, Zia-ur Rahman, and Glenn A Woodell. Retinex image processing: Improved fidelity to direct visual observation. In *Color and Imaging Conference*, volume 1996, pages 124–125. Society for Imaging Science and Technology, 1996.

[100] Daniel J Jobson, Zia-ur Rahman, and Glenn A Woodell. A multiscale retinex for bridging the gap between color images and the human observation of scenes. *IEEE Transactions on Image processing*, 6(7):965–976, 1997.

[101] Daniel J Jobson, Zia-ur Rahman, and Glenn A Woodell. Properties and performance of a center/surround retinex. *IEEE transactions on image processing*, 6(3):451–462, 1997.

[102] Daniel J Jobson, Zia-ur Rahman, Glenn A Woodell, and Glenn D Hines. A comparison of visual statistics for the image enhancement of foresite aerial images with those of major image classes. In *Visual Information Processing XV*, volume 6246, page 624601. International Society for Optics and Photonics, 2006.

[103] Daniel J Jobson and Glenn A Woodell. Properties of a center/surround retinex: Part 2. surround design. *NASA Technical Memorandum*, 110188:15, 1995.

[104] WANG Li Jun and ZHU Rong. Image defogging algorithm of single color image based on wavelet transform and histogram equalization. *Applied Mathematical Sciences*, 7(79):3913–3921, 2013.

[105] Harpoonamdeep Kaur and Rajiv Mahajan. A review on various visibility restoration techniques. *International Journal of Advanced Research in Computer and Communication Engineering*, 3(5), 2014.

[106] Joung-Youn Kim, Lee-Sup Kim, and Seung-Ho Hwang. An advanced contrast enhancement using partially overlapped sub-block histogram equalization. *IEEE transactions on circuits and systems for video technology*, 11(4):475–484, 2001.

[107] Mary Kim and Min Gyo Chung. Recursively separated and weighted histogram equalization for brightness preservation and contrast enhancement. *IEEE Transactions on Consumer Electronics*, 54(3), 2008.

[108] Tae Keun Kim, Joon Ki Paik, and Bong Soon Kang. Contrast enhancement system using spatially adaptive histogram equalization with temporal filtering. *IEEE Transactions on Consumer Electronics*, 44(1):82–87, 1998.

[109] S-J Ko and Yong Hoon Lee. Center weighted median filters and their applications to image enhancement. *IEEE transactions on circuits and systems*, 38(9):984–993, 1991.

[110] Harald Koschmieder. Theorie der horizontalen sichtweite. *Beitrage zur Physik der freien Atmosphare*, pages 33–53, 1924.

[111] Louis Kratz and Ko Nishino. Factorizing scene albedo and depth from a single foggy image. In *Computer Vision, 2009 IEEE 12th International Conference on*, pages 1701–1708. IEEE, 2009.

[112] Taek Mu Kwon. Atmospheric visibility measurements using video cameras: Relative visibility. 2004.

[113] Edwin H Land. Recent advances in retinex theory and some implications for cortical computations: color vision and the natural image. *Proceedings of the National Academy of Sciences*, 80(16):5163–5169, 1983.

[114] Edwin H Land and John J McCann. Lightness and retinex theory. *Josa*, 61(1):1–11, 1971.

[115] J Lavenant, JP Tarel, and D Aubert. Procédé de détermination de la distance de visibilité et procédé de détermination de la présence dun brouillard. *French patent*, 201822, 2002.

[116] Yeejin Lee, Kristofor B Gibson, Zucheul Lee, and Truong Q Nguyen. Stereo image defogging. In *Image Processing (ICIP), 2014 IEEE International Conference on*, pages 5427–5431. IEEE, 2014.

[117] Yong Lee and S Kassam. Generalized median filtering and related nonlinear filtering techniques. *IEEE Transactions on Acoustics, Speech, and Signal Processing*, 33(3):672–683, 1985.

[118] Gun Li, JF Wu, and ZY Lei. Research progress of image haze grade evaluation and dehazing technology. *Laser J.*, 35(9):1–6, 2014.

[119] Li Li, Wei-qi Jin, Chao Xu, and Xia Wang. Color image enhancement using nonlinear sub-block overlapping local equilibrium algorithm under fog and haze weather conditions. *Trans. Beijing Inst. Technol*, 33(5):516–522, 2013.

[120] Zheqi Lin and Xuansheng Wang. Dehazing for image and video using guided filter. *Open J. Appl. Sci*, 2(4B):123–127, 2012.

[121] Anders Lindgren, Fang Chen, Patrick W Jordan, and Haixin Zhang. Requirements for the design of advanced driver assistance systems-the differences between swedish and chinese drivers. *International Journal of Design*, 2(2), 2008.

[122] Zhongli Ma, Jie Wen, Quanyong Liu, and Guanjun Tuo. Near-infrared and visible light image fusion algorithm for face recognition. *Journal of Modern Optics*, 62(9):745–753, 2015.

[123] John McCann. Lessons learned from mondrians applied to real images and color gamuts. In *Color and imaging conference*, volume 1999, pages 1–8. Society for Imaging Science and Technology, 1999.

[124] Earl J McCartney. Optics of the atmosphere: scattering by molecules and particles. *New York, John Wiley and Sons, Inc., 1976. 421 p.*, 1976.

[125] Gaofeng Meng, Ying Wang, Jiangyong Duan, Shiming Xiang, and Chunhong Pan. Efficient image dehazing with boundary constraint and contextual regularization. In *Computer Vision (ICCV), 2013 IEEE International Conference on*, pages 617–624. IEEE, 2013.

[126] WEK Middleton. l952: Vision through the atmosphere.

[127] Charlie Miller and Chris Valasek. A survey of remote automotive attack surfaces. *black hat USA*, 2014, 2014.

[128] John Miller. Self-driving car technologu's benefits, potential risks, and solutions. *The Energy Collective, theenergycollective. com*, pages 1–7, 2014.

[129] O Miller. Robotic cars and their new crime paradigms. *LinkedIn Pulse, Sept*, 3, 2014.

[130] Daisuke Miyazaki, Daisuke Akiyama, Masashi Baba, Ryo Furukawa, Shinsaku Hiura, and Naoki Asada. Polarization-based dehazing using two reference objects. In *Computer Vision Workshops (ICCVW), 2013 IEEE International Conference on*, pages 852–859. IEEE, 2013.

[131] Andrew Moore, John Allman, and Rodney M Goodman. A real-time neural system for color constancy. *IEEE Transactions on Neural networks*, 2(2):237–247, 1991.

[132] Einav Namer and Yoav Y Schechner. Advanced visibility improvement based on polarization filtered images. In *Polarization Science and Remote Sensing II*, volume 5888, page 588805. International Society for Optics and Photonics, 2005.

[133] Srinivasa G Narasimhan and Shree K Nayar. Chromatic framework for vision in bad weather. In *Computer Vision and Pattern Recognition, 2000. Proceedings. IEEE Conference on*, volume 1, pages 598–605. IEEE, 2000.

[134] Srinivasa G Narasimhan and Shree K Nayar. Removing weather effects from monochrome images. In *Computer Vision and Pattern Recognition, 2001. CVPR 2001. Proceedings of the 2001 IEEE Computer Society Conference on*, volume 2, pages II–II. IEEE, 2001.

[135] Srinivasa G Narasimhan and Shree K Nayar. Vision and the atmosphere. *International Journal of Computer Vision*, 48(3):233–254, 2002.

[136] Srinivasa G. Narasimhan and Shree K. Nayar. Contrast restoration of weather degraded images. *IEEE transactions on pattern analysis and machine intelligence*, 25(6):713–724, 2003.

[137] Srinivasa G Narasimhan and Shree K Nayar. Interactive (de) weathering of an image using physical models. In *IEEE Workshop on color and photometric Methods in computer Vision*, volume 6, page 1. France, 2003.

[138] Srinivasa G Narasimhan, Chi Wang, and Shree K Nayar. All the images of an outdoor scene. In *European conference on computer vision*, pages 148–162. Springer, 2002.

[139] Shree K Nayar and Srinivasa G Narasimhan. Vision in bad weather. In *Computer Vision, 1999. The Proceedings of the Seventh IEEE International Conference on*, volume 2, pages 820–827. IEEE, 1999.

[140] Ko Nishino, Louis Kratz, and Stephen Lombardi. Bayesian defogging. *International journal of computer vision*, 98(3):263–278, 2012.

[141] John P Oakley, BL Satherley, Chris G Harrison, and Costas S Xydeas. Enhancement of image sequences from a forward-looking airborne camera. In *Image and Video Processing IV*, volume 2666, pages 266–277. International Society for Optics and Photonics, 1996.

[142] John P Oakley and Brenda L Satherley. Improving image quality in poor visibility conditions using a physical model for contrast degradation. *IEEE transactions on image processing*, 7(2):167–179, 1998.

[143] Horacio ABF Oliveira, Eduardo F Nakamura, Antonio AF Loureiro, and Azzedine Boukerche. Error analysis of localization systems for sensor networks. In *Proceedings of the 13th annual ACM international workshop on Geographic information systems*, pages 71–78. ACM, 2005.

[144] Sylvain Paris and Frédo Durand. A fast approximation of the bilateral filter using a signal processing approach. *International journal of computer vision*, 81(1):24–52, 2009.

[145] Dubok Park, David K Han, and Hanseok Ko. Single image haze removal with wls-based edge-preserving smoothing filter. In *Acoustics, Speech and Signal Processing (ICASSP), 2013 IEEE International Conference on*, pages 2469–2473. IEEE, 2013.

[146] Omprakash Patel, Yogendra PS Maravi, and Sanjeev Sharma. A comparative study of histogram equalization based image enhancement techniques for brightness preservation and contrast enhancement. *arXiv preprint arXiv:1311.4033*, 2013.

[147] Aneesh Paul, Rohan Chauhan, Rituraj Srivastava, and Mriganka Baruah. Advanced driver assistance systems. Technical report, SAE Technical Paper, 2016.

[148] Richard W Pazzi and Azzedine Boukerche. Propane: A progressive panorama streaming protocol to support interactive 3d virtual environment exploration on graphics-constrained devices. *ACM Transactions on Multimedia Computing, Communications, and Applications (TOMM)*, 11(1):5, 2014.

[149] Richard WN Pazzi and Azzedine Boukerche. Mobile data collector strategy for delay-sensitive applications over wireless sensor networks. *Computer Communications*, 31(5):1028–1039, 2008.

[150] Soo-Chang Pei and Tzu-Yen Lee. Nighttime haze removal using color transfer pre-processing and dark channel prior. In *Image Processing (ICIP), 2012 19th IEEE International Conference on*, pages 957–960. IEEE, 2012.

[151] Patrick Perez et al. *Markov random fields and images*. IRISA, 1998.

[152] Ana Belén Petro, Catalina Sbert, and Jean-Michel Morel. Multiscale retinex. *Image Processing On Line*, pages 71–88, 2014.

[153] Dean Pomerleau. Visibility estimation from a moving vehicle using the ralph vision system. In *Intelligent Transportation System, 1997. ITSC'97., IEEE Conference on*, pages 906–911. IEEE, 1997.

[154] Y Qu. Study of removing fog from images based on moving mask. *Comput. Eng. Appl.*, 49(24):186–190, 2013.

[155] Zia-ur Rahman, Daniel J Jobson, and Glenn A Woodell. Multi-scale retinex for color image enhancement. In *Image Processing, 1996. Proceedings., International Conference on*, volume 3, pages 1003–1006. IEEE, 1996.

[156] Zia-ur Rahman, Daniel J Jobson, and Glenn A Woodell. Multiscale retinex for color rendition and dynamic range compression. In *Applications of Digital Image Processing XIX*, volume 2847, pages 183–192. International Society for Optics and Photonics, 1996.

[157] Zia-ur Rahman, Daniel J Jobson, and Glenn A Woodell. Retinex processing for automatic image enhancement. *Journal of Electronic Imaging*, 13(1):100–111, 2004.

[158] Zia-ur Rahman, Daniel J Jobson, Glenn A Woodell, and Glenn D Hines. Automated, on-board terrain analysis for precision landings. In *Visual Information Processing XV*, volume 6246, page 62460J. International Society for Optics and Photonics, 2006.

[159] C Ramya and Dr S Subha Rani. Contrast enhancement for fog degraded video sequences using bpdfhe. *Int. J. Comput. Sci. Inf. Technol*, 3(2):3463–3468, 2012.

[160] Yonglin Ren and Azzedine Boukerche. Modeling and managing the trust for wireless and mobile ad hoc networks. In *Communications, 2008. ICC'08. IEEE International Conference on*, pages 2129–2133. IEEE, 2008.

[161] Cristiano G Rezende, Azzedine Boukerche, Heitor S Ramos, and Antonio AF Loureiro. A reactive and scalable unicast solution for video streaming over vanets. *IEEE Trans. Computers*, 64(3):614–626, 2015.

[162] Ann Marie Rohaly, John Libert, Philip Corriveau, Arthur Webster, et al. Final report from the video quality experts group on the validation of objective models of video quality assessment. *ITU-T Standards Contribution COM*, 1:9–80, 2000.

[163] Zhu Rong and Wang Li Jun. Improved wavelet transform algorithm for single image dehazing. *Optik-International Journal for Light and Electron Optics*, 125(13):3064–3066, 2014.

[164] Samer Samarah, Muhannad Al-Hajri, and Azzedine Boukerche. A predictive energy-efficient technique to support object-tracking sensor networks. *IEEE Transactions on Vehicular Technology*, 60(2):656–663, 2011.

[165] János Schanda. The concept of colour rendering revisited. In *Conference on Colour in Graphics, Imaging, and Vision*, volume 2002, pages 37–41. Society for Imaging Science and Technology, 2002.

[166] Lex Schaul, Clément Fredembach, and Sabine Süsstrunk. Color image dehazing using the near-infrared. In *Image Processing (ICIP), 2009 16th IEEE International Conference on*, pages 1629–1632. IEEE, 2009.

[167] Yoav Y Schechner, Srinivasa G Narasimhan, and Shree K Nayar. Instant dehazing of images using polarization. In *Computer Vision and Pattern Recognition, 2001. CVPR 2001. Proceedings of the 2001 IEEE Computer Society Conference on*, volume 1, pages I–I. IEEE, 2001.

[168] Yoav Y Schechner, Srinivasa G Narasimhan, and Shree K Nayar. Polarization-based vision through haze. *Applied optics*, 42(3):511–525, 2003.

[169] Ming-Jung Seow and Vijayan K Asari. Ratio rule and homomorphic filter for enhancement of digital colour image. *Neurocomputing*, 69(7-9):954–958, 2006.

[170] Ruchika Sharma and Vinay Chopra. A review on different image dehazing methods. *International Journal of Computer Engineering and Applications*, 6(3), 2014.

[171] Hamid R Sheikh, Alan C Bovik, and Lawrence Cormack. No-reference quality assessment using natural scene statistics: Jpeg2000. *IEEE Transactions on Image Processing*, 14(11):1918–1927, 2005.

[172] Sarit Shwartz, Einav Namer, and Yoav Y Schechner. Blind haze separation. In *Computer Vision and Pattern Recognition, 2006 IEEE Computer Society Conference on*, volume 2, pages 1984–1991. IEEE, 2006.

[173] Robby T Tan. Visibility in bad weather from a single image. In *Computer Vision and Pattern Recognition, 2008. CVPR 2008. IEEE Conference on*, pages 1–8. IEEE, 2008.

[174] Ketan Tang, Jianchao Yang, and Jue Wang. Investigating haze-relevant features in a learning framework for image dehazing. In *Proceedings of the IEEE Conference on Computer Vision and Pattern Recognition*, pages 2995–3000, 2014.

[175] Jean-Philippe Tarel, Nicholas Hautiere, Laurent Caraffa, Aurélien Cord, Houssam Halmaoui, and Dominique Gruyer. Vision enhancement in homogeneous and heterogeneous fog. *IEEE Intelligent Transportation Systems Magazine*, 4(2):6–20, 2012.

[176] Jean-Philippe Tarel and Nicolas Hautiere. Fast visibility restoration from a single color or gray level image. In *Computer Vision, 2009 IEEE 12th International Conference on*, pages 2201–2208. IEEE, 2009.

[177] Jean-Philippe Tarel, Nicolas Hautiere, Aurélien Cord, Dominique Gruyer, and Houssam Halmaoui. Improved visibility of road scene images under heterogeneous fog. In *Intelligent Vehicles Symposium (IV), 2010 IEEE*, pages 478–485. IEEE, 2010.

[178] Carlo Tomasi and Roberto Manduchi. Bilateral filtering for gray and color images. In *Computer Vision, 1998. Sixth International Conference on*, pages 839–846. IEEE, 1998.

[179] Tali Treibitz and Yoav Y Schechner. Polarization: Beneficial for visibility enhancement? In *Computer Vision and Pattern Recognition, 2009. CVPR 2009. IEEE Conference on*, pages 525–532. IEEE, 2009.

[180] Tali Treibitz and Yoav Y Schechner. Recovery limits in pointwise degradation. In *Computational Photography (ICCP), 2009 IEEE International Conference on*, pages 1–8. IEEE, 2009.

[181] Abhishek Kumar Tripathi and Sudipta Mukhopadhyay. Removal of fog from images: A review. *IETE Technical Review*, 29(2):148–156, 2012.

[182] Min Wang and Shu-dao Zhou. The study of color image defogging based on wavelet transform and single scale retinex. In *International Symposium on Photoelectronic Detection and Imaging 2011: Advances in Imaging Detectors and Applications*, volume 8194, page 81940F. International Society for Optics and Photonics, 2011.

[183] Wei-Jheng Wang, Bo-Hao Chen, and Shih-Chia Huang. A novel visibility restoration algorithm for single hazy images. In *Systems, Man, and Cybernetics (SMC), 2013 IEEE International Conference on*, pages 847–851. IEEE, 2013.

[184] Yuan-Kai Wang and Ching-Tang Fan. Single image defogging by multiscale depth fusion. *IEEE Transactions on image processing*, 23(11):4826–4837, 2014.

[185] Zhou Wang and Alan C Bovik. A universal image quality index. *IEEE signal processing letters*, 9(3):81–84, 2002.

[186] Zhou Wang, Alan C Bovik, Hamid R Sheikh, and Eero P Simoncelli. Image quality assessment: from error visibility to structural similarity. *IEEE transactions on image processing*, 13(4):600–612, 2004.

[187] Yang Wanting, Wang Ronggui, Fang Shuai, and Zhang Xuan. Variable filter retinex algorithm for foggy image enhancement [j]. *Journal of Computer-Aided Design & Computer Graphics*, 6(010), 2010.

[188] Ryan Whitwam. How googles self-driving cars detect and avoid obstacles. *Extreme Tech.*, 2014.

[189] Di Wu and Qing-song Zhu. The latest research progress of image dehazing. *Acta Automatica Sinica*, 41(2):221–239, 2015.

[190] Chunxia Xiao and Jiajia Gan. Fast image dehazing using guided joint bilateral filter. *The Visual Computer*, 28(6-8):713–721, 2012.

[191] Bin Xie, Fan Guo, and Zixing Cai. Improved single image dehazing using dark channel prior and multi-scale retinex. In *Intelligent System Design and Engineering Application (ISDEA), 2010 International Conference on*, volume 1, pages 848–851. IEEE, 2010.

[192] Zhu Xizhi. The application of wavelet transform in digital image processing. In *MultiMedia and Information Technology, 2008. MMIT'08. International Conference on*, pages 326–329. IEEE, 2008.

[193] Yong Xu, Jie Wen, Lunke Fei, and Zheng Zhang. Review of video and image defogging algorithms and related studies on image restoration and enhancement. *IEEE Access*, 4:165–188, 2016.

[194] Zhiyuan Xu, Xiaoming Liu, and Xiaonan Chen. Fog removal from video sequences using contrast limited adaptive histogram equalization. In *Computational Intelligence and Software Engineering, 2009. CiSE 2009. International Conference on*, pages 1–4. IEEE, 2009.

[195] Garima Yadav, Saurabh Maheshwari, and Anjali Agarwal. Fog removal techniques from images: A comparative review and future directions. In *Signal Propagation and Computer Technology (ICSPCT), 2014 International Conference on*, pages 44–52. IEEE, 2014.

[196] Qingxiong Yang, Kar-Han Tan, and Narendra Ahuja. Real-time o (1) bilateral filtering. In *Computer Vision and Pattern Recognition, 2009. CVPR 2009. IEEE Conference on*, pages 557–564. IEEE, 2009.

[197] Yanjing Yang, Zhizhong Fu, Xinyu Li, Chang Shu, and Xiaofeng Li. A novel single image dehazing method. In *Computational Problem-solving (ICCP), 2013 International Conference on*, pages 275–278. IEEE, 2013.

[198] Yitzhak Yitzhaky, Itai Dror, and Norman S Kopeika. Restoration of atmospherically blurred images according to weather-predicted atmospheric modulation transfer functions. *Optical Engineering*, 36(11):3064–3073, 1997.

[199] Maram Bani Younes and Azzedine Boukerche. Intelligent traffic light controlling algorithms using vehicular networks. *IEEE transactions on Vehicular Technology*, 65(8):5887–5899, 2016.

[200] Jing Yu, Chuangbai Xiao, and Dapeng Li. Physics-based fast single image fog removal. In *Signal Processing (ICSP), 2010 IEEE 10th International Conference on*, pages 1048–1052. IEEE, 2010.

[201] Jing Yu, Dong-bin Xu, and Qing-min Liao. Image defogging: a survey. *Journal of Image and Graphics*, 16(9):1561–1576, 2011.

[202] Xiaoliang Yu, Chuangbai Xiao, Mike Deng, and Li Peng. A classification algorithm to distinguish image as haze or non-haze. In *Image and Graphics (ICIG), 2011 Sixth International Conference on*, pages 286–289. IEEE, 2011.

[203] Benjamin Zhang. Autonomous cars could save the us $ 1.3 trillion dollars a year. *Business Insider*, 2014.

[204] Erhu Zhang, Kaihui Lv, Yongchao Li, and Jinghong Duan. A fast video image defogging algorithm based on dark channel prior. In *Image and Signal Processing (CISP), 2013 6th International Congress on*, volume 1, pages 219–223. IEEE, 2013.

[205] Qiang Zhang and Xiaorun Li. Fast image dehazing using guided filter. In *Communication Technology (ICCT), 2015 IEEE 16th International Conference on*, pages 182–185. IEEE, 2015.

[206] Zheng Zhang, Yong Xu, Jian Yang, Xuelong Li, and David Zhang. A survey of sparse representation: algorithms and applications. *IEEE access*, 3:490–530, 2015.

[207] Zhenxia Zhang, Azzedine Boukerche, and Richard Pazzi. A novel multi-hop clustering scheme for vehicular ad-hoc networks. In *Proceedings of the 9th ACM international symposium on Mobility management and wireless access*, pages 19–26. ACM, 2011.

[208] Zhenxia Zhang, Richard W Pazzi, and Azzedine Boukerche. A mobility management scheme for wireless mesh networks based on a hybrid routing protocol. *Computer Networks*, 54(4):558–572, 2010.

[209] Meiyuan Zhao. Advanced driver assistant system, threats, requirements, security solutions. *Intel Labs*, 2015.

[210] Xiaoxia Zhao, Rulin Wang, and Yang Qiu. An enhancement method of fog-degraded images. In *Second International Conference on Digital Image Processing*, volume 7546, page 75461S. International Society for Optics and Photonics, 2010.

[211] Ma Zhongli and Wen Jie. Single-scale retinex sea fog removal algo-rithm fused the edge information. *Journal of Computer-Aided Design & Computer Graphics*, 27(2):217–225, 2015.

[212] Pu-cheng Zhou, Feng Wang, Hong-kun Zhang, and Mo-gen Xue. Camouflaged target detection based on visible and near infrared polarimetric imagery fusion. In *International Symposium on Photoelectronic Detection and Imaging 2011: Advances in Imaging Detectors and Applications*, volume 8194, page 81940Y. International Society for Optics and Photonics, 2011.

[213] Karel Zuiderveld. Contrast limited adaptive histogram equalization. *Graphics gems*, pages 474–485, 1994.